Aalto University

Alejandro Fernández Navarro

Impact of fusion neutrons on helium production in beryllium and tungsten, and tritium breeding in ITER and DEMO

Final report being equivalent to a Master's thesis required in partial fulfillment for the degree of Master of Science in Technology in the Degree Programme in Engineering Physics and Mathematics.

Supervisor: Professor Mathias Groth

Instructors: Docent Markus Airila, MSc Lauri Rintala

August 31, 2014

AALTO UNIVERSITY
DEPPARTAMENT OF APPLIED PHYSICS

ABSTRACT OF FINAL PROJECT

Author:	Alejandro Fernández Navarro
Title:	Impact of fusion neutrons on helium production on beryllium and tungsten, and tritium breeding in ITER and DEMO
Date:	August 31, 2014 **Number of pages:** VI + 80
Chair:	Tfy-56 Advanced Energy Systems
Supervisor:	Prof. Mathias Groth
Instructors:	Doc. Markus Airila, MSc Lauri Rintala

Abstract:

The project studies blanket designs of ITER and DEMO for neutron shielding, helium production and tritium breeding. On the one hand, a comparison has been made between beryllium and tungsten as first wall materials. On the other hand, tritium breeding blanket models have been studied, focus on the European test blanket module (TBM) concepts, the helium-cooled pebble bed (HCPB) and the helium-cooled lithium-lead (HCLL).

The choice of plasma facing materials and the tritium breeding technology are key issues in the technological development of future fusion power plants. Whereas the ITER design includes beryllium as the first wall material of the blanket and tungsten in the divertor, DEMO will possibly use tungsten for both surfaces, due to beneficial characteristics of this material related to lower tritium retention and lower erosion rates. As future DEMO-type reactors are intended to be tritium self-sufficient, the reactors would dedicate most of the blanket to tritium breeding.

Both analytical (multigroup diffusion theory) and Monte-Carlo methods were utilized to calculate the neutron fluxes and neutron induced reactions. The Serpent code is used to run Monte-Carlo simulations.

The results for the Be-W comparison indicate that W is a better first wall material in terms of blanket shielding capability for high-energy neutrons and showing lower helium production in the first wall. However, the simulations for the HCPB and HCLL models show that the use of a Be first wall instead of W leads to a substantial increment of the tritium breeding ratio (TBR), allowing the use of lithium with lower enrichment.

The assessment of the European tritium breeding blanket concepts indicated that HCPB models have a higher TBR and better shielding capability than HCLL models, being the HCPB with Be as first wall the most efficient breeding blanket.

Finally, lithium depletion simulations for the HCPB and HCLL models showed that these blankets can be easily designed to work without recharging lithium during their estimated lifespan of 5 years.

Language: English

Keywords: Beryllium, tungsten, lithium, tritium breeding, blanket, fusion, ITER, DEMO, HCPB, HCLL

UNIVERSIDAD DE AALTO ABSTRACT DEL PROYECTO FINAL DE CARRERA

DEPARTAMENTO DE FÍSICAS APLICADAS

Autor:	Alejandro Fernández Navarro
Título:	Efecto de neutrones de fusión en la producción de helio en berilio y wolframio, y reproducción de tritio en ITER y DEMO
Fecha:	31 de agosto, 2014 **Número de páginas:** VI + 80
Publicado en:	Tfy-56 Advanced Energy Systems
Supervisor:	Prof. Mathias Groth
Instructores:	Doc. Markus Airila, MSc Lauri Rintala

Abstract:

El Proyecto estudia diseños de blanket para ITER y DEMO en términos de blindaje neutrónico, producción de helio y reproducción de tritio. Por una parte, se ha realizado una comparación entre berilio y wolframio como materiales de "first wall". Por otra parte, se han estudiado diferentes modelos de blankets reproductores de tritio, centrando la atención en los conceptos europeos de test blanket module (TBM), el helium-cooled pebble bed (HCPB) y el helium-cooled lithium-lead (HCLL).

La elección de materiales enfrentados al plasma y la tecnología de reproducción de tritio son aspectos clave en el desarrollo tecnológico de futuras centrales de fusión nuclear. Mientras que el diseño de ITER incluye berilio como material de first wall en el blanket y wolframio en el divertor, DEMO posiblemente utilice wolframio para ambas superficies, debido a las características ventajosas de este material relacionadas con menor retención de tritio y reducidos ratios de erosión. Al estar previsto que los futuros reactores de tipo DEMO sean autosuficientes en tritio, éstos dedicarían la mayor parte del blanket para la reproducción de tritio.

Se han utilizado tanto métodos analíticos (teoría de difusión multigrupo) como el método de Monte-Carlo para calcular los flujos neutrónicos y las reacciones neutrónicas. Las simulaciones de Monte-Carlo fueron realizadas con el código Serpent.

Los resultados de la comparación Be-W indican que el W es un mejor material de first wall, en términos de blindaje del blanket para neutrones de alta energía, y procurando valores inferiores de producción de helio en la first wall. Sin embargo, las simulaciones para los modelos de HCPB y HCLL mostraron que la utilización de una first wall de Be en vez de W conlleva un incremento sustancial del tritium breeding ratio (TBR), permitiendo el uso de litio con menor enriquecimiento.

La evaluación de los conceptos europeos de blankets reproductores evidenció que los modelos HCPB tienen un mayor TBR y una mejor capacidad de blindaje que los modelos HCLL, siendo el HCPB con Be de first wall el blanket reproductor más eficiente.

Por último, las simulaciones de agotamiento de litio, para los modelos HCPB y HCLL, mostraron que estos blankets pueden ser fácilmente diseñados para funcionar sin recargas de litio durante toda su vida útil, estimada en 5 años.

Idioma:	**Keywords:** Berilio, wolframio, litio, reproducción de tritio,
Inglés	blanket, fusión, ITER, DEMO, HCPB, HCLL

Preface

The Final Project was carried out in Finland within jointly between the Aalto University Fusion and Fission research groups, where the group members have made me feel like home.

I am very grateful to my supervisor and group leader Prof. Mathias Groth for giving me the opportunity to do with them a so special project. Thank you to Markus Airila, who guided me along with Mathias throughout the project. Thanks to my instructor, Lauri, to my office mate, Eric, to Risto and to Prof. Rainer Salomaa, who always helped me when I needed.

I do not forget Prof. José Manuel Perlado, director of the Instituto de Fusión Nuclear in the UPM, who encouraged me to get this project, nor can I forget all the professors and teachers who walked with me during my student trip, from the school to the university.

A special mention to all my friends during the Erasmus, my friends in the ETSII, in “Abraxas” and my friends of “La Colmenarehaine” as well. They have made the last few years full of laughter and great experiences. In particular thanks to Jaime for the technical support during my time in Finland.

Last but not least, a big thank you to my family: my grandparents, my uncles and cousins and especially to my parents, Manuel and Aurora and my sister, Alba. They have given me all their love and affection, have taught me to fight for what I want and have encouraged me in my artistic and academic vocations.

All of them have helped me in achieving this project, with which I would like to do my bit in the research and development of fusion energy, as a clean and sustainable energy source.

For those who still say that “fusion is 50 years away and always will be” I leave this quote of George Bernard Shaw:

“People who say it cannot be done should not interrupt those who are doing it”.

Contents

Nomenclature

A	Mass number
DEMO	Demonstration Power Plant
E	Neutron energy
EES	Engineering Equation Solver
g	Neutron energy group
HCLL	Helium-Cooled Lithium Lead
HCPB	Helium-Cooled Pebble Bed
ITER	International Thermonuclear Experimental Reactor
JET	Joint European Torus
LMJ	Lase Megajoule
NIF	National Ignition Facility
PFM	Plasma Facing Material
PPCS	Europea Power Plant Conceptual Study
Q	Fusion power gain
R	Major radius
r	Minor radius
SS	Stainless Steel
TBM	Test Blanket Module
TBR	Tritium Breeding Ratio
WCCB	Water-Cooled Ceramic Breeder
Z	Atomic number

Chapter 1

Introduction

Humanity is at a critical juncture today. The worldwide energy consumption is rapidly growing whereas fossil fuels are depleted. At the same time renewable energies are experiencing an accelerated technological development, and the population becomes aware of the serious issue of global climate change. These factors promote an unprecedented energy revolution either in the near or long term. Nuclear fusion as a clean, inexhaustible and inherently safe energy source could play an important role in the future new-energy model.

During the last 60 years scientists and engineers have sought means to control the energy of the stars for civil purposes. Despite the many technological problems, the international fusion research project ITER is under construction since 2010 and is expected to achieve the first plasma in 2020. This large-scale tokamak reactor will spearhead the fusion energy development, paving the way in the 2030s for the first “demonstration” fusion power plant, referred to as DEMO.

The choice of plasma facing materials (PFMs) for the blanket and divertor[1] is a key issue in the technological development of tokamaks. The ITER design includes beryllium as the first wall material of the blanket and tungsten in the divertor. However, DEMO will possibly use tungsten for both blanket first wall and divertor, due to beneficial characteristics of this material related to lower tritium retention and lower erosion rates. Another important issue for future fusion power plants is the tritium breeding technology. As DEMO-type reactors will use a deuterium-tritium (D-T) fuel and tritium is a radioactive and extremely rare isotope on earth, the power plants are intended to be tritium self-sufficient. Tritium breeding is carried out by neutron induced reactions in lithium materials in the blanket. ITER will test 6 different tritium breeding blanket modules called test blanket modules (TBMs) in the D-T experimental phase. Nevertheless, a fusion power plant would use most of its blanket for tritium breeding to reach self-sufficiency.

The purpose of this project is to assess different blanket designs for ITER and DEMO in two ways. On the one hand, this study compares the use of beryllium and tungsten as first wall material in terms of neutron spectra inside the blanket and helium production in the first wall. Helium collected at grain boundaries of PFMs cause embrittlement and swelling. On the other hand, different tritium breeding blanket models have been run to compare the tritium

[1] The blanket and divertor (in the bottom) cover the interior surfaces of the vaccum vessel in modern coonfigurations of tokamaks, mainly providing neutron shielding to other components (see Figure 2.7).

production and the neutron shielding capability. Lithium depletion simulations have been also run to assess the decrease of tritium breeding with time.

Tritium breeding calculations in this study focus on two European TBM concepts, the helium-cooled pebble bed (HCPB) and the helium-cooled lithium-lead (HCLL). The material compositions of the proposed models have been optimized to reach tritium self-sufficiency and to provide an adequate neutron shielding in a DEMO-type reactor.

Both analytical (multigroup diffusion theory) and Monte-Carlo methods are utilized to calculate the neutron fluxes and neutron induced reactions. The Serpent[2] code [1] is used to run the Monte-Carlo simulations.

The structure of the project comprises six chapters, including this introductory chapter. Chapter 2 begins by laying out the different fusion approaches and giving an overview of the present development of fusion energy technology. It also provides basic information about fusion reactions, the tokamak concept, ITER and DEMO and the different blanket designs. In chapter 3 we analyze the relevant materials in blanket technology, their properties, possible neutron-induced reactions, cross-sections and decays. The formulas to calculate reaction rates and the tritium breeding ratio[3] (TBR) are also shown. Chapter 4 presents the methods, the assumptions and the approaches chosen in this project. A 1-group diffusion method is used to get some initial estimates, 4-group diffusion models are presented in the second section of the chapter, and the Serpent method is shown in the third section. Chapter 5 provides the results of the study, which are divided into two sections: shielding blanket models and tritium breeding blanket models. Finally, chapter 6 summarizes the results, makes comparisons with other papers and presents their implications.

[2] Serpent is a continuous-energy Monte-Carlo code, developed by the VTT Technical Research Centre of Finland [1].

[3] Tritium breeding ratio (TBR) is defined as the tritium production rate in the whole blanket divided by the tritium burning rate in the plasma.

Chapter 2

Fusion energy technology

The use of nuclear fusion as energy source requires a plasma, or ionized gas, with temperatures about 100 million ºC and a confinement time long enough to reach ignition[4]. To achieve these goals two approaches have been implemented in the last few decades: magnetic confinement fusion (tokamaks or stellarators) and inertial confinement fusion (through lasers). Nowadays the tokamak concept, originally developed in Russia, is the most promising way to future fusion power plants. JET tokamak, in the UK, reached 16.1 MW of fusion power and a fusion power gain[5] Q=0.62 in 1997[6]. The international project ITER follows the JET concept and is under construction since 2010. This tokamak is expected to produce 500 MW of fusion power at Q=10 during pulses of 400 s and would open the door in the 2030s to a demonstration power plant referred to as DEMO.

Stellarators can work in steady state with a great plasma stability because of the current-free plasma, but they are far away from reaching break-even (Q=1). The Wendelstein 7-X will be completed in 2015 (Germany) and is the first stellarator with optimized superconducting magnetic coils.

Inertial confinement fusion approach has been mainly developed at the National Ignition Facility (NIF) in the USA. Despite the ambitious fusion campaign carried out in NIF to reach ignition, the many technical problems prevented achieving this goal so far. However, break-even was achieved in September 2013. A similar laser installation has been completed in France in 2014, called Laser Megajoule (LMJ).

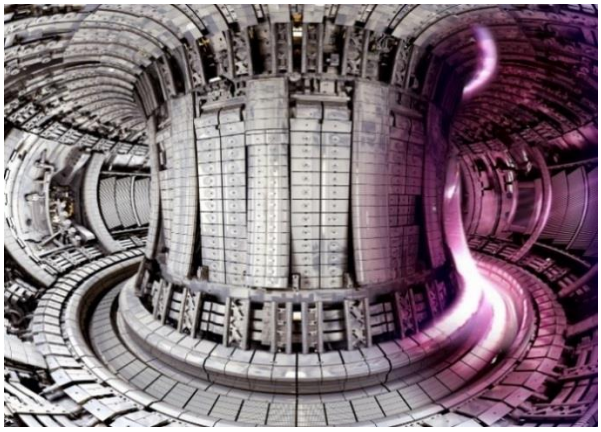

Figure 2.1: In-vessel view of the JET tokamak [2].

[4] Ignition refers to the conditions in which the fusion power output is much higher than the input power.
[5] Fusion power gain, or Q factor, is defined as the ratio of the fusion power output to the input power.
[6] The JET team, *Deuterium-Tritium Operation in Magnetic Confinement Experiments*, p.1, 1999.

2.1 Fusion reactions

In nuclear fusion two light nuclei collide producing a heavier element and releasing energy due to the mass loss in the reaction. The reaction between deuterium (D or $^{2}_{1}\mathrm{H}$) and tritium (T or $^{3}_{1}\mathrm{H}$) has the highest cross-section at the lowest temperature (~10 keV) (Figure 2.2), and because of that D-T fuel is the choice for the future DEMO reactor. This reaction releases 17.6 MeV in the form of kinetic energies of the product nuclei, a helium nucleus and a neutron (Figure 2.3). These neutrons, with ≅14.1 MeV each, are the neutron source for the simulations in this study.

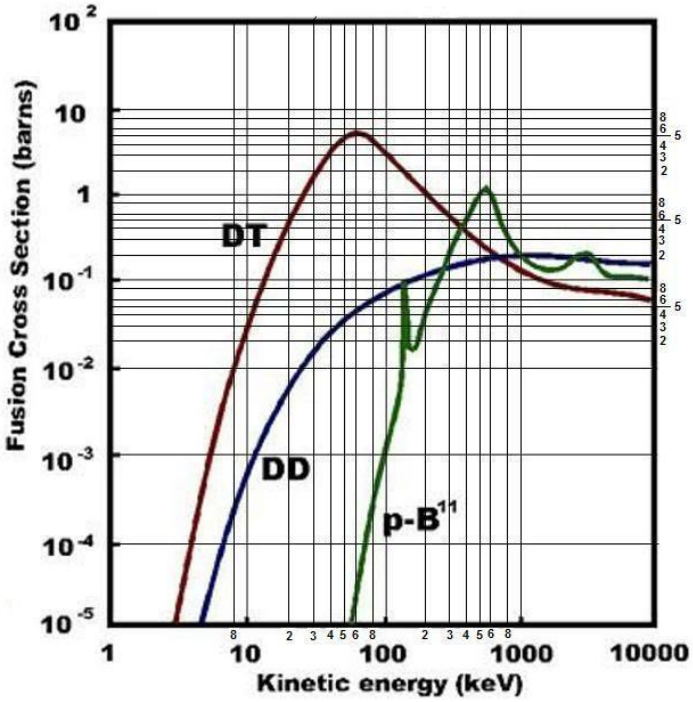

Figure 2.2: Fusion cross-sections of various fusion reactions as a function of kinetic energy of the incident particle [3].

$$\mathrm{D} + \mathrm{D} \xrightarrow{50\%} \mathrm{T}(1.01\ \mathrm{MeV}) + \mathrm{p}(3.02\ \mathrm{MeV})$$
$$\mathrm{D} + \mathrm{D} \xrightarrow{50\%} {}^{3}\mathrm{He}(0.82\ \mathrm{MeV}) + \mathrm{n}(2.45\ \mathrm{MeV})$$
$$\mathrm{D} + \mathrm{T} \longrightarrow {}^{4}\mathrm{He}(3.5\ \mathrm{MeV}) + \mathrm{n}(14.1\ \mathrm{MeV})$$

Figure 2.3: Fusion reaction and energy released for D-D and D-T fuels.

2.2 Tokamak

The word tokamak is the acronym in Russian of "**to**roidal'naya **ka**mera s**ma**gnitnymi **k**atushkami", meaning toroidal chamber with magnetic coils. Specifically, a tokamak has toroidal and poloidal field coils producing a helical magnetic field in the plasma to achieve the confinement (Figure 2.4). Modern configurations of tokamaks include a divertor in the bottom of the chamber to minimize the plasma-wall interaction.

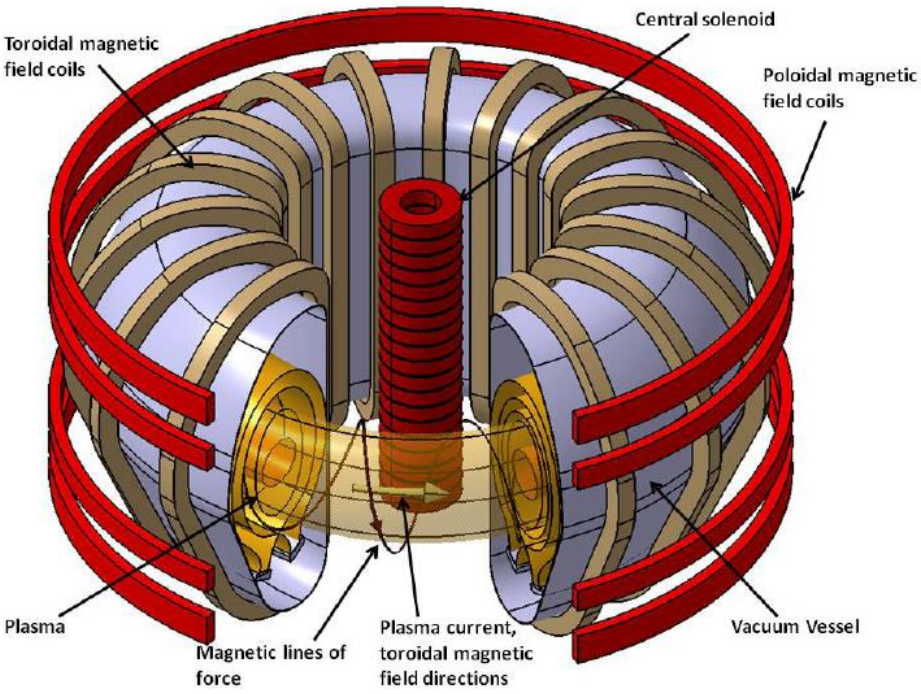

Figure 2.4: Schematic of a tokamak [4].

2.3 ITER and DEMO reactors

ITER[7], "the way" in Latin, is an international fusion research project that aims to demonstrate the technological and scientific feasibility of fusion energy. This large-scale experimental reactor would open the door to the first "demonstration" fusion power plant, DEMO.

ITER is in the building phase since 2010, the first plasma is expected to be achieved in 2020 and the D-T operation phase would start in 2027.

[7] Nowadays ITER means "the way or "the road" in Latin, but initially, it was also the acronym of "International Thermonuclear Experimental Reactor".

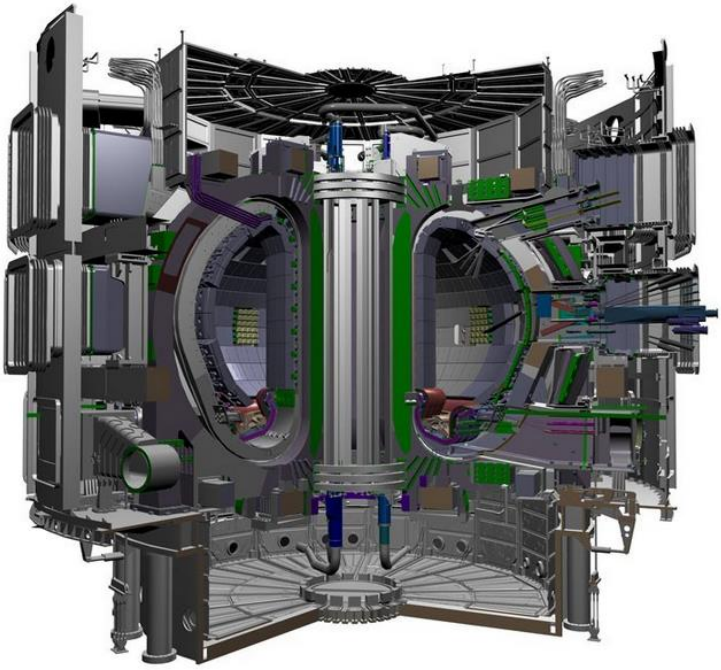

Figure 2.5: ITER design [5].

The Europea Power Plant Conceptual Study (PPCS) of 2005 shows several possible designs and sizes for DEMO (see Figure 2.5). Whereas concepts A and B are near-term models (and more conservatives than C and D), C and D are designs for more advanced power plants. Model B has been chosen as DEMO design in this study considering that is the most economically and technologically feasible choice in the near-term.

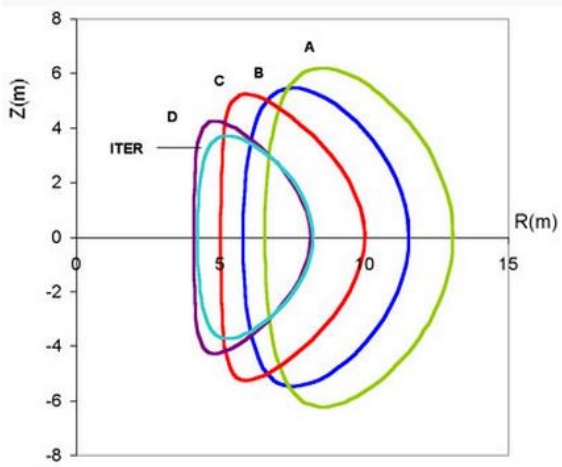

Figure 2.6: Sizes and shape of the plasmas in ITER (similar to model D) and the PPCS [6].

The following Table 2.1 compares the main design parameters of ITER and DEMO. This study considers the nominal parameters of the full D-T (50 %-50 %) operation phase for ITER and the values of the PPCS-B model for DEMO.

Main parameters of ITER and DEMO	Major radius (R)/ minor radius (r) [m]	Nominal fusion power P_f[MW]	First wall neutron loading P_{wn}[MW/m^2]	Performance	Output electrical power [MW]
ITER	6.2/2	500	0.55	400 s pulses Q = 10	–
DEMO	8.6/3	3600	1.89	Steady – state Q ≫ 1	1330

Table 2.1: Main parameters of ITER and DEMO designs [6, 7].

To calculate the neutron power and neutron yield, and hence the neutron source for the models, this study assumes only D-T reactions in the plasma (see Figure 2.3). Appendix A shows that the neutron yield from D-D reactions is about 800 times lower than the neutron yield from D-T reactions, and therefore D-D neutrons can be considered negligible in D-T plasma.

The total first wall surface includes the divertor plates and the different ports (see Figure 2.7). The first wall shape and configuration of ITER was used to calculate the wall surface values for DEMO.

The neutron power, neutron yield and first wall loading in Tables 2.1 and 2.2 are calculated through the following formulas (2.1), (2.2) and (2.3).

$$P_n = P_f * \frac{E_n}{E_{tot}} \tag{2.1}$$

where P_n is the neutron power, P_f the fusion power, E_n the neutron energy (14.1 MeV) and E_{tot} the total energy released (17.6 MeV).

$$I_n = \frac{P_n}{E_n} \tag{2.2}$$

where I_n is the neutron yield and E_n is given in J.

$$P_{wn} = \frac{P_n}{S_t} \tag{2.3}$$

where P_{wn} is the first wall neutron loading and S_t is the total surface area of the first wall.

Other parameters of ITER and DEMO	Neutron power P_n[MW]	Neutron yield I_n[s^{-1}]	Total First wall surface S_t[m^2]	Blanket surface S_b[m^2]	S_b/S_t
ITER	401	$1.78 * 10^{20}$	730	600	0.82
DEMO	2880	$1.28 * 10^{21}$	1520	1250	0.82

Table 2.2: Other useful parameters in this study of ITER and DEMO designs [6, 7].

2.4 Blanket designs

This study considers two types of blanket: the shielding blanket and the tritium breeding blanket. The purpose of the shielding blanket (besides collect thermal energy) is to protect the magnets and other components against the neutrons. A tritium breeding blanket also has the purpose of producing tritium to fuel the plasma. ITER will have a complete shielding blanket that mainly consists of a beryllium first wall, a structure of an austenitic stainless steel (Section 3.1) and water pipes as the cooling system. However, in the D-T phase of ITER, breeding blanket modules called Test Blanket Modules (TBMs) will be tested in 6 of the equatorial ports (see part (3) in Figure 2.7 and Figure 2.8). Unlike ITER, DEMO would use the whole blanket, or a large part of it, to produce tritium. This study considers the use of the whole blanket, i.e. the 82 % (Table 2.2) of the first wall, for tritium breeding calculations.

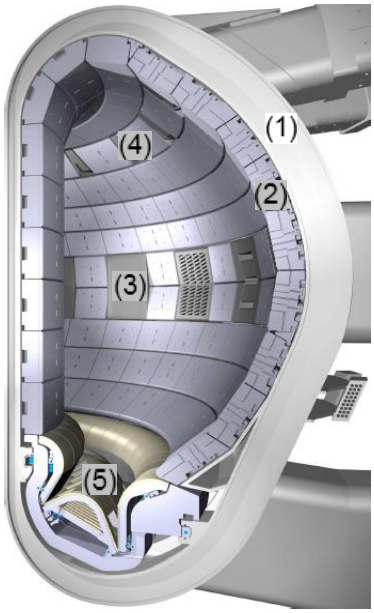

Figure 2.7: Poloidal cross section of ITER: vacuum vessel (1), blanket (2), equatorial ports (3), upper ports (4) and divertor (5) [5].

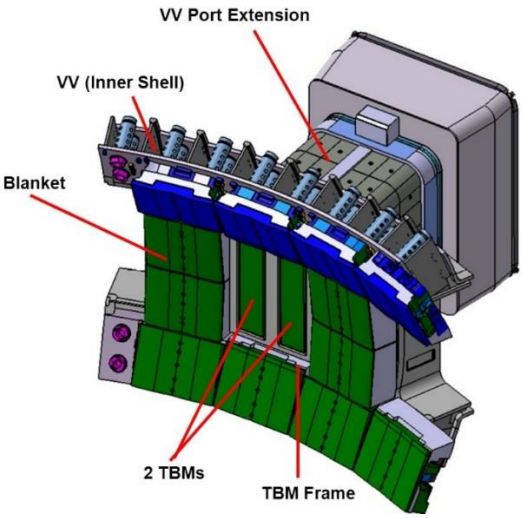

Figure 2.8: Shielding blanket and Test Blanket Modules (TMBs) for ITER [8].

Among the 6 tritium breeding blanket designs for ITER, this study gives focus to two European designs: the Helium-Cooled Pebble Bed (HCPB) and the Helium-Cooled Lithium Lead (HCLL). Also some simple models have been made for a Japanese Water-Cooled Ceramic Breeder (WCCB).

The HCPB concept consists mainly of a beryllium first wall, lithium ceramic (Li_4SiO_4) pebbles as tritium breeder, beryllium pebbles as neutron multiplier material, cooling plates and pipes with helium as coolant, a structure of stainless steel and a back manifold. Unlike the HCPB, the HCLL concept uses a lithium-lead alloy flowing through pipes as tritium breeder and does not have Be pebbles as neutron multiplier. (More information about materials in Chapter 3).

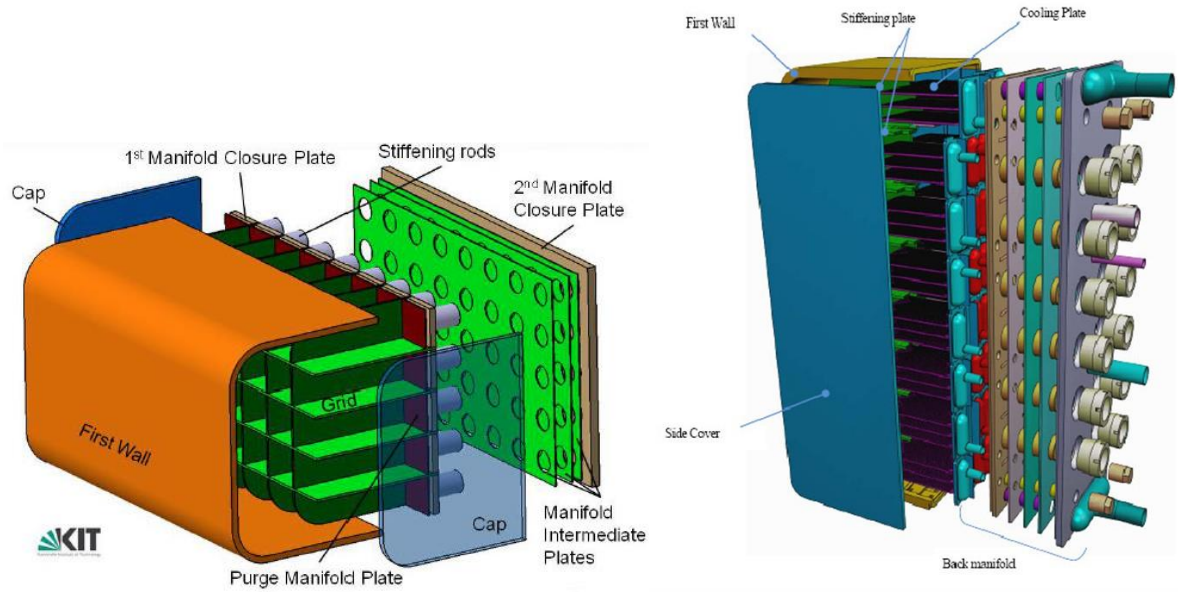

Figure 2.9: HCPB-TBM design (left) and HCLL-TBM design (right) [9].

The thickness of the blanket is an important parameter in this study for shielding and tritium breeding calculations. The shielding blanket of ITER is 45 cm thick [7] and a thickness of 55 cm has been considered for the shielding blanket of DEMO. The HCPB-TBM has a radial thickness of ~70 cm [10] and the HCLL-TBM ~100 cm [11]. The thickness of the tritium breeding blankets have been used for both, ITER and DEMO models. The following table shows the approximate values for the blanket volume, calculated by multiplying the former values by the blanket surface (Table 2.2).

Blanket volumes of ITER and DEMO	Shielding blanket volume [m^3]	HCPB blanket volume [m^3]	HCLL blanket volume [m^3]
ITER	270	420	600
DEMO	690	875	1250

Table 2.3: Blanket volumes for different blanket concepts of ITER and DEMO [6, 7, 10, 11].

Chapter 3

Relevant materials under neutron irradiation

3.1 Relevant materials

Carbon, beryllium, tungsten, lithium, steel, water, helium and other materials are used in present blankets or future blanket designs of tokamaks. In this section we analyze the properties of the relevant materials and their purpose in the current designs/proposals of ITER and DEMO blankets.

Relevant materials	Composition	Phase (operating conditions)	Molar mass (g/mol)	Density (g/cm^3) (room temp.)	Atomic density (cm^{-3})
Beryllium (PFM)	(natural) $^{9}_{4}Be$	Solid	9.01	1.82	$1.216 * 10^{23}$
Tungsten (PFM)	(natural; molar fraction) $^{180}_{74}W(0.12\ \%)$, $^{182}_{74}W(26.5\ \%)$, $^{183}_{74}W(14.3\ \%)$, $^{184}_{74}W(30.6\ \%)$, $^{186}_{74}W(28.4\ \%)$	Solid	183.84	19.3	$6.322 * 10^{22}$
Lithium (T breeder)	(natural; molar fraction) $^{6}_{3}Li(7.5\ \%)$, $^{7}_{3}Li(92.5\ \%)$	Solid	6.94	0.53	$4.634 * 10^{22}$
Lithium orthosilicate (T breeder)	Li_4SiO_4	Solid	119.85	2.28	$1.146 * 10^{22}$
Lithium-lead eutectic (T breeder)	(molar fraction) $Pb(83\ \%), Li(17\ \%)$	Liquid	173.8	9.809	$3.399 * 10^{22}$
SS 316(N) – IG (structural)	$Fe(\sim 70\ wt.\%), Cr(\sim 18\ wt.\%), Ni(\sim 12\ wt.\%)$	Solid	~55.5	7.97	$8.648 * 10^{22}$
Water (coolant)	H_2O	Liquid	18.02	1	$3.343 * 10^{22}$
Helium (coolant)	(natural) $^{4}_{2}He(\sim 100\ \%)$	Supercritical fluid	4.00	(8 MPa, 600 K) $6.49 * 10^{-3}$	$9.769 * 10^{20}$

Table 3.1: Composition, atomic weight and densities for the relevant materials [7, 11, 12, 13, 14, 15].

The choice of the plasma facing materials (PFMs) for the blanket and divertor is a key issue in the technological development of tokamaks due to a number of reasons. The material in question must withstand high neutron fluxes and temperatures, keeping appropriate physical and thermo-mechanical properties and minimizing the erosion rate, induced radioactivity, fuel particle retention and plasma contamination by impurities. The main materials considered for this purpose are carbon (C), beryllium (Be) and tungsten (W). Other mixed PFMs, like W/C or Be/C mixes, are also being investigated.

Helium production in PFMs is an important issue because helium collected at grain boundaries (producing bubbles) induces swelling and cause the embrittlement of the material.

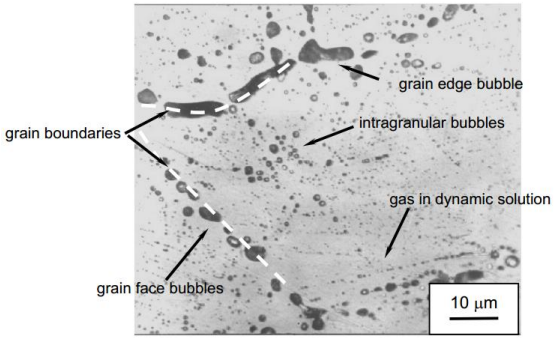

Figure 3.1: Bubbles inside the grain and at grain boundaries in an irradiated beryllium pebble [16].

Carbon, as graphite and carbon fiber composites, has good thermo-mechanical properties like high thermal conductivity and very high melting temperature, low neutron activation cross-section and, being a low-Z, is benign to the plasma as an impurity. Because of that, it has been the most commonly used PFM since the 1980s. However, carbon materials have been dismissed as PFMs for future fusion power plants (DEMO-type reactors) due to serious drawbacks. One of these drawbacks is a high tritium retention rate, producing high levels of radioactivity (see Figure 3.2). Another important drawback is the high erosion yield of carbon, largely due to chemical erosion, restricting the lifetime of the first wall.

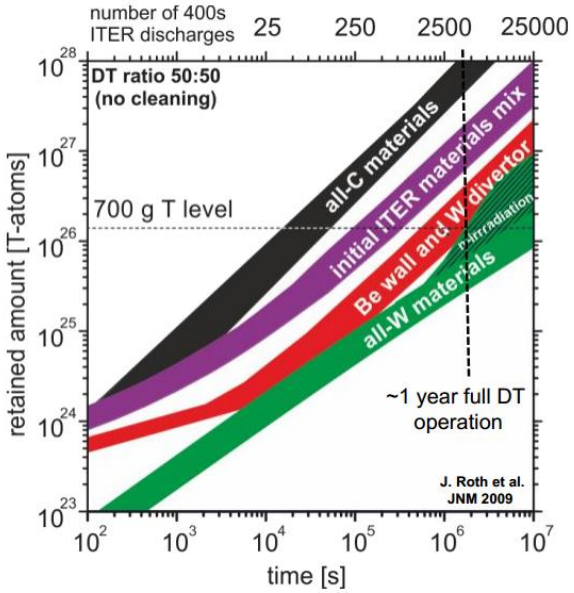

Figure 3.2: Accumulation of tritium up the 700 g ceiling in ITER for different PFMs during nominal operation [17]. Experimentally validated [18].

J. Roth et al. assumed a 700 g ceiling for retained tritium in ITER and concluded the time to reach this ceiling for the different PFMs (Figure 3.2, [17], 2009). For carbon as first wall and divertor plates material the ceiling is reached at around 75 pulses of 400 s, that is, 9 days of the DT operation plan in ITER and only 8 hours hypothetically operating in steady-state. Instead, with Be as first wall and W for the divertor the ceiling is reached for around 3000 nominal pulses, corresponding to one year of DT operation (400 s pulses) and 14 days in steady-state operation. The best option would be the use of all-W materials, reaching the ceiling at around 15000 pulses, 5 years of DT operation in ITER and 69 days in steady state. The use of carbon as PFMs is not feasible because implementing cleaning actions would be needed every 9 days in ITER and every few hours in a DEMO-type reactor. Because of the reasons explained, carbon has been dismissed as first wall material in present ITER-type reactor designs and, therefore, is not included in the models described in chapter 4.

Beryllium as first wall material has been already tested in JET and is the choice for ITER [7]. Be is also a low-Z material as C, a good thermal conductor and retains more than 10 times less tritium than carbon (Figure 3.2). As drawbacks, this material has a low melting point (1560 K), produces higher particle sputtering rates than C and is highly toxic, which concerns manufacturing, operation and decommissioning. Be has been dismissed as the divertor plates material due to the high erosion yield (divertor plates are under high particle bombardment).

Tungsten is a possible option as first wall material in DEMO and is the choice for the divertor plates in ITER. W is a high-Z metal, having the lowest sputtering yield for incident particles with less than 10 keV (compared to C and Be, see Figure 3.3), but its high-Z impurities are damaging for the plasma stability. Other advantages are the melting point, 3695 K, and the lowest tritium retention rate.

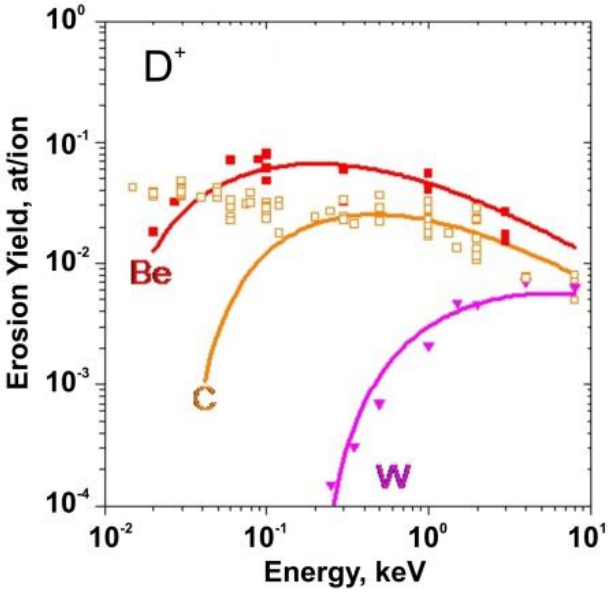

Figure 3.3: Erosion yields of tungsten (W), beryllium (Be), and carbon (C) as a function of the impacting deuterium energy. Lines are theoretical prediction for physical sputtering yields. Dots correspond to experimental results [19].

Tritium breeding technology is based on lithium alloys and compounds, with different degrees of ^{6}Li enrichment. Lithium is a soft alkali metal, one of the lightest elements (Z=3) and has a low melting point (454 K). Natural lithium has a ^{6}Li isotope fraction of 7.5 %, but as

a tritium breeder, it is further enriched to increase the tritium production rate (see Figure 5.12). This is because ^{6}Li has a large (n, T) cross-section for low neutron energies (see Figure 3.9). The HCPB TBM concept contains lithium ceramic pebbles as tritium breeding material. Among the lithium ceramics, lithium orthosilicate (Li_4SiO_4) is the leading choice, but other ceramics are being investigated, like lithium metatitanate (Li_2TiO_3) [20]. The HCLL TBM concept uses the lithium-lead eutectic alloy Pb17Li (83 %Pb, 17 %Li) in the liquid state (melting point 510 K) as tritium breeding material [14].

The structural material of the blanket is an austenitic stainless steel in ITER and a ferritic-martensitic steel in the DEMO conceptual design. The steel forms the structure of the blanket and acts as bulk shield against neutron irradiation. SS 316L(N)-IG is the ITER-grade stainless steel. Among its properties, this Cr-Ni austenitic stainless steel possess a great corrosion resistance, high toughness and good weldability. EUROFER 97 is the European reference material for the DEMO blanket. The main characteristic of this ferritic-martensitic steel is its low activation, a key issue for future reactors, and also experiences lower swelling than stainless steels. SiC composites are also being investigated as structural material [21]. This study uses the steel of ITER as reference, approximating it by iron in the 4-group diffusion models and by the mixture Fe(70 wt.%), Cr(18 wt.%), Ni(12 wt.%) in the Monte-Carlo method models.

Chemical composition (wt.%)	Fe	C	Cr	Mn	Ni	Mo	N	V	Imp.
SS 316(N) – IG	Basis	0.0225	17.50	1.80	12.25	2.50	0.07	(0.004)	~ 1.02
EUROFER 97	Basis	0.11	9.00	0.4	0.006	(<0.005)	0.03	0.20	~ 0.79

Table 3.2: Specification of the chemical composition of the steels SS 316L(N)-IG [7] and EUROFER 97 [22].

The coolant for the ITER blanket will be water, but helium is going to be used in the European designs for the test blanket modules (TBMs), the HCPB and HCLL (see section 2.4). Water is a well-known coolant and moderator in fission power plants. Water combines good physical and thermal properties (liquid in a high range of conditions, high specific heat capacity 4618 J/kgK, thermal conductivity 0.65 W/mK (at 510 K, 4.4 MPa)) and good nuclear properties as neutron moderator (see section 3.2.5). Apart from that, it is available almost everywhere (rivers, lakes, sea etc.). Helium will be used as coolant at 8 MPa and around 600 K, being a supercritical fluid in these conditions. This fluid has good thermophysical properties (specific heat capacity 5187 J/kgK, thermal conductivity 0.26 W/mK) and is transparent to neutrons but has a low density and it is not a good moderator.

3.2 Neutron induced reactions and cross-sections

The performance of the relevant materials under neutron irradiation is analyzed in the next Table 3.3 (main neutron induced reactions and decay channels of the activation products) and the following subsections (cross-sections of the significant reactions).

Material	Reaction	Range of relevance	Decay	Half life
Beryllium	$^{9}Be(n,\ el)$	$\forall E$	-	-
	$^{9}Be(n,2n)\ ^{8}Be$	> 2 MeV	$^{8}Be \underset{\alpha}{\rightarrow}\ ^{4}He$	10^{-16}s
	$^{9}Be(n,\alpha)\ ^{6}He$	> 1 MeV	$^{6}He \underset{\beta^-}{\rightarrow}\ ^{6}Li$	0.8s
	$^{9}Be(n,T)\ ^{7}Li$	> 10 MeV	$T \underset{\beta^-}{\rightarrow}\ ^{3}He$	12.32 y
	$^{9}Be(n,\gamma)\ ^{10}Be$	< 1 eV	$^{10}Be \underset{\beta^-}{\rightarrow}\ ^{10}B$	$1.5 * 10^{6}$y
Tungsten	$W(n,\ el)$	$\forall E$	-	-
	$W(n,n')W^*$	> 0.1 MeV	$W^* \underset{\gamma}{\rightarrow} W$	-
	$^{182}W(n,2n)\ ^{181}W$ $^{183}W(n,2n)\ ^{182}W$ $^{184}W(n,2n)\ ^{183}W$ $^{186}W(n,2n)\ ^{185}W$	> 5 MeV	$^{181}W \underset{CE}{\rightarrow}\ ^{181}Ta$ - - $^{185}W \underset{\beta^-}{\rightarrow}\ ^{185}Re$	121d - - 75d
	$^{182}W(n,\gamma)\ ^{183}W$ $^{183}W(n,\gamma)\ ^{184}W$ $^{184}W(n,\gamma)\ ^{185}W$ $^{186}W(n,\gamma)\ ^{187}W$	< 5 MeV	- - $^{185}W \underset{\beta^-}{\rightarrow}\ ^{185}Re$ $^{187}W \underset{\beta^-}{\rightarrow}\ ^{187}Re$	- - 75d 1d
	$^{182}W(n,\alpha)\ ^{179}Hf$ $^{183}W(n,\alpha)\ ^{180}Hf$ $^{184}W(n,\alpha)\ ^{181}Hf$ $^{186}W(n,\alpha)\ ^{183}Hf$	> 10 MeV	- - $^{181}Hf \underset{\beta^-}{\rightarrow}\ ^{181}Ta$ $^{183}Hf \underset{\beta^-}{\rightarrow}\ ^{183}Ta\ ;\ ^{183}Ta \underset{\beta^-}{\rightarrow}\ ^{183}W$	- - 42d 1h ; 5d
Lithium	$^{6}Li(n,\ el)\ ^{6}Li$ $^{7}Li(n,\ el)\ ^{7}Li$	$\forall E$	- -	- -
	$^{6}Li(n,n')\ ^{6}Li^*$ $^{7}Li(n,n')\ ^{7}Li^*$	> 2 MeV > 0.5 MeV	$^{6}Li^* \underset{\gamma}{\rightarrow}\ ^{6}Li$ $^{7}Li^* \underset{\gamma}{\rightarrow}\ ^{7}Li$	- -
	$^{6}Li(n,p)\ ^{6}He$	> 3 MeV	$^{6}He \underset{\beta^-}{\rightarrow}\ ^{6}Li$	0.8s
	$^{7}Li(n,D)\ ^{6}He$	> 10 MeV	$^{6}He \underset{\beta^-}{\rightarrow}\ ^{6}Li$	0.8s
	$^{6}Li(n,T)\ ^{4}He$	< 10 MeV	$T \underset{\beta^-}{\rightarrow}\ ^{3}He$	12.32 y
	$^{7}Li(n,n+T)\ ^{4}He$	> 3 MeV	$T \underset{\beta^-}{\rightarrow}\ ^{3}He$	12.32 y
	$^{6}Li(n,\gamma)\ ^{7}Li$ $^{7}Li(n,\gamma)\ ^{8}Li$	< 10 eV	- $^{8}Li \underset{\beta^-}{\rightarrow}\ ^{8}Be\ ;\ ^{8}Be \underset{\alpha}{\rightarrow}\ ^{4}He$	- 0.8s ; 10^{-16}s
	$^{7}Li(n,2n)\ ^{6}Li$	> 10 MeV	-	-
	$^{6}Li(n,n+D)\ ^{4}He$	> 2 MeV	-	-
	$^{6}Li(n,2n+\alpha)H$ $^{7}Li(n,2n+\alpha)D$	> 5 MeV > 10 MeV	$^{6}He \underset{\beta^-}{\rightarrow}\ ^{6}Li$ -	0.8s -

Table 3.3: Significant neutron induced reactions and decay channels of the PFMs, Be, W and the tritium breeder element, Li [23, 24].

3.2.1 Beryllium

Beryllium acts as moderator, neutron multiplier and He producer under high-energy neutron irradiation (Figure 3.4). Note that Be is used as PFM and that the energy of the neutron current at the first wall is 14.1 MeV. As moderator, it has an average logarithmic energy loss of $\xi = 0.21$ and the moderating ratio for 1 MeV is ~400. The elastic scattering cross-section (n, elastic) is around 2 b for high energies (E>0.1 MeV) and 7 b (almost constant) for lower energies. The neutron multiplier reaction (n, 2n) has a cross-section around 0.5 b for E>2 MeV and negligible for lower energies. He production is due to the (n, α) reaction and to the (n, 2n) reaction (through alpha decay). The cross-section of (n, α) has a maximum of 0.1 b at 3 MeV and is negligible for energies E<1 MeV. Neutron capture (n, γ) is only significant for E<1 eV and the tritium production reaction (n, T) is negligible for E<10 MeV. The cross-sections of the rest of reactions are negligible in the whole neutron spectrum. Data retrieved from ENDF/B-VII.1 library, (March 2014) [24].

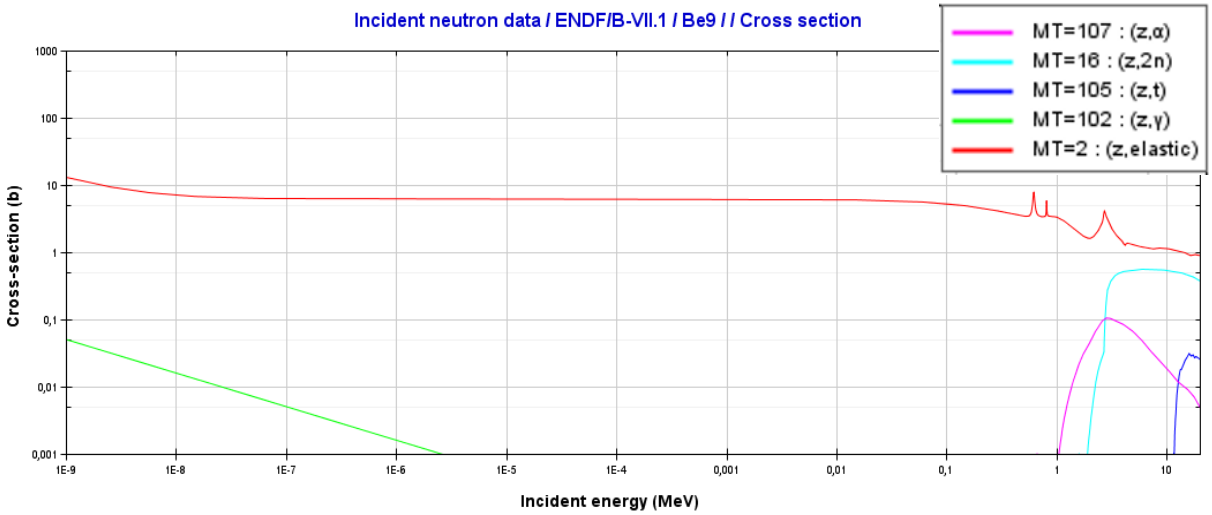

Figure 3.4: Significant cross-sections for ^{9}Be under neutron irradiation [24]. Reaction MT-numbers according to ENDF format [25].

3.2.2 Tungsten

Tungsten is a neutron absorber for medium and low energies and a good neutron multiplier for high neutron energies (Figure 3.5, 3.6, 3.7, 3.8). The absorption is mainly due to the neutron capture (n, γ) reaction, with a cross-section increasing rapidly towards thermal energies, it is around 0.1 b for high energies, there are large resonances for medium energies and it reaches 10-200 b at 1 meV (depending on the isotope). The neutron multiplier reaction (n, 2n) has a cross-section around 2 b for E>5-6 MeV and negligible for lower energies. The elastic scattering cross-section (n, elastic) is around 5 b for high energies, is resonant for medium energies and around 6 b (constant) for lower energies, except for ^{186}W that it decreases towards lower energies. The inelastic scattering (n, n') cross-section is about 1-5 b for high neutron energies and negligible for lower energies. The He production is almost negligible, with a little cross-section of about 1 mb for E>10 MeV. Other reactions are significant for energies E>15 MeV, like (n,p), (n,D), (n,T), (n,n+p), (n, n+D), (n, n+ α) or (n, 3n), but they are not interesting in this study. Data retrieved from JEFF-3.1.2 General Purpose Library, (February 2014) [23].

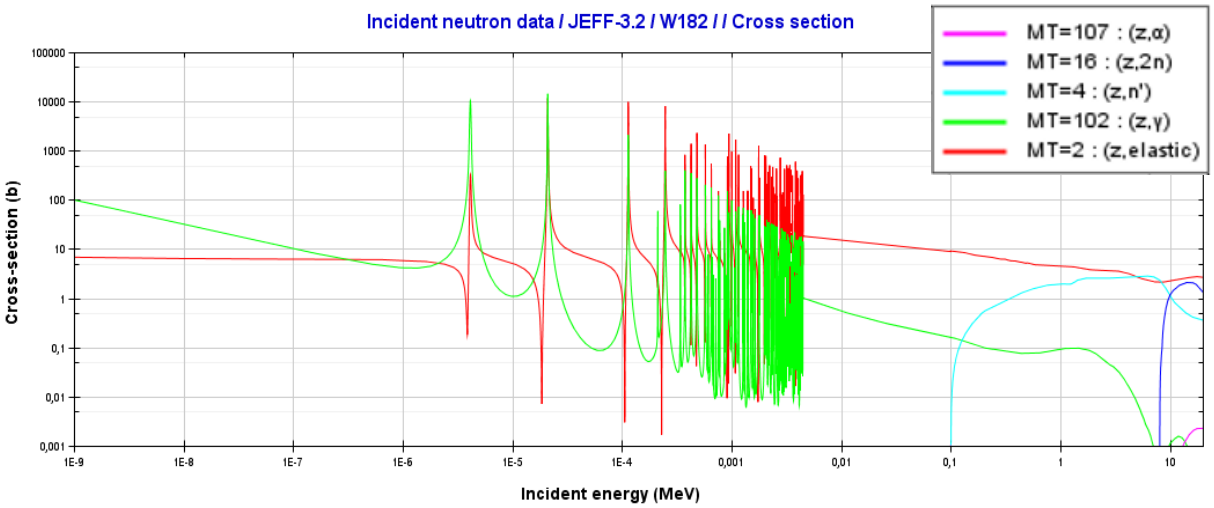

Figure 3.5: Significant cross-sections for ^{182}W under neutron irradiation [23]. Reaction MT-numbers according to ENDF format [25].

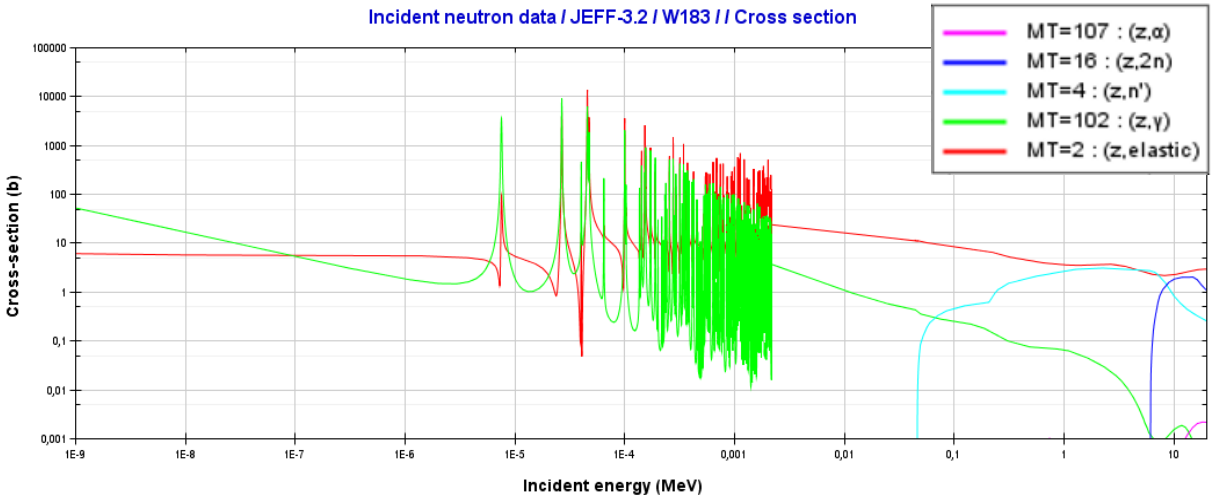

Figure 3.6: Significant cross-sections for ^{183}W under neutron irradiation [23]. Reaction MT-numbers according to ENDF format [25].

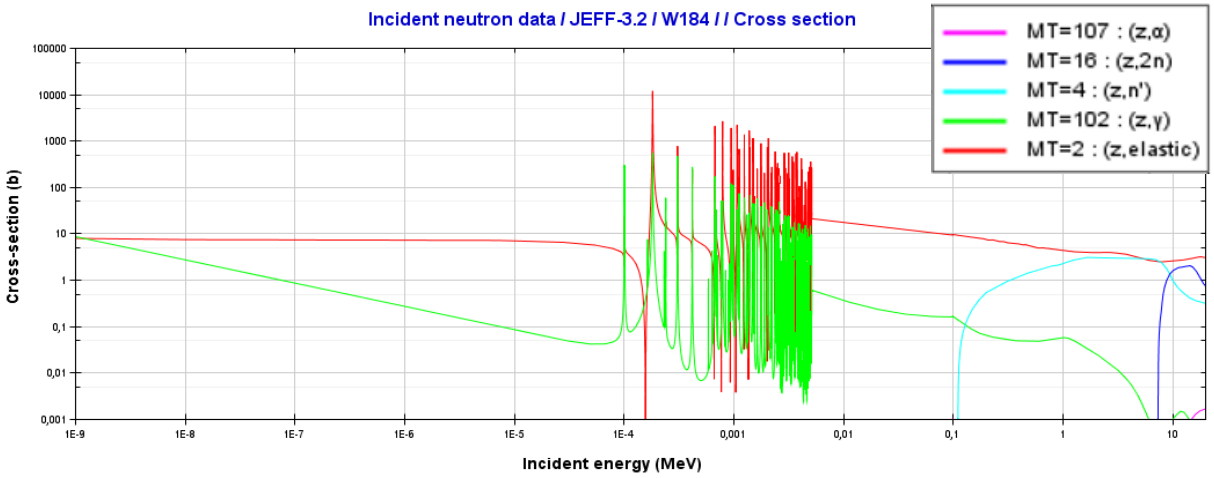

Figure 3.7: Significant cross-sections for ^{184}W under neutron irradiation [23]. Reaction MT-numbers according to ENDF format [25].

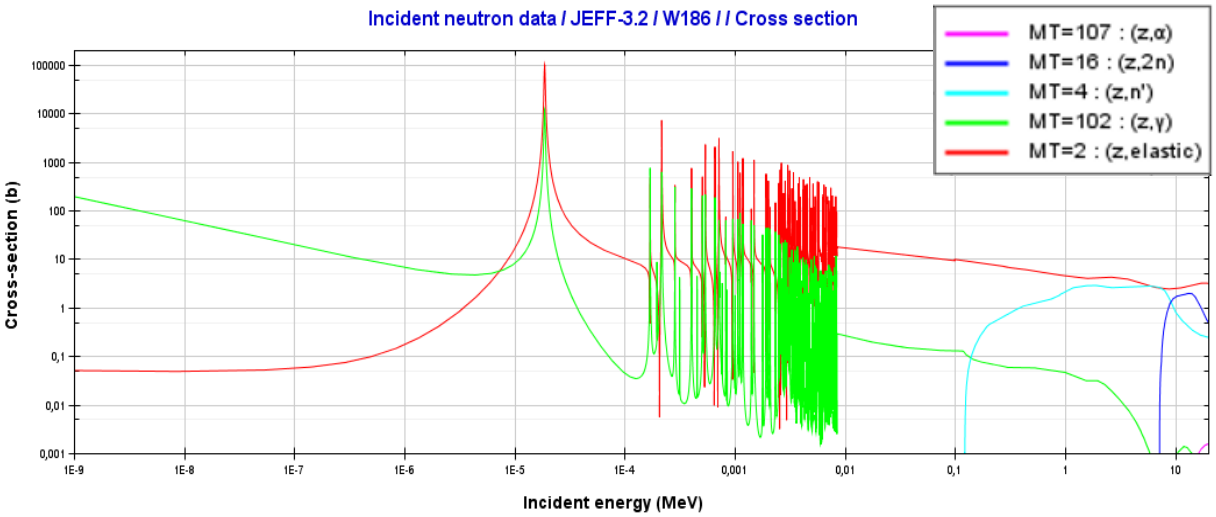

Figure 3.8: Significant cross-sections for ^{186}W under neutron irradiation [23]. Reaction MT-numbers according to ENDF format [25].

3.2.3 Lithium

Lithium is principally a tritium producer, especially for low energy neutrons with ^{6}Li. The cross-section of the $^{6}\mathrm{Li}(\mathrm{n},\mathrm{T})$ reaction increases rapidly, as ≅1/v (v is the neutron velocity), towards low energies, reaching almost 5000 b at 10^{-3} eV, (this reaction produces also He). ^{7}Li breeds also tritium through the $(\mathrm{n},\mathrm{n}+\mathrm{T})$ reaction ((z,Xt) in Figure 3.10), reaching the maximum cross-section around 7 MeV, 0.4 b, and it is negligible for E<3 MeV. The neutron capture reaction is only significant for thermal neutrons. The neutron multiplier reaction $^{6}\mathrm{Li}(\mathrm{n},\mathrm{n}+\mathrm{D})$ ((z, Xd) in Figure 3.9) is important for E>2 MeV. Other reactions are significant for energies around 10 MeV, like $^{A}\mathrm{Li}(\mathrm{n},\ 2\mathrm{n}+\alpha)$, $^{6}\mathrm{Li}(\mathrm{n},\ \mathrm{p})$, $^{7}\mathrm{Li}(\mathrm{n},\ 2\mathrm{n})$ and $^{7}\mathrm{Li}(\mathrm{n},\ \mathrm{D})$. Data retrieved from ENDF/B-VII.1 library, (March 2014) [24].

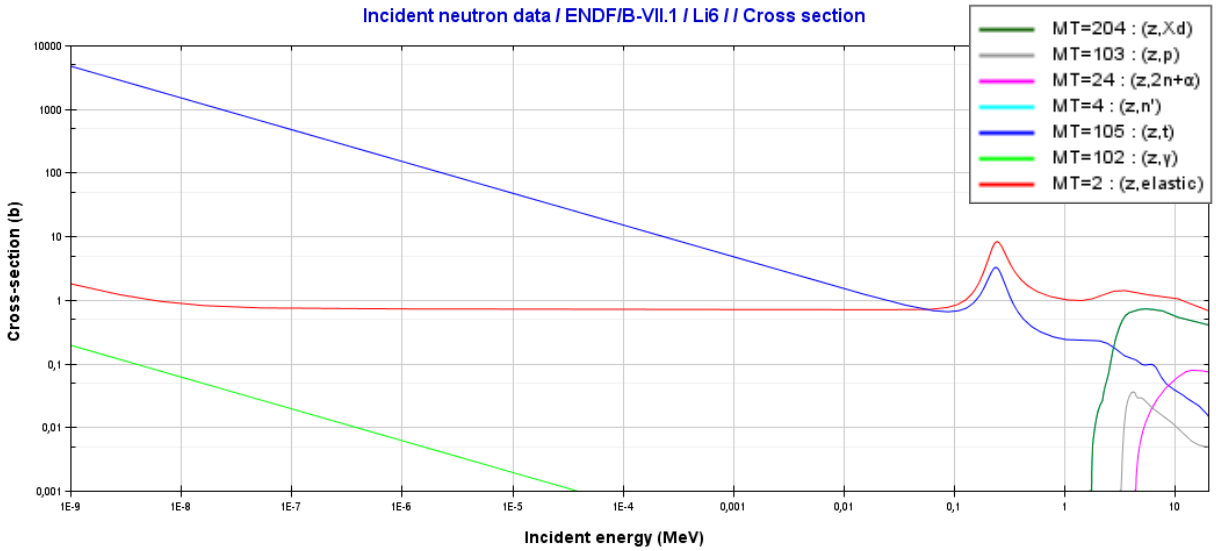

Figure 3.9: Significant cross-sections for ^{6}Li under neutron irradiation [24]. Reaction MT-numbers according to ENDF format [25].

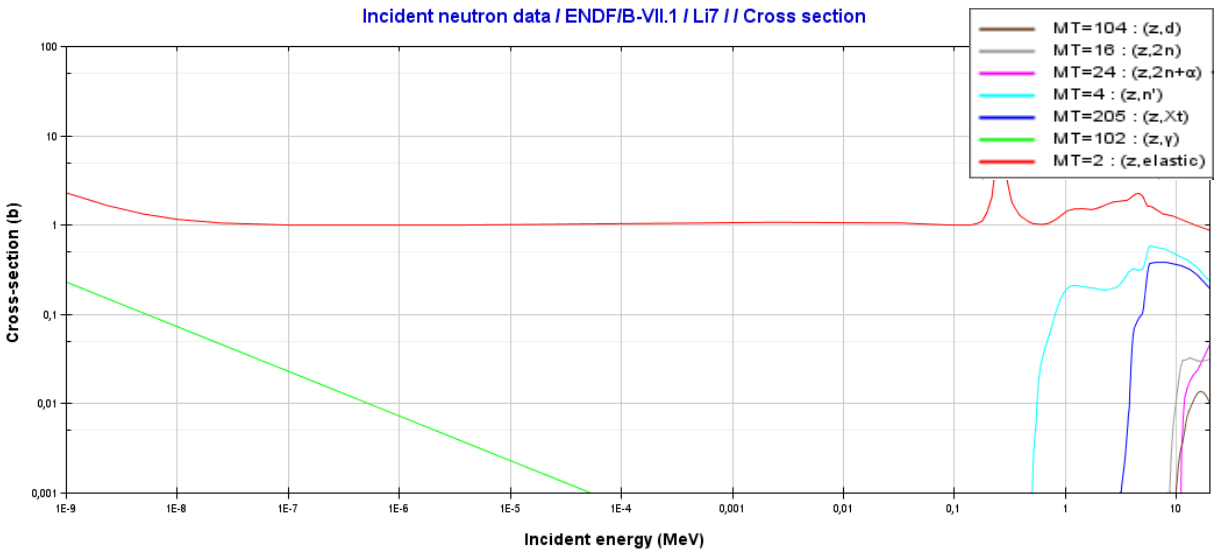

Figure 3.10: Significant cross-sections for $^{7}\mathrm{Li}$ under neutron irradiation [24]. Reaction MT-numbers according to ENDF format [25].

3.2.4 Lead

As the HCLL concept uses a lithium-lead alloy ($\mathrm{Li_{17}Pb_{83}}$) as tritium breeder, the performance of lead under neutron irradiation is an important issue. Lead is a good neutron multiplier with incident high energy neutrons, favoring the increase of the tritium production rate in lithium. The cross-section of the (n, 2n) reaction is around 2 b for E>8 MeV and the (n, 3n) reaction is significant for E>14 MeV. The following Figure 3.11 shows the relevant cross-sections for $^{206}\mathrm{Pb}$, but they are representative also for the other three stable isotopes of lead, $^{204}\mathrm{Pb}$, $^{207}\mathrm{Pb}$ and $^{208}\mathrm{Pb}$. Data retrieved from ENDF/B-VII.1 library, (March 2014) [24].

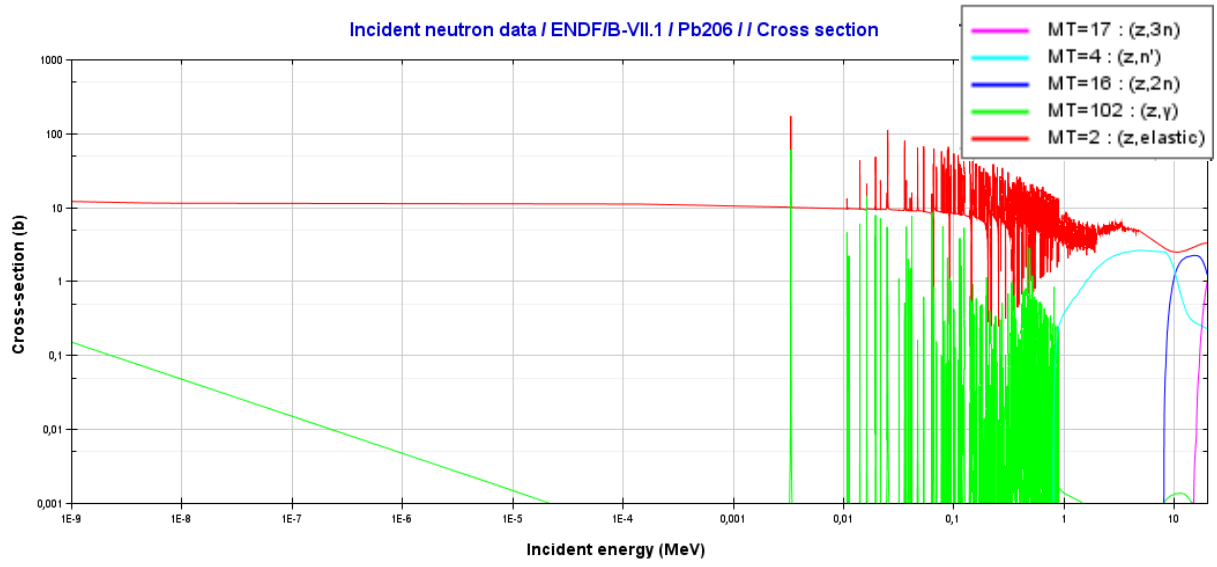

Figure 3.11: Significant cross-sections for $^{206}\mathrm{Pb}$ under neutron irradiation [24]. Reaction MT-numbers according to ENDF format [25].

3.2.5 Steel

The steel used in ITER, SS 316(N)-IG (see Table 3.2), is taken as reference in this study. It is approximated by iron in the 4-group diffusion models and by the mixture Fe(70 wt.%), Cr(18 wt.%), Ni(12 wt.%) in the Serpent models. Figure 3.12 shows the cross-sections for iron[8] (approximated by ^{56}Fe), which is the most important element in this material. Iron, like tungsten, is a neutron absorber for medium and low energies and a neutron multiplier for E>10 MeV. Data retrieved from JEFF-3.1.2 General Purpose Library, (February 2014) [23].

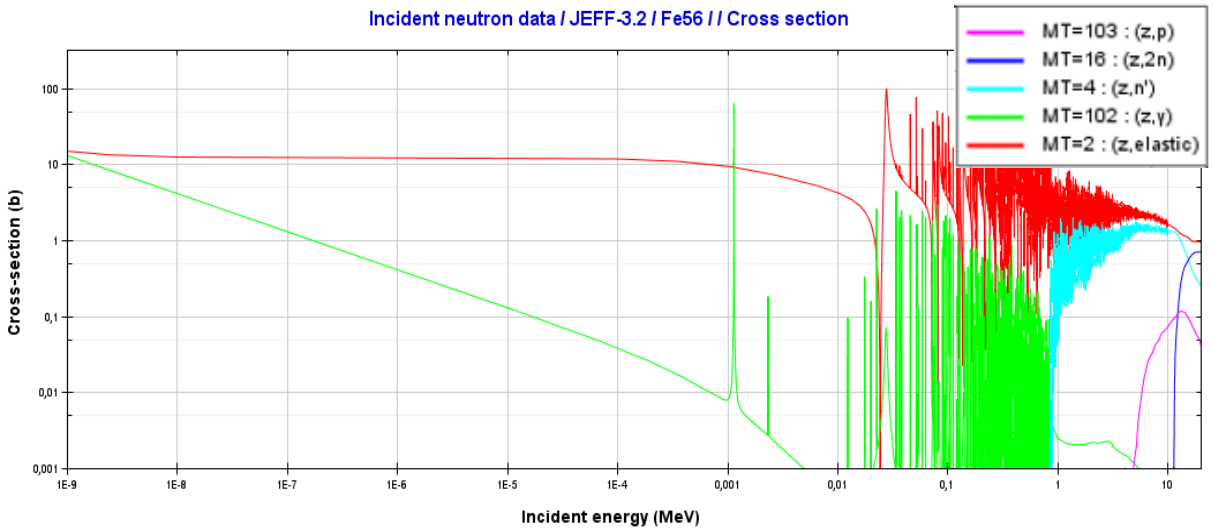

Figure 3.12: Significant cross-sections for ^{56}Fe under neutron irradiation [23]. Reaction MT-numbers according to ENDF format [25].

3.2.6 Water

Water is going to be used as coolant in ITER, and it also plays a role as neutron moderator. Hydrogen is a great neutron moderator with an elastic scattering cross-section that increases towards low energies and reaches more than 100 b at 10^{-3} eV. Its average logarithmic energy loss is $\xi = 1$ and the moderating ratio for 1 MeV neutrons is ~100000. Oxygen has an almost constant elastic scattering cross-section around 4 b, other reactions are only relevant above 3 MeV. Data retrieved from JEFF-3.1.2 General Purpose Library, (February 2014) [23].

[8] Natural iron contains ^{54}Fe(5.8 at.%), ^{56}Fe(91.8 at.%), ^{57}Fe(2.1 at.%) and ^{58}Fe(0.3 at.%).

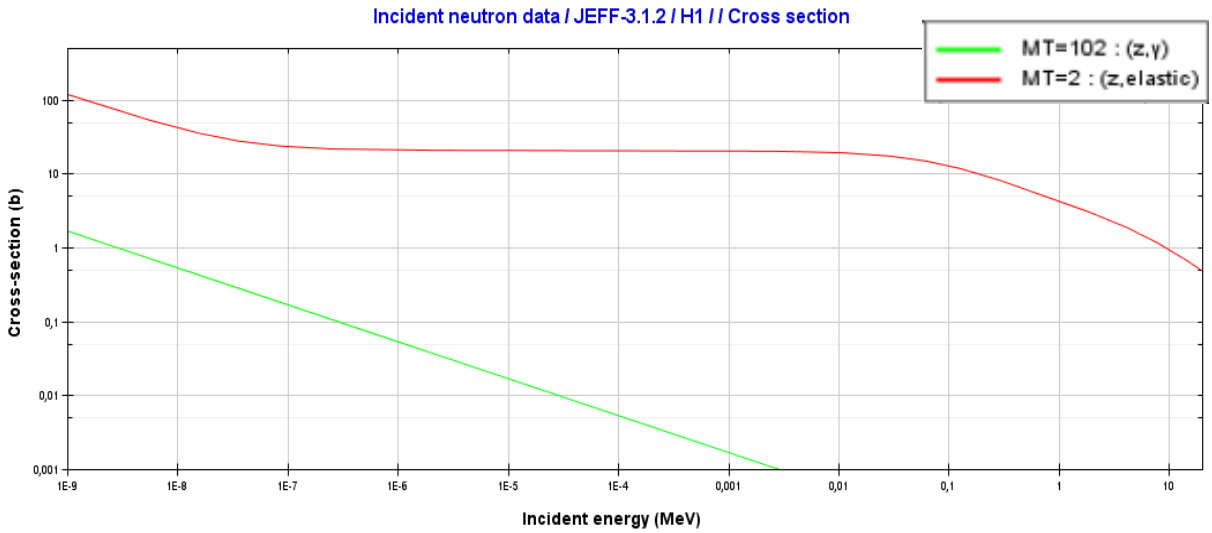

Figure 3.13: Significant cross-sections for hydrogen under neutron irradiation [23]. Reaction MT-numbers according to ENDF format [25].

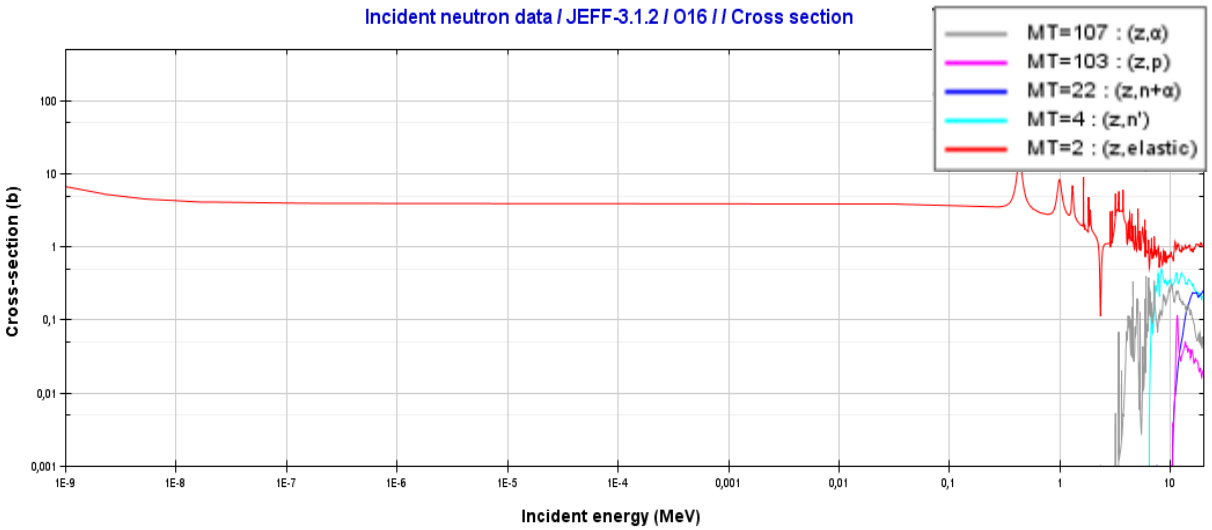

Figure 3.14: Significant cross-sections for oxygen under neutron irradiation [23]. Reaction MT-numbers according to ENDF format [25].

3.2.7 Helium

Helium is transparent to neutrons, presenting only a cross-section for elastic scattering. This cross-section, of 0.8 b, is almost constant for E<0.1 MeV and has a peak of 8 b around 1 MeV. Data retrieved from ENDF/B-VII.1 library, (March 2014) [24].

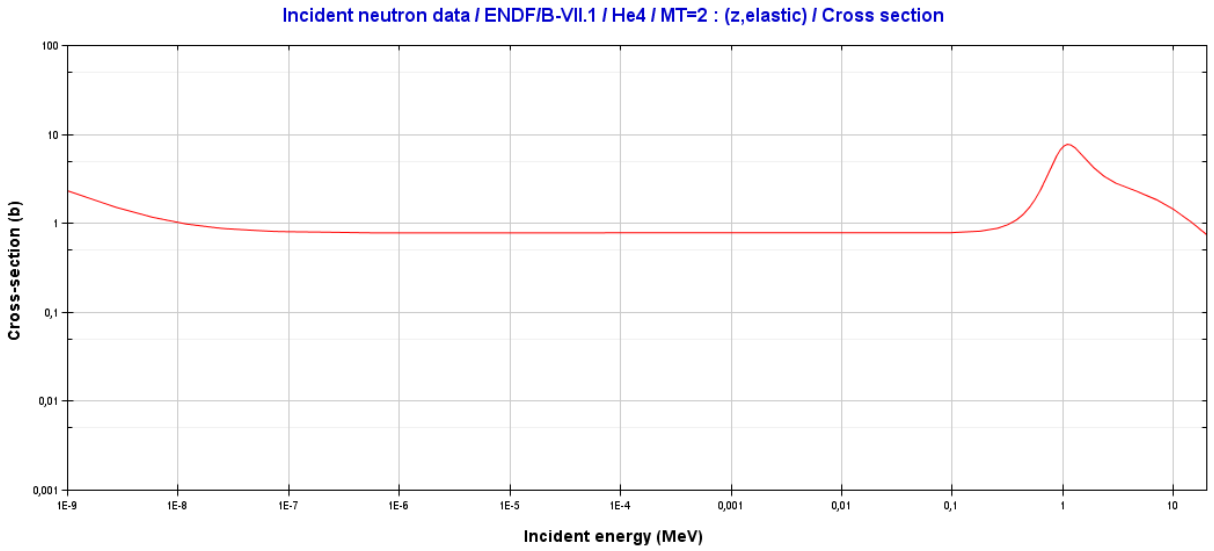

Figure 3.15: Significant cross-sections for helium under neutron irradiation [24]. Reaction MT-number according to ENDF format [25].

3.3 Reaction rates and tritium breeding ratio

This section shows the formulas for the reaction rates and the tritium breeding ratio (TBR) and explains how the results are obtained by the different methods in this study (1-group/4-group diffusion methods and Serpent [1] (Monte-Carlo method).

3.3.1 Reaction rates

The volumetric reaction rate (number of reactions per unit volume and time) for a reaction "r" is defined as:

$$R_r = N \int \sigma_r(E)\Phi(E)dE \tag{3.1}$$

where Φ is the neutron flux, σ_r is the cross-section of the reaction r and N is the atomic density of the target material in the medium considered.

The "total" reaction rate, i.e. the reaction rate in the whole blanket, is defined as the volumetric reaction rate integrated over the volume of the medium in the blanket (V_m).

$$R_r^t = \int_{V_m} R_r(r)d^3r \tag{3.2}$$

The reaction rates in the analytical methods (1-group and 4-group diffusion methods) are calculated by summing the results for each energy group "g":

$$R_r = N \sum_g \Phi_g \sigma_{rg} \tag{3.3}$$

See Appendices B.1 and B.2 for the definition and derivation of the group constants Φ_g and σ_{rg} in the analytical methods.

As a homogenized medium is considered in the analytical methods, the volume of the medium is equal to the volume of the blanket ($V_m^{1g/4g} = V_b$).

$$R_r^t = R_r V_b \tag{3.4}$$

The Serpent code provides the reaction rates in $[b\ cm^{-2}s^{-1}]$ or $[b\ s^{-1}]$ units, corresponding to the following equations:

$$r_r[b\ cm^{-2}s^{-1}] = \frac{1}{A_m}\int_{A_m}\int_{E} \sigma_r(E)\Phi(r,E)d^2rdE \tag{3.5}$$

$$r_r^t[b\ s^{-1}] = \int_{A_m}\int_{E} \sigma_r(E)\Phi(r,E)d^2rdE \tag{3.6}$$

where σ_r is given in barns and A_m is the area (cm^2) of the 2D medium in which the reaction occurs (see the geometry approach in section 4.3.1 and Figure 4.7).

To obtain the volumetric and total reaction rates, the following formulas are used:

$$R_r[cm^{-3}s^{-1}] = r_r N * 10^{-24} \tag{3.7}$$

$$R_r[appm/s]^{9} = r_r * 10^{-18} \tag{3.8}$$

$$R_r^t[s^{-1}] = r_r^t N L_{tor} * 10^{-24} \tag{3.9}$$

where L_{tor} is the toroidal length of the tokamak (equations 4.42 for ITER and 4.43 for DEMO).

3.3.2 Tritium breeding ratio

DEMO and future fusion reactors are expected to breed enough tritium to be self-sufficient, i.e. to produce at least the same amount of tritium as burnt in the plasma. The tritium bred-to-burnt ratio is called tritium breeding ratio (TBR). Specifically TBR is the tritium production rate in the whole blanket divided by the tritium burning rate in the plasma. Thus, considering ideal conditions the reactor would be self-sufficient when TBR=1, but this study assumes a tritium extraction efficiency of 90 %[10], so self-sufficiency is reached at TBR≃1.1.

$$TBR = \frac{R_{Tbred}^t}{R_{Tburnt}^t} \tag{3.10}$$

The tritium burning rate is equal to the total neutron yield in the plasma, because for every tritium nucleus reacting there is one neutron produced[11] (Figure 2.3). In order to reach self-sufficiency ($TBR \geq 1.1$) the tritium breeding rate is:

[9] Appm means atomic parts per million

[10] Estimation for tritium extraction efficiency from Fabrizio Franza, Tritium transport analysis in HCPB DEMO blanket with the FUS-TPC Code. Karlsruhe Institute of Technology, 2013, page 31.

[11] Assuming only D-T reactions. See Appendix A

$$R^{t}_{Tbred} \geq 1.1 * R^{t}_{Tburnt} \quad (3.11)$$

Calculating for ITER and DEMO (see neutron yields in Table 2.2):

$$TBR^{ITER} \geq 1.1 \Rightarrow R^{tITER}_{Tbred} \geq 1.958 * 10^{20}\ s^{-1} \quad (3.12)$$

$$TBR^{DEMO} \geq 1.1 \Rightarrow R^{tDEMO}_{Tbred} \geq 1.408 * 10^{21}\ s^{-1} \quad (3.13)$$

Chapter 4

Analysis methods

Both analytical (multigroup diffusion theory) and Monte-Carlo methods are utilized to calculate the neutron fluxes and neutron induced reactions required in this project. The first method is based on the 1-group diffusion theory and is intended to give initial estimates of neutron fluxes and helium production in shielding blankets, and tritium breeding ratio (TBR) in breeding blankets. The second method, a 4-group diffusion method, is aimed to give better estimates to understand the physics of the problem and the performance of the materials under neutron irradiation. This method allows to obtain qualitative findings about neutron spectra, helium production and tritium breeding. The last method utilizes the Monte-Carlo code Serpent [1] to run more complex models of the previous cases, create alternatives and optimize material compositions of the blankets proposed.

4.1 1-group diffusion method

The first approach of the problem is a simple one-dimensional model of the blanket, applying the 1-group diffusion theory. Some initial estimates are expected to be obtained through the 1-group diffusion method. Particularly, estimates about neutron fluxes and helium production for shielding blankets, and the TBR for breeding blankets.

The problem is approximated to a plane isotropic 14.1 MeV neutron source in the border of a 1D semi-infinite homogeneous medium. The geometry approach is shown in the next Figure 4.1.

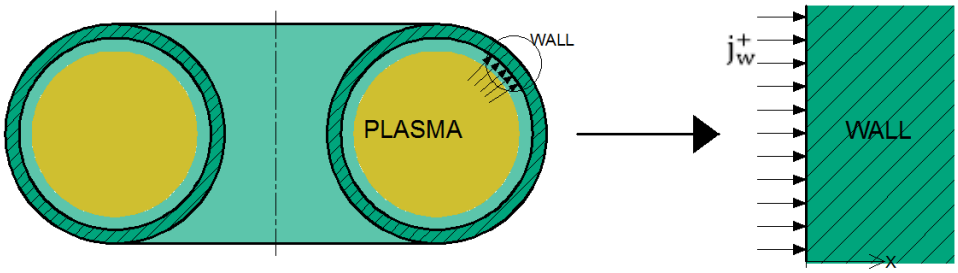

Figure 4.1: Geometry approach for 1-group diffusion models: one-dimensional medium.

The 1-group diffusion theory assumes one neutron speed, a uniform medium, neutron flux varying spatially slowly, small absorption relative to scattering and neutrons scattered isotropically.

Through integrating the general equation (B.1), considering steady state, no fission or other sources inside the wall and a plane isotropic source s_0 at the edge of the semi-infinite medium, the equation obtained is:

$$\Phi(x) = \frac{s_0 L}{D} e^{-x/L} \tag{4.1}$$

where the source, s_0 at x=0, is the neutron partial current at the wall surface of the tokamak, $s_0 = j_w^+$, as Figure 4.1 shows. L is the diffusion length and D is the diffusion coefficient.

See appendix B.1 for a full derivation of the equation (4.1).

The surface neutron current density is defined as the neutron yield in the reactor (P_n/E_n) divided by the total first wall surface (S_t):

$$j_w^+ = \frac{P_n}{E_n S_t} \tag{4.2}$$

Nominal parameters of ITER and DEMO are used in this formula (See section 2.3):

$$j_w^+(\mathrm{ITER}) = 2.4 * 10^{17}\ s^{-1}m^{-2} \tag{4.3}$$

$$j_w^+(\mathrm{DEMO}) = 8.4 * 10^{17}\ s^{-1}m^{-2} \tag{4.4}$$

The diffusion coefficient and diffusion length are defined as follows:

$$D = \frac{1}{3(\Sigma_t - \mu_0 \Sigma_s)} \tag{4.5}$$

$$L = \left(\frac{D}{\Sigma_a}\right)^{\frac{1}{2}} \tag{4.6}$$

where Σ_t, Σ_s and Σ_a are the total, scattering and absorption cross-sections respectively, and μ_0 is the average cosine of scattering angle, approximated as $\mu_0 = 2/3A$ (with A the mass number of the isotope).

For calculation of the diffusion coefficient and length D and L, respectively, the scattering, absorption, and total cross-sections of 14.1 MeV incident neutrons are needed. For this purpose, the JEFF-3.1.2 library [23] was used primarily, but also the ENDF/B-VII.0 [24] and EXFOR [26] were used. The macroscopic cross-sections were calculated using the pure material densities from Table 3.1.

Neutron flux profiles through the first wall (equation 4.1) are calculated using the D and L values obtained.

The neutron flux value chosen to calculate the reaction rates is the average neutron flux over the first 5 cm of the blanket (equation 4.7). This flux can be considered as the neutron flux in the first wall for He production calculations (but note that the real first wall in ITER is 1 cm thick instead of 5 cm).

$$\langle \Phi \rangle = \frac{1}{a} \int_0^a \Phi(x) dx = \frac{s_0 L^2}{aD} (1 - e^{-a/L}) \tag{4.7}$$

4.2 4-group diffusion method

4-group models have been run to study approximated blankets, for ITER and DEMO, made of Be, W, Li, and more realistic mixtures, including iron as neutron sink and water as moderator. The following results have been calculated: He production in Be and W materials and the TBR as a function of the $^{6}\mathrm{Li}$ fraction for the tritium breeding blankets.

The program "Engineering Equation Solver" (EES) [27] was utilized to calculate the averaged cross-sections, through integration over the energy, and to solve the set of equations, through iteration.

4.2.1 4-group diffusion approximation and equations

The problem has been simplified to an infinite, homogenized medium with a uniform 14.1 MeV neutron source. The multigroup diffusion theory is used to calculate neutron spectra, through four energy groups. In turn, the neutron fluxes obtained are used to calculate reaction rates.

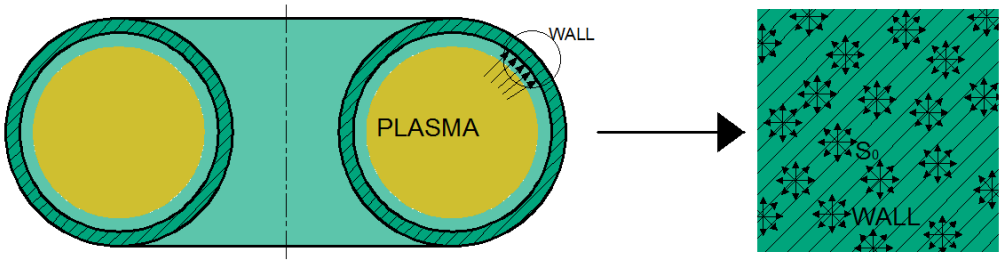

Figure 4.2: Geometry approach for 4-group diffusion models: infinite medium.

A set of four equations is obtained for the 4-group diffusion method. These equations are based on the general form of the equations of the multigroup diffusion theory (formula B.5). After neglecting the leakage term (infinite medium) and the time dependence (steady-state), and assuming only down-scattering, the set of equations remains:

$$\Sigma_{t0}\Phi_0 = S_0 \tag{4.8}$$

$$\Sigma_{t1}\Phi_1 = \Sigma_{s01}\Phi_0 + S_1 \tag{4.9}$$

$$\Sigma_{t2}\Phi_2 = \Sigma_{s02}\Phi_0 + \Sigma_{s12}\Phi_1 + S_2 \tag{4.10}$$

$$\Sigma_{t3}\Phi_3 = \Sigma_{s13}\Phi_1 + \Sigma_{s23}\Phi_2 + S_3 \tag{4.11}$$

See Appendix B.2 for the definition and derivation of the group constants.

The four energy groups, $E = 14.1\ \mathrm{MeV}$, $1\ \mathrm{MeV} \le E < 14.1\ \mathrm{MeV}$, $100\ \mathrm{keV} \le E < 1\ \mathrm{MeV}$ and $E < 100\ \mathrm{keV}$, are chosen according to the characteristics of the problem (see Appendix B.2).

$$g = 0\text{: } E = E_0 \tag{4.12}$$

$$g = 1\text{: } E_1 \le E < E_0 \tag{4.13}$$

$$g = 2: E_2 \leq E < E_1 \tag{4.14}$$

$$g = 3: E < E_2 \tag{4.15}$$

where: $E_0 = 14.1\ \text{MeV}; E_1 = 1\ \text{MeV}; E_2 = 100\ \text{keV}$.

The averaged cross-sections, Σ_{tg} and $\Sigma_{sg'g}$, depend on the neutron flux, $\Phi(E)$. But this dependence is removed by assuming $\Phi(E)$=constant in every energy group to solve the problem analytically. This study considers homogenized materials, so the final cross-sections are the summation of the cross-sections for the different materials (equation B.34).

4.2.2 Averaged cross-sections

The averaged cross-sections are calculated through integrating the cross-sections over the energy as shown in equation (B.21). The averaged scattering cross-sections between groups ($\Sigma_{sg'g}$) for Be, W, Li, Fe and O are calculated through equations (B.24) and (B.25), for hydrogen, through equations (B.29) to (B.33). Detailed information about the neutron induced reactions and cross-sections for the materials used can be found in section 3.2.

The main neutron reactions for ^{9}Be (only stable isotope of Be) are: (n, el) (elastic scattering), $(n, 2n)$, (n, α), (n, T) and (n, γ) (neutron capture). The tritium and gamma reactions are negligible (minute cross-section in a minute energy range), so they are not considered in this method. The (n, 2n) reaction is an important neutron source and He production source (through alpha decay) and the alpha reaction is needed for the He production calculations.

For tungsten, the main neutron reactions are: (n, el), $(n, 2n)$, (n, α), (n, γ) and (n, n'), but inelastic scattering is neglected to simplify the calculations. Natural tungsten is mainly made of ^{182}W, ^{183}W, ^{184}W and ^{186}W (see Table 3.1). The cross-sections for ^{182}W and ^{183}W are very similar (compare Figure 3.5 and 3.6), so the cross-sections of ^{182}W are used for both isotopes, to simplify the calculations.

For lithium, the main neutron reactions are: (n, el), (n, γ), (n, n'), $^{6}Li(n, t)$, $(n, n + t)$ $^{6}Li(n, n + d)$ and $^{7}Li(n, n + t)$. The gamma reaction is negligible (small cross-section in a very small energy range) and Inelastic scattering is neglected to simplify the calculations. The steel was simplified to ^{56}Fe (There is 91,75 %^{56}Fe in natural iron). For the calculations only elastic scattering and neutron capture are interesting. For water, the averaged cross-sections of H and ^{16}O have been calculated. The main neutron reactions for H are elastic scattering and neutron capture. For oxygen are considered elastic scattering and the alpha reaction.

4.2.3 Neutron source

The uniform 14.1 MeV neutron source S_0 for 4-group models is defined as the total neutron yield in the reactor (P_n/E_n) times the blanket-total surface ratio ($S_b/S_t \cong 0.82$), divided by the blanket volume (V_b):

$$S_0 = \frac{0.82\ P_n}{E_n V_b} \tag{4.16}$$

This neutron source reproduces the average neutron flux inside the blanket and is utilized in a medium in which the leakage term is neglected (infinite). Thus, the method assumes that all the neutrons arriving to the blanket are absorbed in the blanket. This assumption is quite reasonable because according to the ITER "Nuclear Analysis report", only 1 % of the neutron flux arriving to the blanket escapes from the blanket (2004).

As the neutron source depends on the neutron yield and blanket volume, there is a difference between ITER and DEMO cases, but also between shielding and tritium breeding blankets.

The neutron yields can be seen in Table 2.2 and the shielding blanket volumes in Table 2.3. For the tritium breeding blanket models a blanket thickness of 1 m is considered for both, ITER and DEMO cases, leading to $V_b \approx 600\ m^3$ and $V_b \approx 1250\ m^3$, respectively.

The neutron sources obtained for each case are:

$$S_0^{shield,ITER} \approx 5.4 * 10^{11}\ cm^{-3}s^{-1} \tag{4.17}$$

$$S_0^{shield,DEMO} \approx 1.5 * 10^{12}\ cm^{-3}s^{-1} \tag{4.18}$$

$$S_0^{breeding,ITER} \approx 2.4 * 10^{11}\ cm^{-3}s^{-1} \tag{4.19}$$

$$S_0^{breeding,DEMO} \approx 8.4 * 10^{11}\ cm^{-3}s^{-1} \tag{4.20}$$

4.2.4 Shielding blanket models

The shielding blanket approximation (Figure 4.3) is based on the blanket design for ITER, inspired by data from "ITER Nuclear Analysis Report" [7]. Two cases are considered: a blanket with Be as first wall material, like in ITER, and a blanket with W as first wall. The model consists of an infinite homogenized medium with the Be-Fe-H2O or W-Fe-H2O material composition shown in Figure 4.3. Note that the stainless steel used in ITER (see section 3.1) has been approximated by iron for the 4-group diffusion method.

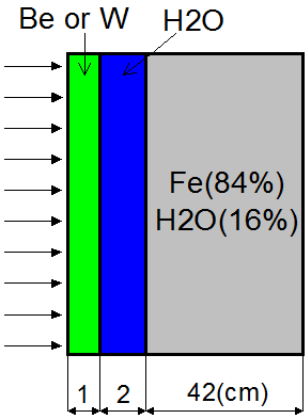

Figure 4.3: Shielding blanket approximation of ITER for the 4-group diffusion models.

- Material composition

The atomic density of each material "m" is the density of the pure material times its volume fraction in the medium.

$$N_m = N_{mp} x_m \tag{4.21}$$

Pure material densities are found in Table 3.1. The volume fractions are calculated from the Figure 4.3 as follows:

$$x_{Be/W} = \frac{a_{fw}}{a_t} \tag{4.22}$$

$$x_{H2O} = \frac{a_{hs}}{a_t} + 0.16 * \frac{a_{bs}}{a_t} \tag{4.23}$$

$$x_{Fe} = 0.84 * \frac{a_{bs}}{a_t} \tag{4.24}$$

where a_m are the thickness of each layer in the blanket: $a_{fw} = 1\ \text{cm}$ (first wall), $a_{hs} = 2\ \text{cm}$ (heat sink), $a_{bs} = 42\ \text{cm}$ (bulk shield) and the total thickness $a_t = 45\ \text{cm}$.

The density for each isotope of mass number A in the material "m" can be calculated by $N_A = N_m x_A$ ($N_9 = N_{Be}$ for natural beryllium, $N_A = N_w x_A$ for natural tungsten and $N_{56} \cong N_{Fe}$). $N_1 = 2 * N_{H2O}$ for hydrogen and $N_{16} = N_{H2O}$ for oxygen in water.

- Set of equations

Macroscopic cross-sections Σ_{rg} are calculated through the formula (B.34), using the densities previously calculated and the averaged microscopic cross-sections of section 4.2.2.

The ^{9}Be (n, 2n) reaction introduces a neutron source in the system that has to be taken into account in the equations. The energy balance[12] of this reaction shows that it is an endothermic reaction, absorbing 1.7 MeV. For incidents 14.1 MeV neutrons (energy group 0), the outgoing energy, 12.4 MeV, is shared between the two neutrons and the isotope ^{8}Be. Thus, the model assumes that all the outgoing neutrons are in the group 1 ($1\ \text{MeV} \leq E < 14.1\ \text{MeV}$). For incident neutrons in the group 1, the outgoing energy is $E = E_n - 1.7\ \text{MeV}$. In this case the model assumes that half of the outgoing neutrons are still in the group 1 and the other half are born in the following group ($100\ \text{keV} \leq E < 1\ \text{MeV}$).

In the model with W, the (n,2n) reaction also appears. In this case the absorbed energies are 8.1 MeV for ^{182}W, 6.2 MeV for ^{183}W, 7.5 MeV for ^{184}W and 7.2 MeV for ^{186}W. The same assumptions as in the previous case have been considered.

The set of equations for both cases (Be or W as first wall) is:

$$\Sigma_{t0}\Phi_0 = S_0 \tag{4.25}$$

$$\Sigma_{t1}\Phi_1 = \Sigma_{s01}\Phi_0 + 2\Sigma_{2n0}\Phi_0 + \Sigma_{2n1}\Phi_1 \tag{4.26}$$

[12]The energy absorbed in a nuclear reaction is defined as: $Q = (\sum m_f - \sum m_i)c^2$, where m_f and m_i are the final and initial masses, respectively, and $c^2 = 931.5\ \text{MeV/amu}$.

$$\Sigma_{t2}\Phi_2 = \Sigma_{s02}\Phi_0 + \Sigma_{s12}\Phi_1 + \Sigma_{2n1}\Phi_1 \quad (4.27)$$

$$\Sigma_{t3}\Phi_3 = \Sigma_{s13}\Phi_1 + \Sigma_{s23}\Phi_2 \quad (4.28)$$

where $\Sigma_{2ng}\Phi_g$ is the neutron source due to the (n, 2n) reaction with an incident neutron of group g.

4.2.5 Tritium breeding blanket models

Two main breeding models have been implemented through the 4-group diffusion method. One of them is an almost pure lithium medium (80 % Li, 20 % Fe). This model is intended to show roughly the performance of this element. The other model is inspired by the Japanese TBM design for ITER, the WCCB (water-cooled ceramic breeder). The approximation made for this model (Figure 4.4) uses lithium instead of lithium ceramic (Li_4SiO_4) and iron instead of steel. The WCCB model without Be has been also implemented to assess the importance of Be as neutron multiplier.

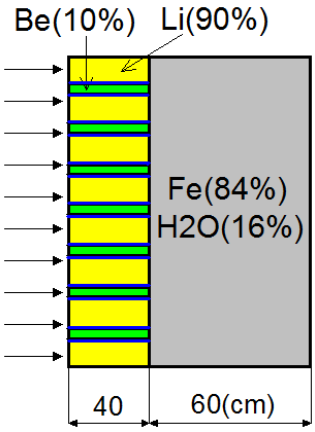

Figure 4.4: WCCB blanket approximation.

- Material composition

The model with an almost pure lithium medium requires a fraction of some neutron absorber material, due to the negligible absorption cross-section of ^{7}Li for low energies, and also due to the missing leakage term in the model. In other words, a neutron sink in the energy group 3 is needed to obtain a realistic neutron spectrum. 20 % of ^{56}Fe has been introduced in the model for this purpose. Therefore, with volume fractions $x_{Li} = 0.8$ and $x_{56} = 0.2$. The model is run for different degrees of ^{6}Li enrichment.

The WCCB model has a 40 cm layer for tritium breeding and 60 cm of bulk shield (see Figure 4.4). 10 % of Be is introduced in the lithium breeding layer as a neutron multiplier. The bulk shield is made of 84 % of Fe and 16 % of water. Using these data the volume fractions and material densities are calculated as in previous cases.

The case without Be has $x_{Li} = 0.4$, the rest of volume fractions and densities are equal to the previous case.

- Set of equations

Reactions (n, n+D) and (n,n+T) act as neutron sources in the system. Reaction (n, n+D) absorbs 1.5 MeV and the (n,n+T) reaction absorbs 2.5 MeV. The outgoing energy, $\mathrm{E} = \mathrm{E_n} - 1.5\ \mathrm{MeV}$ or $\mathrm{E} = \mathrm{E_n} - 2.5\ \mathrm{MeV}$, is shared between the neutron, the He nucleus and the deuterium or tritium nucleus respectively. Because the outgoing neutron takes a great part of this energy, the model assumes that all the outgoing neutrons are born in the first energy group, for both, reactions in the group 0 and in the group 1.

The set of equations for an almost pure lithium medium is:

$$\Sigma_{t0}\Phi_0 = S_0 \tag{4.29}$$

$$\Sigma_{t1}\Phi_1 = \Sigma_{s01}\Phi_0 + \Sigma^6_{D0}\Phi_0 + \Sigma^7_{T0}\Phi_0 + \Sigma^6_{D1}\Phi_1 + \Sigma^7_{T1}\Phi_1 \tag{4.30}$$

$$\Sigma_{t2}\Phi_2 = \Sigma_{s12}\Phi_1 \tag{4.31}$$

$$\Sigma_{t3}\Phi_3 = \Sigma_{s23}\Phi_2 \tag{4.32}$$

where $\Sigma^6_{Dg}\Phi_g$ and $\Sigma^7_{Tg}\Phi_g$ are the neutron sources due to the (n, n+D) and (n, n+T) reactions, respectively, with an incident neutron of group g.

The simplified WCCB blanket model has the following equations:

$$\Sigma_{t0}\Phi_0 = S_0 \tag{4.33}$$

$$\begin{aligned}\Sigma_{t1}\Phi_1 = {} & \Sigma_{s01}\Phi_0 + \Sigma^6_{D0}\Phi_0 + \Sigma^7_{T0}\Phi_0 + \Sigma^6_{D1}\Phi_1 \\ & + \Sigma^7_{T1}\Phi_1 + 2\Sigma_{2n0}\Phi_0 + \Sigma_{2n1}\Phi_1\end{aligned} \tag{4.34}$$

$$\Sigma_{t2}\Phi_2 = \Sigma_{s02}\Phi_0 + \Sigma_{s12}\Phi_1 + \Sigma_{2n1}\Phi_1 \tag{4.35}$$

$$\Sigma_{t3}\Phi_3 = \Sigma_{s13}\Phi_1 + \Sigma_{s23}\Phi_2 \tag{4.36}$$

Finally, the set of equations for the WCCB model without Be is:

$$\Sigma_{t0}\Phi_0 = S_0 \tag{4.37}$$

$$\Sigma_{t1}\Phi_1 = \Sigma_{s01}\Phi_0 + \Sigma^6_{D0}\Phi_0 + \Sigma^7_{T0}\Phi_0 + \Sigma^6_{D1}\Phi_1 + \Sigma^7_{T1}\Phi_1 \tag{4.38}$$

$$\Sigma_{t2}\Phi_2 = \Sigma_{s02}\Phi_0 + \Sigma_{s12}\Phi_1 \tag{4.39}$$

$$\Sigma_{t3}\Phi_3 = \Sigma_{s13}\Phi_1 + \Sigma_{s23}\Phi_2 \tag{4.40}$$

4.3 Monte-Carlo (Serpent) method

The different cases and new ones have been implemented using the Monte-Carlo code Serpent [1]. These simulations allow to achieve more accurate results, create more alternatives and optimize the material composition of the blankets proposed.

Serpent is a continuous-energy Monte-Carlo code, developed by the VTT Technical

Research Centre of Finland and primarily intended for burnup calculations. However, the code is quite versatile and has an external source mode that allows its use for this purpose.

The Monte-Carlo method basically attempts to model a macroscopic system through simulation of its microscopic interactions. A solution is determined by random sampling of the relationships, or the microscopic interactions, until the result converges. Serpent uses (like any MNCP code) a universe-based combinational solid geometry model, which consists of material cells defined by surface types. Neutron transport is based on a combination of typical surface-to-surface ray-tracing and the Woodcock delta-tracking method. Serpent reads continuous-energy cross sections from ACE format data libraries. The interaction physics is based on classical collision kinematics, ENDF reaction laws and probability table sampling in the unresolved resonance region.

4.3.1 Spatial model geometry for a tokamak chamber

The geometry is approximated as an annular model with rotational symmetry (1D), representing the poloidal cross section of a tokamak. This geometry is quite simple but gives quite accurate neutron fluxes compared to complex 3D models of ITER[13].

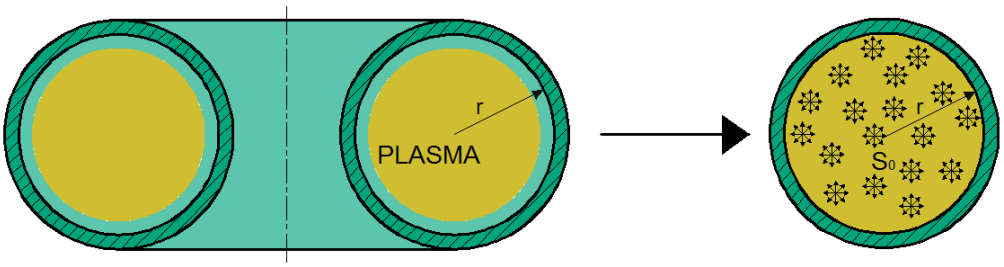

Figure 4.5: Spatial model geometry for a tokamak chamber for Serpent simulations: annular shape.

The approximation was done by keeping the blanket surface and the major radius of ITER and DEMO designs (see Tables 2.1 and 2.2). Thus, the minor radius in the models is $\mathrm{r} = 2.45\ \mathrm{m}$ for ITER and $\mathrm{r} = 3.68\ \mathrm{m}$ for DEMO, instead of 2 m and 3 m respectively in the actual case.

This geometry allows to obtain rather realistic reaction rates integrated over the whole blanket, by multiplying the results of the model by the toroidal length $\mathrm{L_{tor}}$ of the reactor. This is interesting for calculating the TBR (tritium breeding ratio).

$$\mathrm{L_{tor}} = 2\pi\mathrm{R} \tag{4.41}$$

where R is the major radius,

$$\mathrm{L_{tor}^{ITER}} = 38.96\ \mathrm{m} \tag{4.42}$$

$$\mathrm{L_{tor}^{DEMO}} = 54.04\ \mathrm{m} \tag{4.43}$$

[13] 3D MCNP model of ITER from ITER Nuclear Analysis Report, Nuclear Analysis Group, ITER Naka&Garching Joint Work Sites (July 2004) [7].

4.3.2 Neutron source

The neutron source for these models is the total neutron yield in the reactor (P_n/E_n) times the blanket-total surface ratio ($S_b/S_t \cong 0.82$), divided by the toroidal length (L_{tor}). This source is uniformly distributed over the inner ring as Figure 4.5 shows.

$$S_0 = \frac{0.82\ P_n}{E_n L_{tor}} \tag{4.44}$$

Nominal values for ITER and DEMO are replaced in this formula (Table 2.2), obtaining the following neutron sources:

$$S_0^{ITER} \approx 3.74 * 10^{16}\ cm^{-1}s^{-1} \tag{4.45}$$

$$S_0^{DEMO} \approx 1.94 * 10^{17}\ cm^{-1}s^{-1} \tag{4.46}$$

4.3.3 Shielding blanket models

The approximation of ITER blanket (Figure 4.6) is more accurate than in previous methods (1-group and 4-group) due to two improvements. The material composition Ni:12 wt.%, Cr:18 wt.%, Fe:70 wt.% is used to model the austenitic steel SS 316L(N)-IG utilized in ITER (see section 3.1). Also, the design of the heat sink has been improved by introducing a fraction of steel. The previous simplification (2 cm of pure water) produced an over-moderated spectrum in the first wall comparing to the 3D MCNP model of ITER from reference [7].

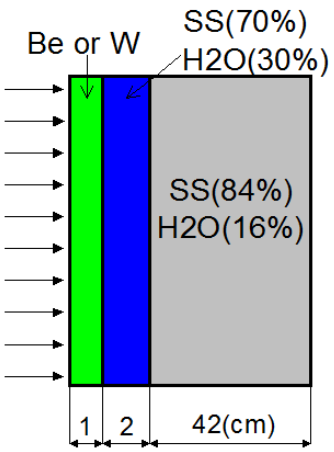

Figure 4.6: Shielding blanket approximation of ITER for Serpent models.

In Serpent models each blanket layer is a homogenized medium. Atomic densities in these media are calculated in the same way as shown in section 4.2.4.

The Figure 4.7 shows the geometry plots made by Serpent for the ITER and DEMO models. The relative size between the reactors is shown in these plots. In the DEMO case a thicker blanket has been chosen, 55 cm instead of 45 cm, to shield properly against neutron power 7 times higher than ITER. A 10 cm layer of void and a 10 cm layer of steel have been added to the models behind the blanket, modeling the vacuum vessel case, to reproduce adequately neutron attenuation. (Note that first wall and heat sink layers are very thin in the plots).

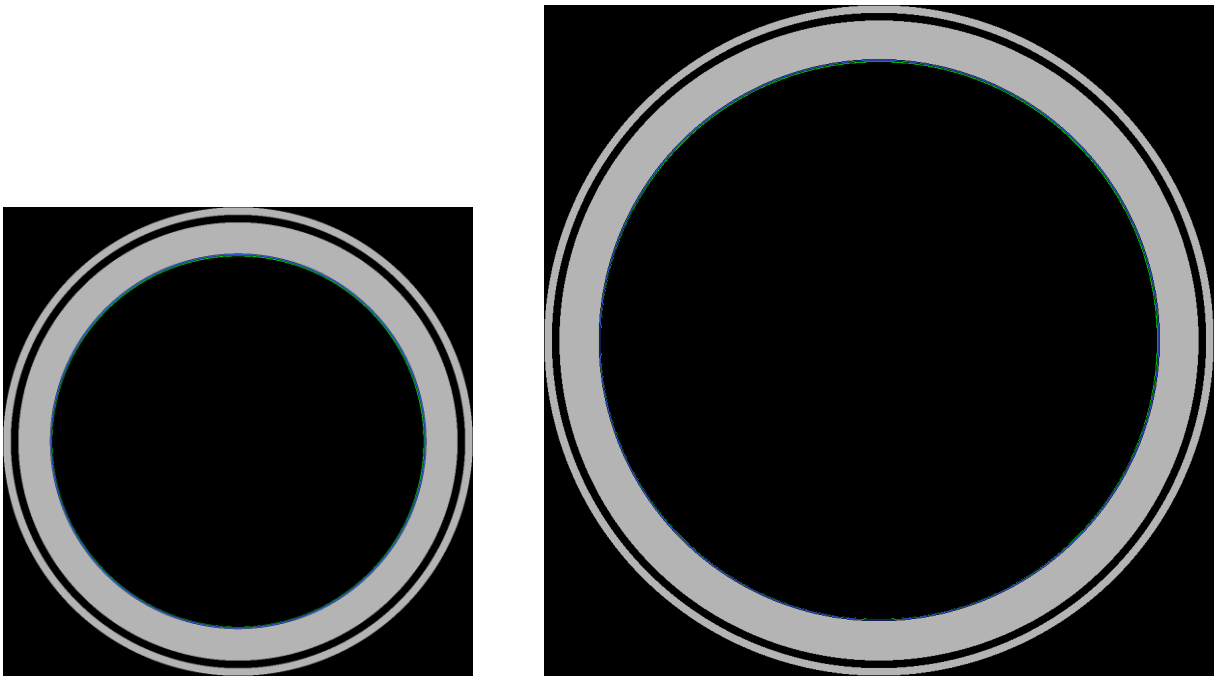

Figure 4.7: Serpent geometry plots of the shielding blanket models of ITER (left) and DEMO (right).

4.3.4 Tritium breeding blanket models

4.3.4.1 Simplified water-cooled ceramic breeder (WCCB)

The same tritium breeding model made with the 4-group method was run with Serpent (see Figure 4.4). This model was inspired by the Japanese WCCB design. The model has been run in an infinite homogeneous medium to compare to the 4-group diffusion model, and afterwards taking into account the geometry (breeding layer and bulk shield layer) as Figure 4.8 shows.

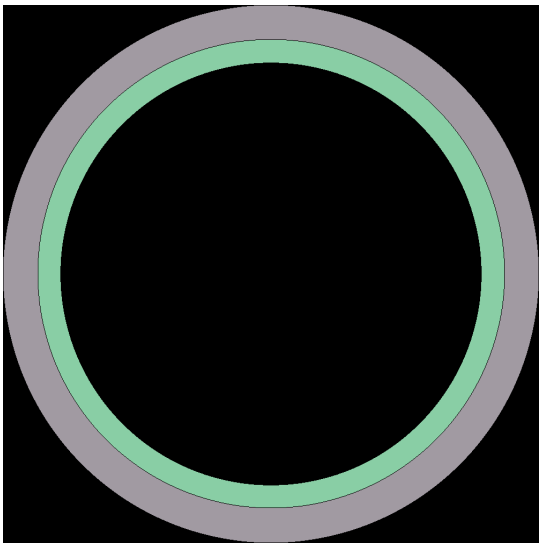

Figure 4.8: Serpent WCCB geometry plot.

4.3.4.2 HCPB and HCLL models.

Two breeding blankets have been modeled based on the European TBM designs for ITER, the HCPB (helium-cooled pebble bed) and the HCLL (helium-cooled lithium lead) (see section 2.4). A schematic of these models is shown in Figure 4.9.

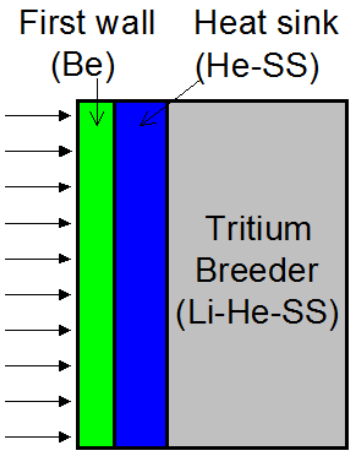

Figure 4.9: Schematic of HCPB and HCLL blanket models.

Two types of design limit have been proposed to ensure the blanket requirements in a DEMO-type reactor (protect the components of the reactor against neutrons and to reach tritium self-sufficiency).

- Design limits for the neutron flux: Two design limits for the neutron flux have been chosen, a maximum total neutron flux behind the blanket and a maximum high-energy neutron flux behind the blanket. For a DEMO-type reactor these limits are:

$$\Phi_{\max}^{\text{tot}} = 1.4 * 10^{13}\ \text{cm}^{-2}\text{s}^{-1} \tag{4.47}$$

$$\Phi_{\max}^{\text{high}} = 4.6 * 10^{12}\ \text{cm}^{-2}\text{s}^{-1} \tag{4.48}$$

  The calculation of these values can be found in Appendix D.

- Design limit for TBR: Assuming a tritium extraction efficiency of 90 %[14], the minimum TBR required for reaching self-sufficiency is (see section 3.3.2):

$$\text{TBR}_{\min} \backsimeq 1.1 \tag{4.49}$$

After consulting different models and approaches (see Bibliography [13, 20, 21, 28, 29]), at first, models with a certain material composition[15] have been run. From these first simulations the following results have been obtained: TBR is slightly lower than 1 for both models (enrichment 50 %Li6); the total neutron flux and high energy neutron flux after the

[14] Estimation for tritium extraction efficiency from [20] Fabrizio Franza, Tritium transport analysis in HCPB DEMO blanket with the FUS-TPC Code. Karlsruhe Institute of Technology, 2013, page 31.
[15] Starting material composition for the HCLL model from [10] Fusion Technology, Annual Report of the Association EURATOM-CEA 2005, page 167.

blanket are slightly higher than design limits in the HCLL model, and acceptable neutron flux values for the HCPB model.

Starting from these models, different combinations of composition have been run to increase the TBR at least until 1.1 in both models, and to reduce the neutron flux for the HCLL model until the design limits. Changes in the composition have been made while keeping reasonable[16] values for the amount of steel, ensuring a minimum amount for the structure, plates and pipes, and a minimum value of helium to ensure enough cooling (at a certain pressure, temperatures and flow rate).

The following findings were obtained during the optimization:

- Increasing the He fraction through decreasing stainless steel (SS) fraction leads to increasing neutron fluxes (He is a moderator and SS is an absorber). On the one hand, this is good because the TBR is increased. On the other hand, there is an increase in the neutron fluxes behind the blanket, especially harmful in HCLL model.

- This change in the neutron flux behind the blanket is bigger if He-SS fraction is altered in the breeding layer, than for the same fraction variation in the heat sink (see Figure 4.9). The change in the TBR instead is approximately the same. Therefore, to increase the TBR and, at the same time, decreasing the neutron fluxes behind the blanket, in the HCLL model, the next procedure was followed: the TBR has been maximized through increasing the He fraction in the heat sink, and the neutron flux behind the blanket has been minimized through increasing the SS fraction in the breeding layer.

- In the HCPB model, the optimized $Li_4SiO_4 - Be$ composition (i.e. for the maximum TBR) is 18 $\%Li_4SiO_4 - 82\ \%Be$, (see chapter 6 for discussion). This is the $Li_4SiO_4 - Be$ composition in the final model, Figure 4.10.

The final material compositions achieve the design limits at least for one ^6Li fraction, in both models. Layer thickness and material compositions are shown in Figure 4.10 (HCPB) and Figure 4.11 (HCLL). The geometry plots by Serpent (Figure 4.12) show the layers of Figure 4.10 and 4.11 and an external steel ring representing the vacuum vessel case.

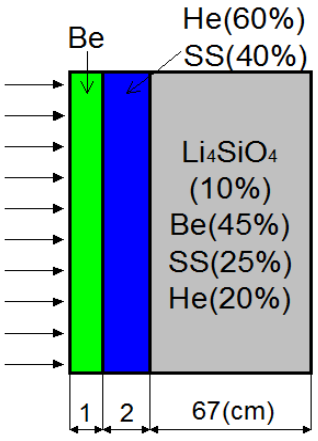

Figure 4.10: HCPB model. Optimized material composition.

[16] Minimum material fractions considered: 50 % of coolant in heat sink; 10 % of coolant in bulk shield; 20 % of steel in bulk shield.

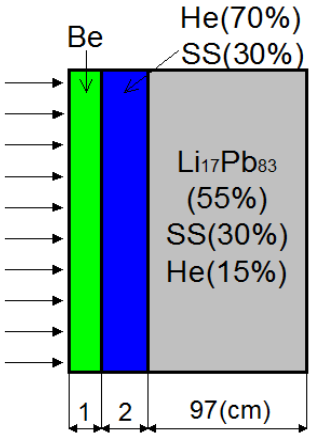

Figure 4.11: HCLL model. Optimized material composition.

Figure 4.12: Serpent geometry plots of the HCPB (left) and the HCLL (right) blanket models of DEMO. Note the different blanket thickness but the same inner radius.

4.3.4.3 Alternatives for HCPB and HCLL models.

A possible option for the HCPB and HCLL models for a DEMO-type reactor is to cover the first wall with W instead of Be. Tungsten as a first wall material has some advantages (thermo-mechanical properties, low He production, low T retention etc.) but also some drawbacks (high-Z impurities in the plasma, sputtering yield for high energies etc.) (see section 3.1).

These new proposals have the same material composition as the previous section, except the first wall material, as the following figures show.

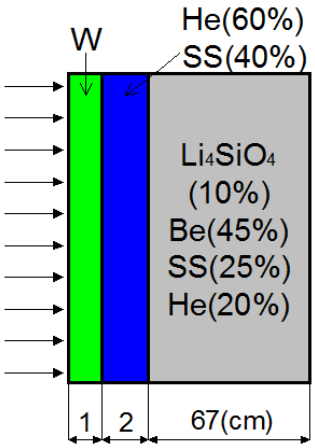

Figure 4.13: Alternative-HCPB model. Optimized material composition.

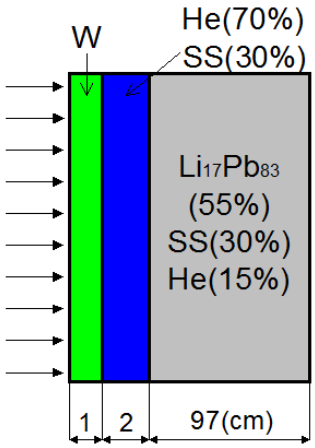

Figure 4.14: Alternative-HCLL model. Optimized material composition.

Chapter 5

Results

The results have been divided into results for shielding blanket models and results for tritium breeding blanket models. Shielding blanket models focus on the ITER-type reactor, because ITER is going to have this type of blanket and the results can be compared with other studies. Tritium breeding calculations focus on the DEMO-type reactor, because the fusion power plants are intended to have a complete breeding blanket. Neutron flux results from shielding models have been used to calculate the design limits for the tritium breeding models.

For the Be-W comparison in shielding models, we have calculated the neutron spectrum at different points of the blanket and the helium production in the first wall. For the assessment of tritium breeding blankets we have assessed the TBR (based on the tritium production rate), the neutron fluxes through the blanket and behind it and finally the lithium depletion with time.

5.1 Shielding blanket models

Neutron fluxes and helium production rates have been calculated through the 1-group diffusion theory, 4-group diffusion theory and Monte-Carlo simulations with Serpent code. 1-group diffusion model gives values for 14.1 MeV neutrons in a 1D, first-wall made of Be or W, the 4-group diffusion model shows results for a dimensionless homogeneous medium (see section 4.2.1) and the model with Serpent has an annular shape of rotational symmetry (1D), representing the poloidal cross section of the tokamak (see section 4.3.1). (The material composition of the 4-group model is shown in Figure 4.3 and the composition and geometry of the Serpent model are shown Figures 4.6 and 4.7).

5.1.1 Neutron fluxes

Serpent predictions of neutron fluxes at the first wall show that the use of Be as first wall material produces 14 % higher total neutron flux and a softer neutron spectrum than the use of W (Table 5.1 and Figure 5.1). Be as first wall material moderates effectively the 14.1 MeV neutrons producing a spectrum with almost the same low-energy neutron flux ($E < 0.1$ MeV) as the high energy neutron flux ($E > 0.1$ MeV). In the case of W there is a slightly bigger high-energy neutron flux than in Be and about the half low-energy neutron flux, due to the high

absorption cross-section of W. The total neutron flux is slightly higher in the Be case due to a more efficient neutron multiplying performance.

$\Phi_{fw}[cm^{-2}s^{-1}]$ ITER	1 group Be	4 group Be	Serpent Be	1 group W	4 group W	Serpent W
$E = 14.1MeV$	$4 * 10^{13}$	$5.6 * 10^{12}$	$3.7 * 10^{13}$	$3 * 10^{13}$	$5.4 * 10^{12}$	$3.8 * 10^{13}$
$E > 0.1MeV$	–	$1.3 * 10^{14}$	$1.3 * 10^{14}$	–	$1.4 * 10^{14}$	$1.5 * 10^{14}$
$E < 0.1MeV$	–	$6.8 * 10^{14}$	$1.1 * 10^{14}$	–	$4.3 * 10^{14}$	$6.3 * 10^{13}$
Total	$4 * 10^{13}$	$8.1 * 10^{14}$	$2.4 * 10^{14}$	$3 * 10^{13}$	$5.6 * 10^{14}$	$2.1 * 10^{14}$

Table 5.1: Neutron fluxes in the ITER first wall comparing Be and W materials. Results from 1-group diffusion, 4-group diffusion[17] and Serpent models.

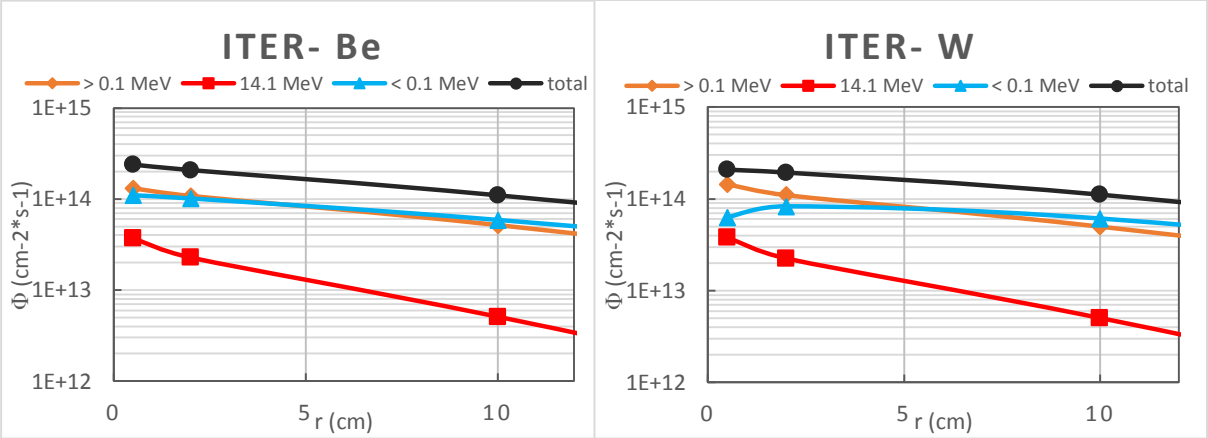

Figure 5.1: Serpent predictions of neutron fluxes for the shielding blanket model of ITER for the first 12 cm of blanket. Model with Be as first wall material (left) and model with W (right).

The 4-group diffusion model provides results in the same order of magnitude as the Serpent model, allowing to make acceptable qualitative predictions. Compared to the Serpent model, on the one hand, the 4-group model significantly underestimates the 14.1 MeV neutron flux (a factor of 7). On the other hand, this analytical model overestimates low-energy neutron fluxes by 6-7 times. The total neutron flux is overestimated in the 4-group model by a factor about 3. The 1-group diffusion model gives a good estimate for the 14.1 MeV neutron flux compared to the Serpent result, but ignores the rest of energies (important even in the first wall), giving a total neutron flux underestimated by 6 times for a Be first wall and a factor of 7 for W.

Results for DEMO are about 3.5 times higher in the 1-group and Serpent models and a factor close to 3 for the 4-group diffusion model.

Following the first few centimeters of blanket, in which the differences between the Be-model and W-model are significant, the rest of the blanket presents similar neutron fluxes for both models, with slight differences (Figures 5.2 and 5.3). The first points on the left of the

[17] The 4-group diffusion model has no spatial dependence, so the neutron fluxes obtained are also used to calculate the He production in the first wall.

following graphs, at $r = 0.5$ cm, corresponds to the neutron fluxes at the first wall. The second points, at $r = 2$ cm, are the fluxes at the heat sink layer. The three following measurements are inside the bulk shield and the points at $r = 50$ cm shows neutron fluxes just after the blanket.

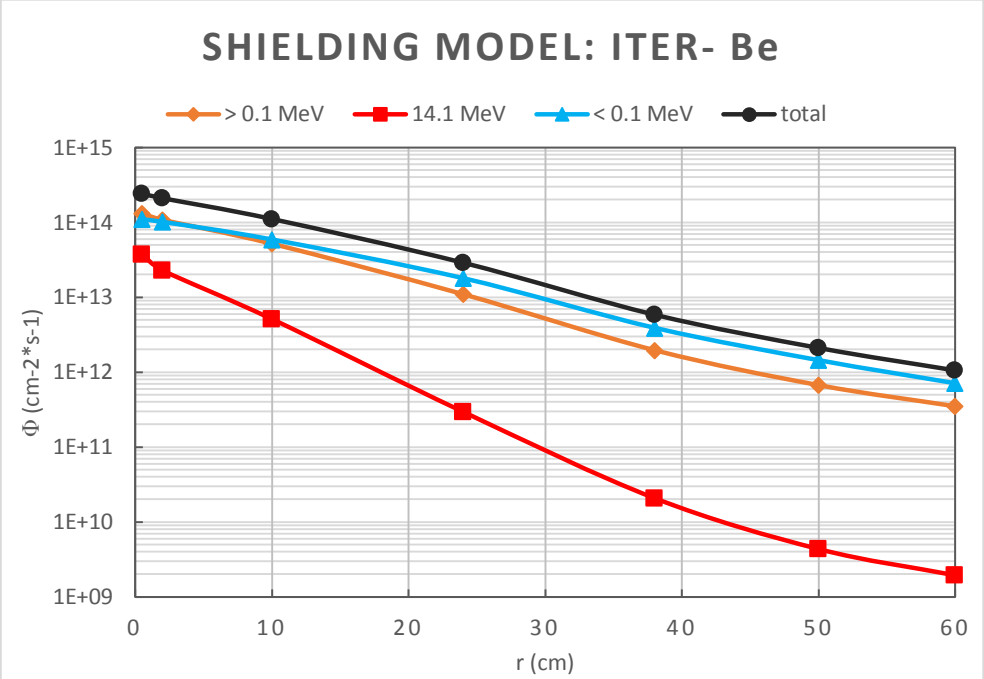

Figure 5.2: Serpent predictions of neutron fluxes for the shielding blanket model of ITER with Be as first wall material, as a function of its radial length.

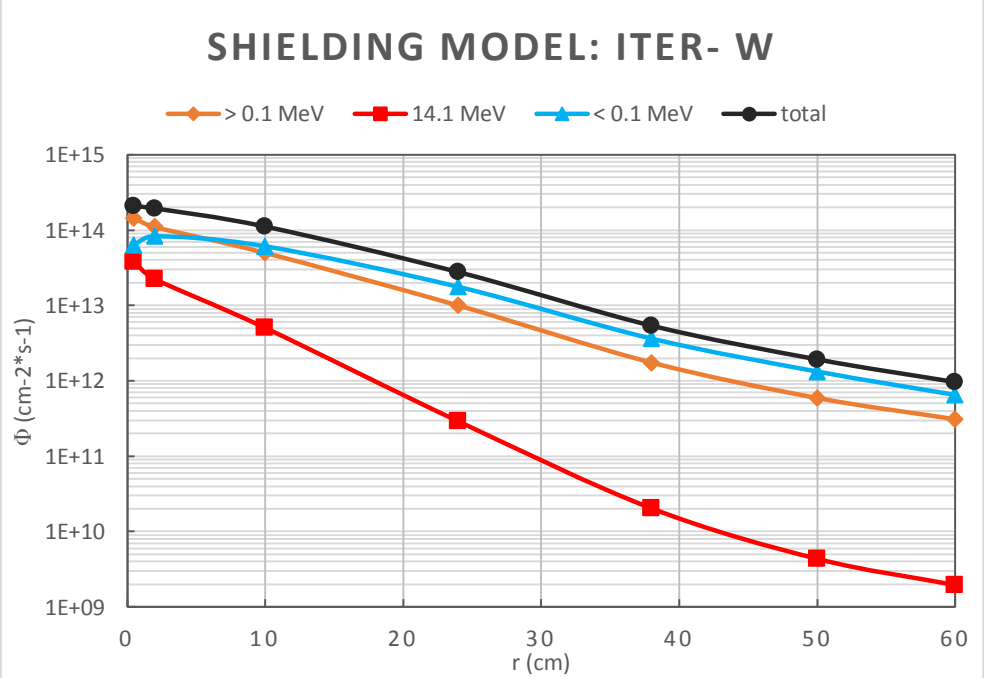

Figure 5.3: Serpent predictions of neutron fluxes for the shielding blanket model of ITER with W as first wall, as a function of its radial length.

The shielding capability of the blanket is measured by the attenuation factor, i.e. the ratio between the neutron flux at the first wall and the neutron flux behind the blanket (Table 5.2). The attenuation factor of the total neutron flux is similar in the Be and W models but the blanket with W provides better shielding against high-energy neutrons, leading to less radiation damage. The 14.1 MeV neutron flux is reduced by a factor of 8000-9000 in both models, the high-energy neutron flux is attenuated 200 times for the Be-model and 250 times for the W-model and the total neutron flux presents an attenuation factor of 100 for both models. These attenuation factors are also used to calculate the design limits for the HCPB and HCLL blanket models (see Appendix D).

Φ_{fw}/Φ_{bb} ITER	Serpent Be	Serpent W
$E = 14.1MeV$	8409	8837
$E > 0.1MeV$	197	254
$E < 0.1MeV$	79	48
Total	114	111

Table 5.2: Serpent predictions of neutron attenuation factors in ITER for Be and W first wall materials.

5.1.2 Helium production

The helium production is an issue of relevance for Be as PFM but not for W. The He production for a W first wall is almost negligible, having a He production rate 1000 times lower than a Be first wall (Table 5.3).

According to [30], the critical bulk concentration for He in Be with a grain radius of 5 μm is 23.3 appm and 71.4 appm for W. If the grain radius is 10 times smaller, 0.5 μm, the critical concentration is 10 times higher, 233 appm and 714.3 appm respectively. In ITER, with grain radius of 5 μm the critical He concentration in Be is reached at 8 months of the DT operation plan (according to Serpent results in Table 5.3). If the radius is 0.5 μm the critical concentration is reached at 7 years. For DEMO, working in steady state unlike ITER, (Serpent results: $R_{He} = 2.21 * 10^{-4}$ appm/s in Be and $R_{He} = 1.15 * 10^{-7}$appm/s in W) the critical He concentration in a Be first wall is reached after only 1 full operating day with thick grain radius (5 μm), and 12 days if the thin grain radius (0.5 μm) is used. For a W first wall, the critical concentration is reached in 20 full operating years with thick grain radius and 200 years with the thin one.

ITER; R_{He}[appm/s]	1 − group	4 − group	Serpent
Be	$4.3 * 10^{-5}$	$1.0 * 10^{-4}$	$3.47 * 10^{-5}$
W	$3.6 * 10^{-8}$	$1.9 * 10^{-8}$	$3.33 * 10^{-8}$

Table 5.3: Helium production rate in the first wall of ITER, made of Be or W. Results for 1-group diffusion, 4-group diffusion and Serpent models. Units appm/s[18].

[18] appm/s units (atomic parts per million/s) are used to compare the results from the different methods because these units do not depend on the density of the medium (different in each method).

Coincidentally, the 1-group diffusion method gives slightly more accurate results than the 4-group diffusion method, compared to the Serpent results. The He production rate in the 1-group model is slightly overestimated (compared to the Serpent result) and in the 4-group model is almost 3 times overestimated for Be first wall and less than 2 times underestimated for W first wall. The high accuracy in the results of the 1-group diffusion method can be explained by the shape of the cross-sections of Be and W (see Figures 3.3 to 3.7). The cross-sections for He production ((n,2n) and (n,α) reactions for Be and (n,α) for W) for high energies are more or less constant and negligible for the rest of energies. This means that the cross-section in 14.1 MeV (only energy of the model) coincides with the average cross-section (in the range where is not negligible) and because of that the results obtained are very accurate.

5.2 Tritium breeding blanket models

Many tests and cases have been run with 1-group diffusion, 4-group diffusion and Serpent methods before arriving to complete breeding blanket models, based on the HCPB (helium-cooled pebble bed) and HCLL (helium-cooled lithium lead) concepts (see section 2.4).

Results are shown for the DEMO case but the TBR for ITER is nearly the same due to the parallelism between the models.

5.2.1 Test models

The 1-group diffusion method is not suitable for tritium breeding calculations. This is mainly due to the shape of the tritium breeding cross-section of $^{6}\mathrm{Li}$ (see Figure 3.9). As it increases quickly towards low neutron energies, the tritium production rate calculated in the only energy of the model, 14.1 MeV, is much lower than in the real case. Thus, the maximum TBR obtained, $\mathrm{TBR}_{\max} = 0.61$, is for pure $^{7}\mathrm{Li}$ and with an infinite blanket.

The first model run with the 4-group diffusion method consists in an almost pure Li medium (80 % Li, 20 % Fe). With this model it is intended to roughly assess the performance of this element. A breeding blanket with the material composition of this model, would have (in DEMO case) a TBR=5.8 for almost pure $^{7}\mathrm{Li}$, ($\mathrm{x}_{\mathrm{Li6}} = 0.01$), and a $\mathrm{TBR} \geq 1.1$ for $\mathrm{x}_{\mathrm{Li6}} \leq 0.86$ (see Figure 5.4), according to the results of the 4-group diffusion model. Obviously this enormous TBR value is far from reality, but the results give the qualitative performance of Li and confirm that there is room to achieve $\mathrm{TBR} \geq 1.1$ (self-sufficient reactor with a tritium extraction efficiency of 90 %).

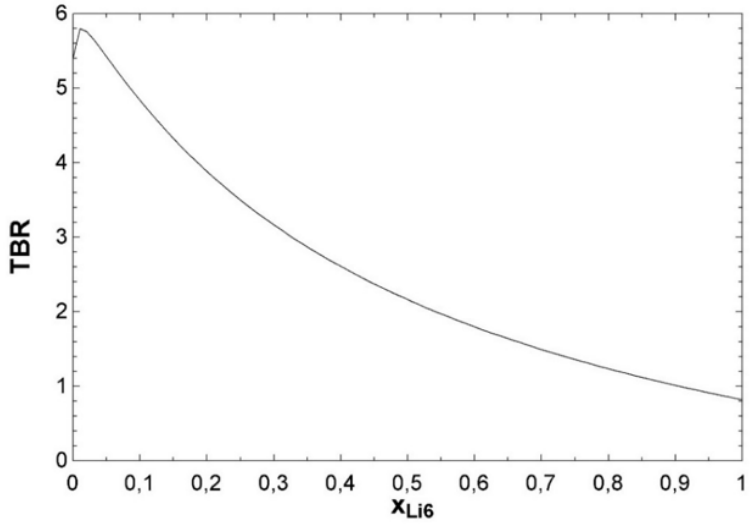

Figure 5.4: Tritium breeding ratio as a function of ^{6}Li volume fraction in Li. 4-group diffusion model for DEMO with a composition 80 % Li, 20 % Fe.

The following tritium breeding blanket model was inspired by the Japanese WCCB (water-cooled ceramic breeder) concept. This design has been run in an infinite homogeneous medium with the 4-group diffusion method (blue lines Figure 5.5) and also with the Serpent code (green lines). In addition, it has been modeled with Serpent in an annular way (orange and yellow lines Figure 5.5) taking into account the geometry (breeding layer and bulk shield). For each method two cases have been run: one with some Be (composition 90 % Li, 10 % Be) and the other one without Be, to assess the influence of this element in the neutron spectrum and TBR since it is a neutron multiplier. (See the WCCB approximation in Figure 4.4).

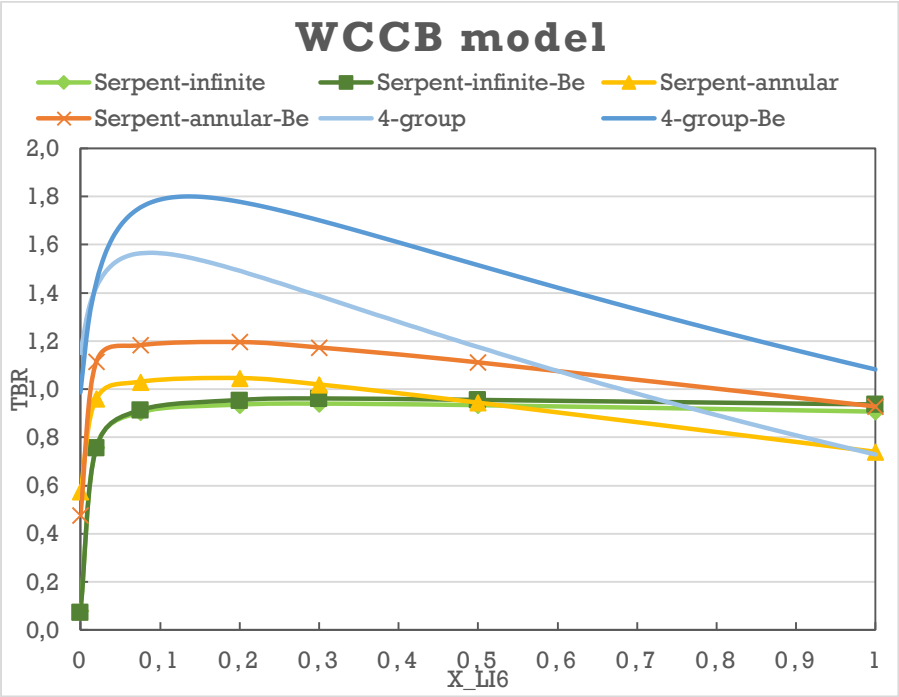

Figure 5.5: TBR as a function of ^{6}Li fraction for the WCCB model. Comparison between 4-group diffusion and Serpent methods and between models with and without Be.

These models reach the highest TBR in the range between natural lithium and 30 % ^{6}Li enrichment. The TBR increases significantly if added only a 10 % of Be to the Li breeding layer. In the 4-group method the difference is 0.26 units at $x_{Li6} = 0.14$. In the infinite Serpent model, the growth is almost negligible, but in the annular model the TBR in the case with Be is 0.15 higher at $x_{Li6} = 0.2$.

The infinite Serpent models reach lower TBR (0.96 at $x_{Li6} = 0.3$) and the graph is flatter than the annular Serpent models ($TBR_{max} = 1.2$ at $x_{Li6} = 0.2$). This is because in the annular model the breeding layer is facing the plasma, receiving higher neutron fluxes than in the homogeneous infinite model, and ^{7}Li produce more tritium (higher TBR for low x_{Li6}) in the annular model because the spectrum in this model is harder (see ^{7}Li(n,n+T) cross-section Figure 3.10).

The 4-group diffusion method generally overestimates the TBR, reaching TBR = 1.81 (model with Be at $x_{Li6} = 0.14$). This is because this method normally overestimates neutron fluxes, especially for low-energy neutrons (see the 4-group Monte-Carlo comparison in Appendix C). Overestimation is much higher for low ^{6}Li fraction. Serpent model in an infinite medium does not reach TBR=1 for any ^{6}Li – ^{7}Li composition, but the annular model goes until TBR=1.20 (case with Be at $x_{Li6} = 0.2$).

5.2.2 HCPB and HCLL models

Serpent annular models based on the HCPB and HCLL concepts have been run and the material composition has been optimized for a DEMO-type reactor (Figures 4.10 and 4.11). These models, like the actual HCPB and HCLL TBM designs for ITER, have a Be first wall, but alternative models with W as a first wall material have also been implemented (Figures 4.13 and 4.14).

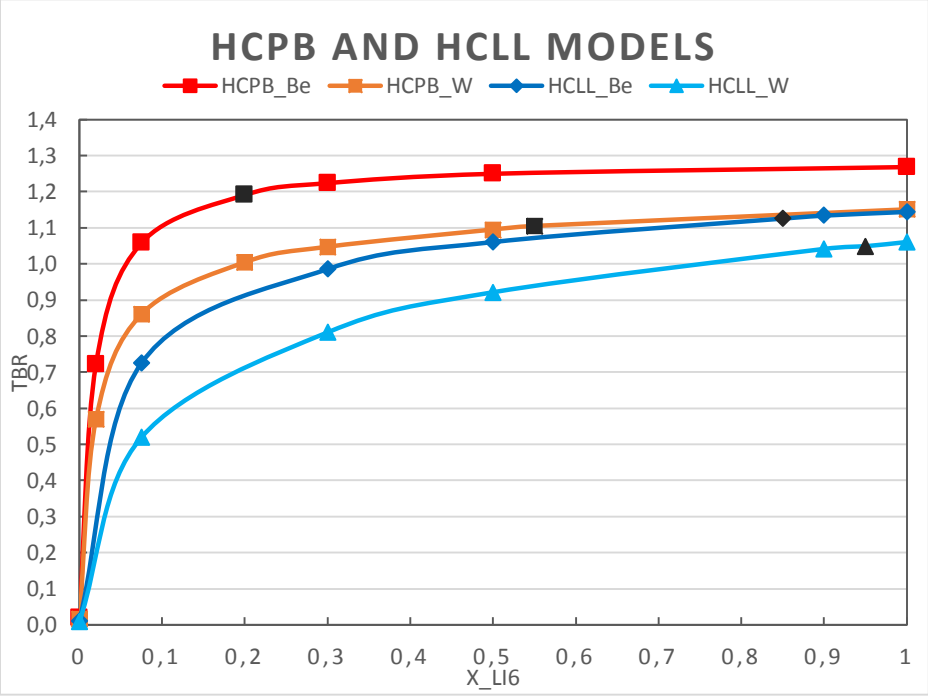

Figure 5.6: TBR as a function of ^{6}Li enrichment for HCPB and HCLL models. Comparison between models with Be and W as a first wall. Black marks represents the reference ^{6}Li fraction and its TBR.

The HCPB models have higher TBR than the HCLL models, and models with Be as first wall material have higher TBR than models with W, thus the HCPB-Be is the most efficient blanket. Both HCPB models have higher TBR than the HCLL models for every $^{6}\mathrm{Li}$ fraction, reaching TBR=1.27 for pure $^{6}\mathrm{Li}$ in the HCPB model with Be. The material of the thin first wall (Be or W), of only one centimeter, affects significantly to the TBR, producing differences up to 0.2 in HCPB models and up to 0.21 in HCLL models.

The shape of the TBR graph (increasing towards pure $^{6}\mathrm{Li}$) is because the $^{7}\mathrm{Li}$ contribution to the TBR is negligible due to a soft spectrum caused by the neutron moderation by helium (see He and Li cross-sections in section 3.2). The $^{7}\mathrm{Li}$ contribution to the TBR is between 2 and 4 orders of magnitude lower than $^{6}\mathrm{Li}$ contribution. Unlike these models, the WCCB model peaks at low $^{6}\mathrm{Li}$ enrichment (Figure 5.5) due to a harder spectrum that makes significant $^{7}\mathrm{Li}$ contribution to the TBR. The hard spectrum in the WCCB model is due to the use of water as moderator instead of helium (compare hydrogen and helium cross-sections in section 3.2) and also to the geometry approach (breeding layer facing the plasma).

Black marks in Figure 5.6 are the reference points chosen for each model, which present the highest TBR possible with the lowest enrichment (enrichment processes are expensive), and keeping the design limits $\mathrm{TBR}_{\mathrm{min}} = 1.1$ and the maximum neutron fluxes behind the blanket. HCPB-Be model gets TBR=1.1 at 10 % $^{6}\mathrm{Li}$ but enriching only until 20 % $^{6}\mathrm{Li}$ it is obtained TBR=1.2. HCPB-W model gets the TBR=1.1 at 55 % $^{6}\mathrm{Li}$, this point is chosen because it is already a relatively high enrichment and the TBR curve is very flat (reaching only TBR=1.15 at 100 % $^{6}\mathrm{Li}$). The HCLL-Be model has TBR=1.1 at 71 % $^{6}\mathrm{Li}$ enrichment, but at this point neutron fluxes are higher than the design limits (see Table 5.5). The lowest $^{6}\mathrm{Li}$ fraction, satisfying the design limits, is $\mathrm{x}_{\mathrm{Li6}} = 0.85$ with TBR=1.13. Finally, HCLL-W model reaches TBR=1.06 at 100 % $^{6}\mathrm{Li}$, not high enough to get tritium self-sufficiency with 90 % extraction efficiency, but TBR can be enhanced through increasing the lithium alloy fraction in the blanket or increasing the helium fraction (by decreasing stainless steel). However, the reference point for the HCLL-W model would be at almost pure $^{6}\mathrm{Li}$, i.e. ~95 % $^{6}\mathrm{Li}$, TBR≈1.1.

HCPB, HCLL (DEMO)	***HCPB − Be***	**HCPB − *W***	**HCLL − Be**	**HCLL − W**
$\mathbf{TBR_{max}}$ $\mathbf{(x_{Li6} = 1)}$	1.27	1.15	1.14	1.06
$\mathbf{TBR \geq 1.1}$	$x \geq 0.1$	$x \geq 0.55$	$x \geq 0.71$	–
$\mathbf{x_{Li6ref}}$	0.2	0.55	0.85	0.95
$\mathbf{TBR_{ref}}$	1.20	1.10	1.13	1.05

Table 5.4: Maximum TBR (reached for pure $^{6}\mathrm{Li}$), range in which $\mathrm{TBR} \geq 1.1$ and reference point ($^{6}\mathrm{Li}$ fraction and $\mathrm{TBR}_{\mathrm{ref}}$). Values for HCPB and HCLL models, with Be or W.

The neutron fluxes of these models (Figures 5.7, 5.8, 5.9 and 5.10) are similar to the fluxes obtained in the shielding models (see section 5.1.1). For example, the same qualitative characteristics are observed when comparing the models with Be and W, softer neutron spectrum in the first wall in the Be case, etc.

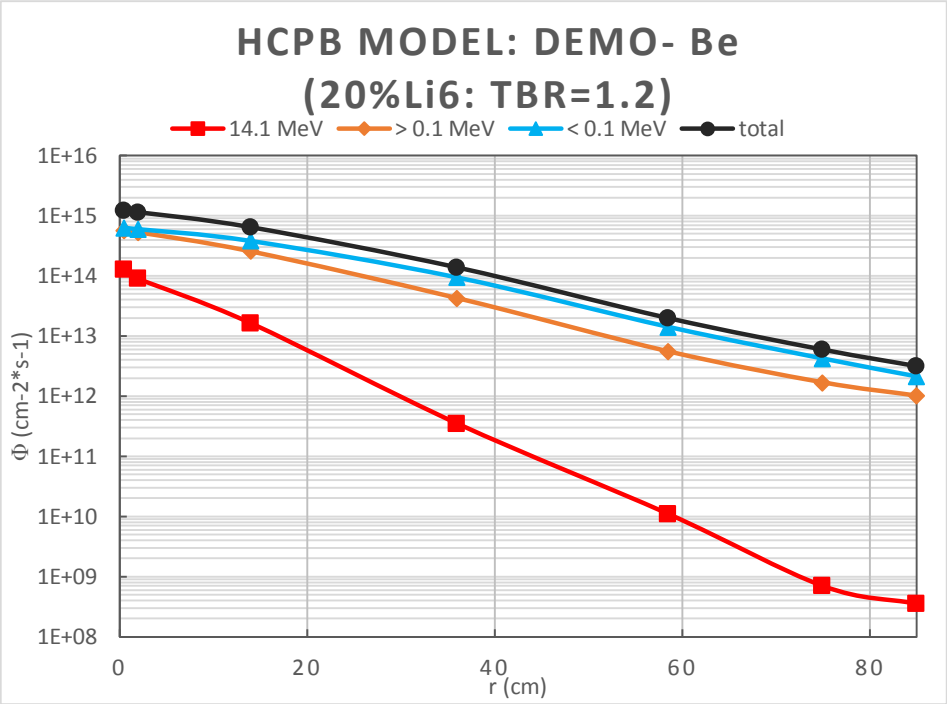

Figure 5.7: Serpent results of neutron fluxes at the reference ^{6}Li enrichment of the HCPB model for DEMO (with Be as first wall), as a function of its radial length.

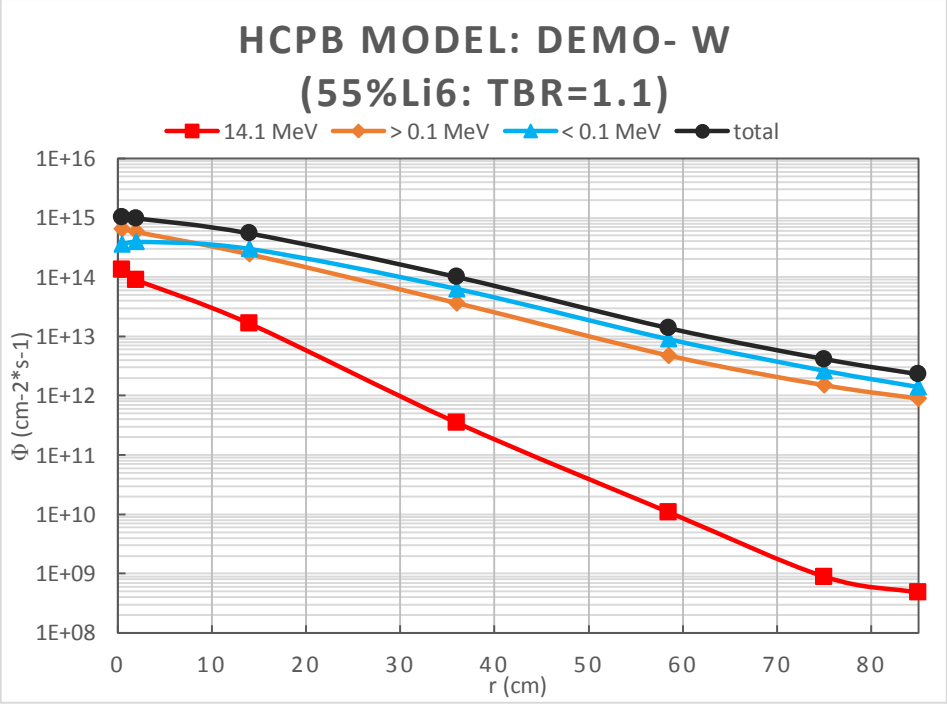

Figure 5.8: Serpent results of neutron fluxes at the reference neutron spectrum at the optimal ^{6}Li enrichment of the HCPB model for DEMO (with W as first wall), as a function of its radial length.

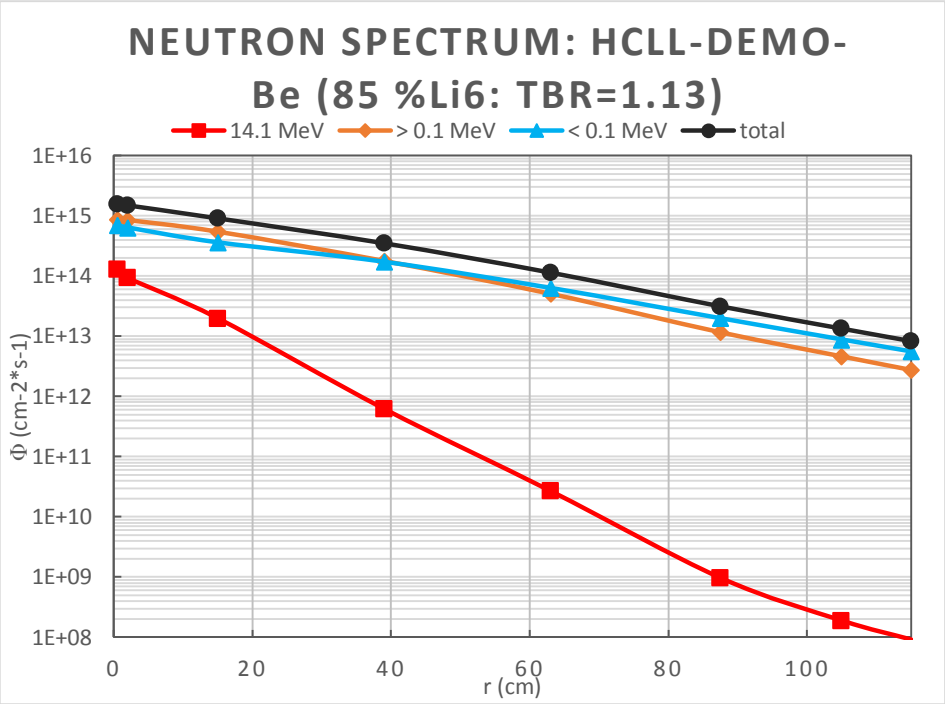

Figure 5.9: Serpent results of neutron fluxes at the reference neutron spectrum at the optimal ^{6}Li enrichment of the HCLL model for DEMO (with Be as first wall), as a function of its radial length.

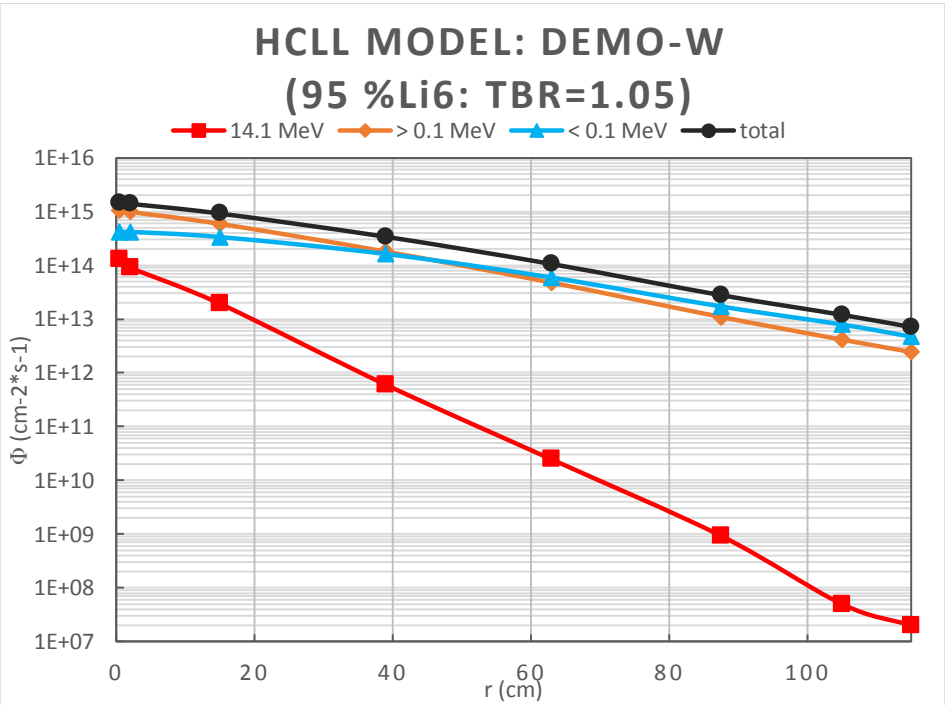

Figure 5.10: Serpent results of neutron fluxes at the reference neutron spectrum at the optimal ^{6}Li enrichment of the HCLL model for DEMO (with W as first wall), as a function of its radial length.

HCPB models satisfy the design limits for the neutron flux with a comfortable margin (Table 5.5), and reach the necessary TBR for a lower ^{6}Li enrichment than the HCLL models (Table 5.4). Because of that, HCPB blankets have more degrees of freedom for the material composition. HCLL model with Be was especially hard to optimize, due to high neutron fluxes and not so high TBRs. However, it was found a reasonable material composition and enrichment that satisfy all the design limits. The HCLL-W model has slightly lower neutron fluxes and lower TBR than the HCLL-Be model, at the reference point.

$\Phi_{bb}[cm^{-2}s^{-1}]$ DEMO	Design limits	HCPB − Be 20 % ^{6}Li	HCPB − W 55 % ^{6}Li	HCLL − Be 85 % ^{6}Li	HCLL − W 95 % ^{6}Li
$E = 14.1\ MeV$	–	$7.0 * 10^{8}$	$8.8 * 10^{8}$	$1.9 * 10^{8}$	$5.0 * 10^{7}$
$E > 0.1\ MeV$	$4.6 * 10^{12}$	$1.7 * 10^{12}$	$1.5 * 10^{12}$	$4.6 * 10^{12}$	$4.1 * 10^{12}$
$E < 0.1\ MeV$	–	$4.2 * 10^{12}$	$2.6 * 10^{12}$	$8.8 * 10^{12}$	$8.0 * 10^{12}$
Total	$1.4 * 10^{13}$	$5.9 * 10^{12}$	$4.1 * 10^{12}$	$1.3 * 10^{13}$	$1.2 * 10^{13}$

Table 5.5: Serpent results for neutron fluxes after the blanket at the reference ^{6}Li enrichment for the different models. Comparison to the design limits for the neutron flux.

The lithium depletion simulations show that the TBR takes between 5 and 10 years[19] (depending on the model) to drop until 1 (Figure 5.11 and Table 5.12). This means that a HCPB-Be blanket (fastest depletion) could work without recharging lithium for around 4 years and the HCLL-Be for at least 8 years. Note that an initial tritium overproduction can compensate the subsequent underproduction, if tritium is stored (taking into account its half-life of 12.32 years).

As the HCPB-Be is the most efficient model (highest TBR at the lowest ^{6}Li enrichment, 20 %), the ^{6}Li density is the lowest and because of that the relative ^{6}Li depletion is significantly faster (and therefore the TBR decrease as well) than in the other models.

[19] A unity power plant capacity factor is assumed.

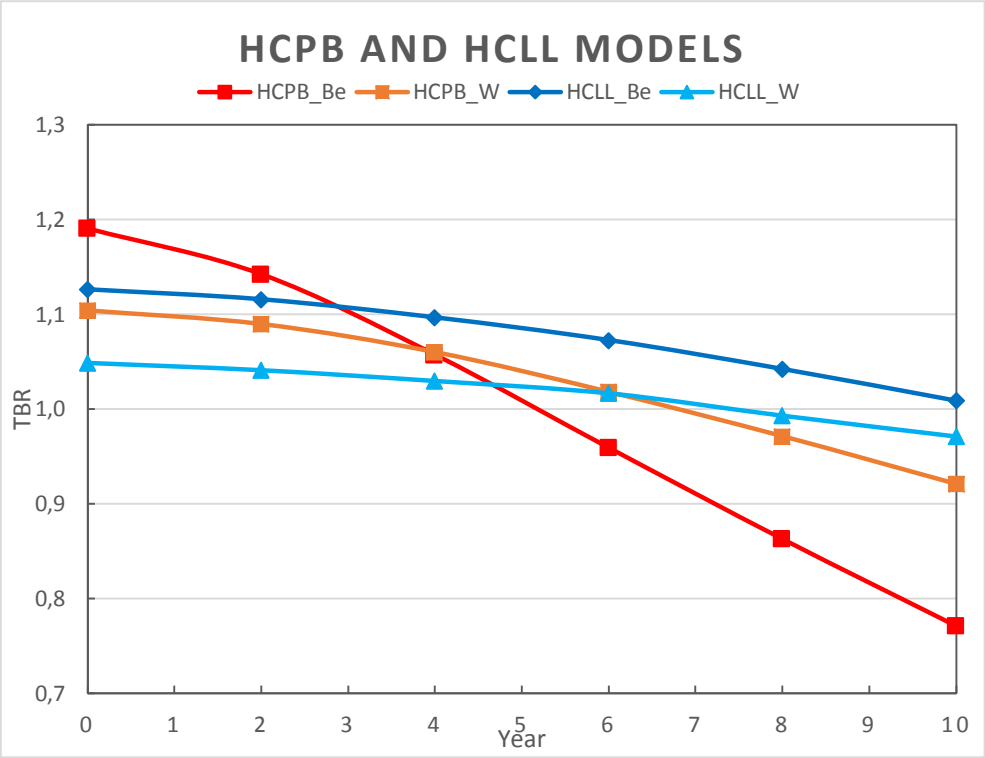

Figure 5.11: Serpent results for TBR reduction with time (due to the ^{6}Li depletion) at the reference ^{6}Li enrichment for the different models.

Depletion of ^{6}Li DEMO	HCPB − Be (20% ^{6}Li)	HCPB − W (55% ^{6}Li)	HCLL − Be (85% ^{6}Li)	HCLL − W (95% ^{6}Li)
$N_{Li6}(t)/N_{Li6}(0)$ $t = 10$ years	0.55	0.83	0.88	0.90
t(year) for TBR = 1	5.2	6.8	10.5	7.6

Table 5.6: Serpent results for ^{6}Li depletion after 10 years and time required for the TBR to be reduced to TBR=1, at the reference ^{6}Li enrichment for the different models.

Chapter 6

Summary and discussion

The first of the two major objectives of this study is to assess the main candidates for the DEMO first wall, Be or W, in terms of the neutron spectrum created inside the blanket and helium production in the first wall. The second objective is to make an assessment of the European helium-cooled pebble bed (HCPB) and helium-cooled lithium lead (HCLL) blanket concepts, comparing the TBR (tritium breeding ratio), the shielding capability and the lithium depletion with time in a DEMO-type reactor. A minor objective is to compare the analytical and Monte-Carlo methods and to assess the limitations of the former ones.

Shielding blanket models based on the ITER parameters have been assessed. The HCPB and HCLL models have been developed by consulting several papers on this topic, using some output data from the shielding models and through an optimization process.

Both analytical (multigroup diffusion theory) and Monte-Carlo methods are utilized to calculate the neutron fluxes and neutron induced reactions required in this project. 1-group and 4-group diffusion methods have been utilized to understand the performance of the materials under neutron irradiation, to obtain initial estimates and also some qualitative findings. More complex models have been run by the Monte-Carlo code Serpent. An assessment of the limitations of the 4-group diffusion method (Appendix C) showed that this method generally overestimates neutron fluxes, especially for low-energy neutrons, mainly due to the difficulty of taking into account the neutron flux dependence when calculating analytically the group constants. This problem can be solved using neutron spectra from Monte Carlo models or using numerical methods. Other limitations are neglecting the inelastic scattering in the 4-group model or the assumption of keeping all the born neutrons in the group 1 from neutron multiplicative reactions. The Serpent shielding blanket model of ITER, with a symmetric annular geometry representing the poloidal cross section of the tokamak, provides quite accurate neutron fluxes compared to the 3D MCNP model of ITER of [7][20].

The results for the Be-W comparison indicates that W is a better first wall material in terms of blanket shielding capability for high-energy neutrons and helium production in the first wall. Be as first wall material produces a softer spectrum (neutron moderation) with a higher total neutron flux (neutron multiplication) than W in the first few centimeters of the blanket, but this trend is progressively changed through the blanket, thus the W case presents a 29% higher global attenuation factor for high-energy neutrons than Be. Helium production causes the

[20] Compare Table 8.1 from [7] to Table 5.1 in this study.

embrittlement and swelling of materials. The He production rate in the Be first wall is 1000 times higher than for W. In the ITER first wall made of Be, the critical He bulk concentration [30] is reached after 7 years of the DT operation plan if the material has thin grain radius ($\sim 0.5\ \mu m$). In a DEMO-type reactor it would take only 1-12 full operating days (depending on the grain radius) to reach the critical He concentration in Be, whereas the He production in W is not a relevant issue (20 to 200 full-power-years to reach the critical concentration). These results can be understood by comparing the cross-sections of these materials which show that Be has a much bigger He production cross-section, lower capture cross-section and it is a better moderator (low-Z) than W. Taking into account other advantages of W as first wall material, like lower tritium retention and lower sputtering yield than Be (section 3.1), we could conclude that W is the most appropriate candidate.

Nevertheless, a Be-W comparison in the tritium breeding models (HCPB and HCLL) showed that the use of a Be first wall leads to a substantial increment of the TBR, about 20 % higher than the model with W, allowing the use of lithium with lower enrichment, and hence reducing costs. This is due to the spectrum characteristics in the first centimeters of the blanket commented previously.

The assessment of the European tritium breeding blanket concepts indicates that HCPB models have a higher TBR and better shielding capability than HCLL models, being the HCPB with Be as first wall the most efficient breeding blanket, reaching tritium self-sufficiency for only 10 % ^{6}Li enrichment, whereas the HCPB-W needs 55 % in ^{6}Li. The HCLL-Be model needs over 70 % ^{6}Li enrichment to reach self-sufficiency. In addition, in HCLL models, lower enrichment means higher neutron fluxes behind the blanket, so their optimal enrichment is about 90 % ^{6}Li. These results are consistent with the reference enrichment values for these blanket concepts found in several papers [9, 20, 21, 29, 31 and 32].

The optimization process of these models showed that about the half of the blanket volume has to be dedicated to the lithium-lead alloy in HCLL models, or to the lithium ceramic plus beryllium pebbles in HCPB models, to reach tritium self-sufficiency. Be pebbles as neutron multiplier material, have a great impact in the breeding performance of the HCPB model, being the optimal composition 18 % Li_4SiO_4 – 82 % Be. This composition is very similar to the reference composition showed in [21] (17 %-83 %).

The ^{6}Li depletion simulations (^{7}Li contribution to the TBR is negligible) indicates that the TBR decreases significantly faster in the HCPB-Be blanket than in the other models, due to the low initial enrichment. However, the HCPB-Be blanket could still work without recharging lithium for at least 4 full-power-years, and the other blanket models could work for 6-9 years. As the DEMO blanket is expected to be replaced every 5 full-power-years [6] due to radiation damage in steel, the breeding blankets can be easily designed to work during this period without any lithium recharge.

The use of Serpent code, despite this code primarily being intended for burnup calculations, has been found to work satisfactory for this study. The external source mode allowed to get good statistical accuracy (relative error ~ 0.1 %) for short running times (10-60 min). However, if a more complex geometry is required, maybe other alternatives should be considered, like a CAD geometry model supporting the Monte-Carlo code.

Future studies on tritium breeding for DEMO should include a 2D model representing the poloidal cross section of the DEMO reactor (this study uses an annular approach of the cross section with rotational symmetry). The spatial and energy distribution of the neutron source should be included in this proposed model to get more accurate results. Other limitations of the HCPB and HCLL models in this study are the material composition,

which would need a further analysis, and the geometry approach of the blanket. Other supporting studies are needed to complete the model, like an assessment of the tritium extraction efficiency (90 % considered in this study) and an analysis of the blanket surface area available for tritium breeding (this study considers the whole blanket, which is the 82 % of the total first wall).

Appendix A

Importance of D-D neutrons in a D-T plasma

This appendix assess the importance of the neutrons from D-D reactions in a D-T plasma by comparing the fusion reaction rates.

Assuming a typical plasma temperature for a D-T plasma, T=10 keV, the fusion cross-sections (see Figure A.1) for D-D and D-T are $\langle \sigma v \rangle_{DD} \approx 1.2 * 10^{-24}\ \mathrm{m}^3/s$ and $\langle \sigma v \rangle_{DT} \approx 1.2 * 10^{-22} \mathrm{m}^3/s$ respectively.

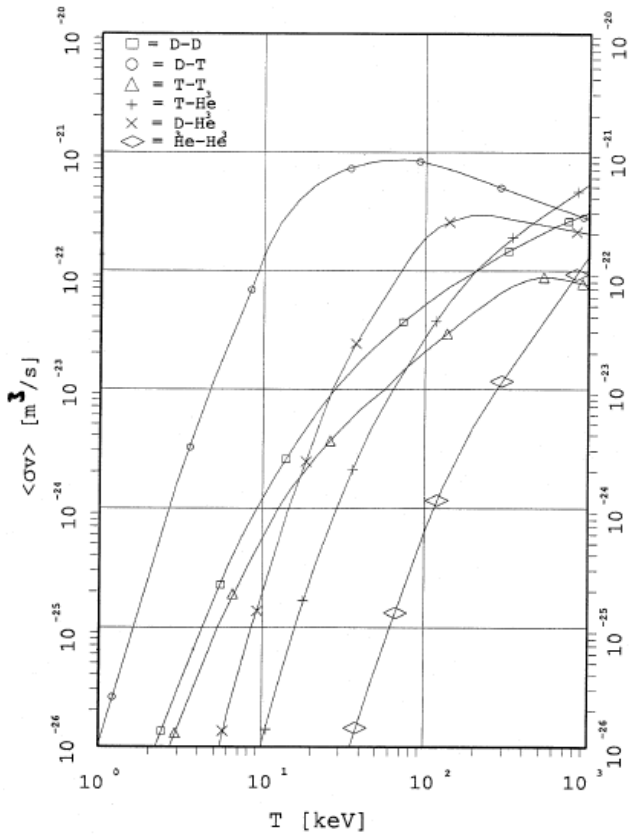

Figure A.1: Fusion cross-sections for different isotopes [33].

The fusion reaction rate is defined as

$$R_f = N_i N_j \langle \sigma v \rangle \tag{A.1}$$

where N_i and N_j are the atomic densities of the plasma species.

Assuming a 50 %-50 % D-T plasma, $N_D = N_T = N$.

In every D-T fusion reaction one neutron is produced (see Figure 2.3), so the neutron production rate for D-T reactions is:

$$R_n^{DT} = R_f^{DT} = N_D N_T \langle \sigma v \rangle_{DT} = N^2 \langle \sigma v \rangle_{DT} \tag{A.2}$$

For D-D reactions, on the one hand, only the half of the reactions produce one neutron (see Figure 2.3), on the other hand, only D nuclei are taken into account ($N_i = N_j = \frac{1}{2} N_D$).

$$R_n^{DD} = \frac{1}{2} R_f^{DD} = \frac{1}{2}\frac{1}{2} N_D \frac{1}{2} N_D \langle \sigma v \rangle_{DD} = \frac{1}{8} N^2 \langle \sigma v \rangle_{DD} \tag{A.3}$$

Comparing both reaction rates:

$$\frac{R_n^{DT}}{R_n^{DD}} = \frac{8\langle \sigma v \rangle_{DT}}{\langle \sigma v \rangle_{DD}} = 800 \tag{A.4}$$

This means that in a D-T plasma there is about 800 more neutrons from D-T reactions than from D-D reaction. Therefore, D-D neutrons in a D-T plasma were considered negligible in this study.

Appendix B

Neutron diffusion

B.1 1-group diffusion equations

The 1-group diffusion theory assumes one neutron speed, a uniform medium, neutron flux varying spatially slowly, small absorption relative to scattering and neutrons scattered isotropically. The general equation for neutron diffusion is derived from the Fick's Law which relates net currents and flux gradients:

$$\frac{\partial \mathrm{n}}{\partial \mathrm{t}} = \mathrm{s} + \nu\Sigma_\mathrm{f}\Phi - \Sigma_\mathrm{a}\Phi + \nabla \mathrm{D}\nabla\Phi \tag{B.1}$$

where n is the neutron density, s is a neutron source, Σ_f and Σ_a are the fission and absorption macroscopic cross-sections, respectively and D is the diffusion coefficient.

Steady-state is considered $\left(\frac{\partial \mathrm{n}}{\partial \mathrm{t}} = 0\right)$ and there are no fission or other neutron sources inside the wall $(s = \nu\Sigma_\mathrm{f}\Phi = 0)$.

$$\nabla \mathrm{D}\nabla\Phi - \Sigma_\mathrm{a}\Phi = 0 \tag{B.2}$$

Assuming a one-dimensional medium (x) and D constant the equation can be written as:

$$\frac{\mathrm{d}^2\Phi(\mathrm{x})}{\mathrm{dx}^2} - \frac{1}{\mathrm{L}^2}\Phi(\mathrm{x}) = 0 \tag{B.3}$$

where L is the diffusion length ($\mathrm{L}^2 = \mathrm{D}/\Sigma_\mathrm{a}$).

Through integrating equation (B.3) and considering a plane isotropic source s_0 at the edge (x=0) of a semi-infinite medium, the equation obtained is:

$$\Phi(\mathrm{x}) = \frac{\mathrm{s}_0\mathrm{L}}{\mathrm{D}}\mathrm{e}^{-\mathrm{x}/\mathrm{L}} \tag{B.4}$$

B.2 4-group diffusion equations

The set of equations of the multigroup diffusion theory in its general form is:

$$\frac{1}{v_g}\frac{\partial \Phi_g}{\partial t} - \nabla \cdot D_g \nabla \Phi_g + \Sigma_{tg}\Phi_g = \sum_{g'=1}^{G} \Sigma_{sg'g}\Phi_{g'} + S_g \qquad g = 0,1,\dots,G \tag{B.5}$$

where S_g is the neutron source in each group, including fission. However, there are no fission sources in this study.

An infinite medium and steady state are assumed. Thus, the leakage term and the time dependence can be neglected in the set of equations of the multigroup diffusion theory.

$$\nabla \cdot D_g \nabla \Phi_g = 0 \tag{B.6}$$

$$\frac{1}{v_g}\frac{\partial \Phi_g}{\partial t} = 0 \tag{B.7}$$

The four energy groups are:

$$g = 0: E = E_0 \tag{B.8}$$

$$g = 1: E_1 \leq E < E_0 \tag{B.9}$$

$$g = 2: E_2 \leq E < E_1 \tag{B.10}$$

$$g = 3: E < E_2 \tag{B.11}$$

where: $E_0 = 14.1\ \text{MeV}; E_1 = 1\ \text{MeV}; E_2 = 100\ \text{keV}$. These groups are chosen according to the characteristics of the problem: we are interested in the 14.1 MeV neutron flux (g=0) because the neutron source has this energy. The group 1 ($1\ \text{MeV} \leq E < 14.1\ \text{MeV}$) is chosen because important reactions like neutron multiplier reactions and He producer reactions only occur in this energy range (see Figures 3.3 to 3.11). We are also interested in the high-energy neutron flux (g=0 + g=1 + g=2) because the radiation damage to the materials is due to these neutrons. g=3 contains all the neutrons with lower energies than 100 keV.

Assuming only down-scattering, the set of four equations is:

$$\Sigma_{t0}\Phi_0 = S_0 \tag{B.12}$$

$$\Sigma_{t1}\Phi_1 = \Sigma_{s01}\Phi_0 + S_1 \tag{B.13}$$

$$\Sigma_{t2}\Phi_2 = \Sigma_{s02}\Phi_0 + \Sigma_{s12}\Phi_1 + S_2 \tag{B.14}$$

$$\Sigma_{t3}\Phi_3 = \Sigma_{s13}\Phi_1 + \Sigma_{s23}\Phi_2 + S_3 \tag{B.15}$$

Where the group constants are:

$$\Phi_g = \int_{E_g}^{E_{g-1}} \Phi(E)dE \tag{B.16}$$

$$\Sigma_{tg} = \Sigma_{ag} + \sum_{g'} \Sigma_{sgg'} \tag{B.17}$$

where Φ_g is the neutron flux averaged in the group g, Σ_{tg} and Σ_{ag} are the total and the absorption cross-sections and $\Sigma_{sgg'}$ is the elastic scattering cross-section between groups.

The cross-section of the reaction r in the group g, and the elastic scattering cross-sections between groups are written as:

$$\Sigma_{rg} = \frac{\int_{E_g}^{E_{g-1}} \Sigma_r(E)\Phi(E)dE}{\int_{E_g}^{E_{g-1}} \Phi(E)dE} \tag{B.18}$$

$$\Sigma_{sg'g} = \frac{\int_{E_{g'}}^{E_{g'-1}} \int_{E_g}^{E_{g-1}} \Sigma_s(E' \to E)\Phi(E')dEdE'}{\int_{E_{g'}}^{E_{g'-1}} \Phi(E')dE'} \tag{B.19}$$

The elastic scattering transfer function, $\Sigma_s(E' \to E)$, is defined as:

$$\Sigma_s(E' \to E) = \begin{cases} \frac{\Sigma_s(E')}{E'(1-\alpha)}; & E \le E' \le \frac{E}{\alpha}; \\ 0 & \text{otherwise} \end{cases} \qquad \alpha = \left(\frac{A-1}{A+1}\right)^2 \tag{B.20}$$

Assuming $\Phi(E) = \text{constant}$ in every energy group, the neutron flux dependence in the cross-sections is removed and the problem can be solved analytically:

$$\Sigma_{rg} = \frac{\int_{E_g}^{E_{g-1}} \Sigma_r(E)dE}{\int_{E_g}^{E_{g-1}} dE} = \frac{\int_{E_g}^{E_{g-1}} \Sigma_r(E)dE}{E_{g-1} - E_g} \tag{B.21}$$

$$\Sigma_{sg'g} = \frac{\int_{E_{g'}}^{E_{g'-1}} \int_{E_g}^{E_{g-1}} \Sigma_s(E' \to E)dEdE'}{E_{g'-1} - E_{g'}} \tag{B.22}$$

Upscattering only occurs in the thermal range, so can be neglected using these four groups.

Note that, because of the shape of the scattering transfer function, only hydrogen, i.e. $\alpha = 0$, can scatter neutrons to two groups under the initial energy group.

Two cases are considered for solving the latter equation: the general case where $0 < \alpha < 1$ and the special case where $\alpha = 0$.

- General case: $0 < \alpha < 1$

For $g' = 1,2$, if the final energy E is in the range $\alpha E' \le E \le E_{g'}$ and the initial energy E', $E_{g'} \le E' \le \frac{E}{\alpha}$, then:

$$\Sigma_{sg'g} = \frac{\int_{E_{g'}}^{E_{g'}/\alpha} \int_{\alpha E'}^{E_{g'}} \frac{\Sigma_s(E')}{E'(1-\alpha)} dE dE'}{E_{g'-1} - E_{g'}} = \frac{\int_{E_{g'}}^{E_{g'}/\alpha} \Sigma_s(E') \frac{E_{g'}/E' - \alpha}{1-\alpha} dE'}{E_{g'-1} - E_{g'}}$$
$$= \frac{\Sigma_{sg'} E_{g'}}{E_{g'-1} - E_{g'}} \left(\frac{\ln\alpha}{\alpha - 1} - 1 \right) \quad \text{(B.23)}$$

In particular:

$$\Sigma_{s12} = \frac{\Sigma_{s1} E_1}{E_0 - E_1} \left(\frac{\ln\alpha}{\alpha - 1} - 1 \right) \quad \text{(B.24)}$$

$$\Sigma_{s23} = \frac{\Sigma_{s2} E_2}{E_2 - E_3} \left(\frac{\ln\alpha}{\alpha - 1} - 1 \right) \quad \text{(B.25)}$$

For scattering from the group 0, trivially: $\Sigma_{s01} = \Sigma_{s0}$.

- Special case: $\alpha = 0$

For $g' = 1,2$, if the final energy E is in the range $0 \le E \le E_{g'}$ and the initial energy E', $E_{g'} \le E' \le E_{g'-1}$ then:

$$\Sigma_{sg'others} = \frac{\int_{E_{g'}}^{E_{g'-1}} \int_0^{E_{g'}} \frac{\Sigma_s(E')}{E'} dE dE'}{E_{g'-1} - E_{g'}} = \frac{\int_{E_{g'}}^{E_{g'-1}} \Sigma_s(E') \frac{E_{g'}}{E'} dE'}{E_{g'-1} - E_{g'}} = \frac{\Sigma_{sg'} E_{g'}}{E_{g'-1} - E_{g'}} \ln\left(\frac{E_{g'-1}}{E_{g'}} \right) \quad \text{(B.26)}$$

For scattering to the group $g = g' + 2$, if the final energy E is in the range $0 \le E \le E_{g'+1}$ and the initial energy E', $E_{g'} \le E' \le E_{g'-1}$ then:

$$\Sigma_{sg'g'+2} = \frac{\Sigma_{sg'} E_{g'+1}}{E_{g'-1} - E_{g'}} \ln\left(\frac{E_{g'-1}}{E_{g'}} \right) \quad \text{(B.27)}$$

Then for scattering to the group $g = g' + 1$:

$$\Sigma_{sg'g'+1} = \Sigma_{sg'others} - \Sigma_{sg'g'+2} = \frac{\Sigma_{sg'}(E_{g'} - E_{g'+1})}{E_{g'-1} - E_{g'}} \ln\left(\frac{E_{g'-1}}{E_{g'}} \right) \quad \text{(B.28)}$$

In particular:

$$\Sigma_{s13} = \frac{\Sigma_{s1} E_2}{E_0 - E_1} \ln\left(\frac{E_0}{E_1} \right) \quad \text{(B.29)}$$

$$\Sigma_{s12} = \frac{\Sigma_{s1}(E_1 - E_2)}{E_0 - E_1} \ln\left(\frac{E_0}{E_1} \right) \quad \text{(B.30)}$$

$$\Sigma_{s23} = \frac{\Sigma_{s2}(E_2 - E_3)}{E_1 - E_2} \ln\left(\frac{E_1}{E_2} \right) \quad \text{(B.31)}$$

For scattering from the group 0 (in which E=14.1 MeV) to the rest of the groups, trivially: $\Sigma_{s0others} = \Sigma_{s0}$.

For scattering from g'=0 to g=2, the final energy E is $E \leq E_1$ and the initial energy E' is $E' = E_0$, then:

$$\Sigma_{s02} = \Sigma_{s0} \frac{E_1}{E_0} \tag{B.32}$$

$$\Sigma_{s01} = \Sigma_{s0others} - \Sigma_{s02} = \Sigma_{s0} \left(1 - \frac{E_1}{E_0}\right) \tag{B.33}$$

As homogenized materials are considered in this study, the final cross-section for reaction r is the summation of the cross-sections for the different materials, i.e.

$$\Sigma_{rg} = \sum_{A} N_A \sigma_{rg}^A \tag{B.34}$$

where σ_{rg}^A is the cross-section of the reaction r in the group g for the isotope with mass number A, and N_A is its density in the medium,

$$N_A = \frac{d_A N_a}{M_A} v_A \tag{B.35}$$

where d_A is the mass density, N_a the Avogadro constant, M_A the atomic mass and v_A the volume fraction in the medium.

Appendix C

Assessment of the limitations of the 4-group diffusion method

A comparison between the 4-group diffusion and the Monte Carlo method has been made to assess the accuracy of the multigroup diffusion theory, to find its main limitations, to determine what kind of uncertainities have to be expected when running the models and to find out how it could be improved.

Comparing the output data from the 4-group diffusion calculations and the Monte Carlo model from the study “Tritium breeding ratio and energy amplification in an infinite lithium blanket” [34] and recalculating the group constants it is shown that the main limitation of the multigroup diffusion theory is the difficulty of taking into account the neutron flux dependence when calculating the group constants. Another source of uncertainities, in this case, is to neglect inelastic scattering in the 4-group model. The 4-group diffusion method generally overestimates neutron fluxes, especially low energy neutron fluxes.

- **Blanket approximation**

The problem is simplified to an infinite, homogenized medium with a uniform 14.1 MeV neutron source.

For both multigroup and Monte Carlo models, the material fractions are: $\mathrm{N}_1 = 1.337 * 10^{28}\ \mathrm{m}^{-3}$; $\mathrm{N}_{16} = 0.669 * 10^{28}\ \mathrm{m}^{-3}$; $\mathrm{N}_{\mathrm{Li}} = 3.712 * 10^{28}\ \mathrm{m}^{-3}$; $\mathrm{N}_{\mathrm{a}} = 0.167 * 10^{28}\ \mathrm{m}^{-3}$, where $\mathrm{N}_1, \mathrm{N}_{16}$ and N_{Li} are the densities of $^{1}\mathrm{H}, ^{16}\mathrm{O}$ and Li respectively, and N_{a} is the density of the theoretical absorber a, which cross-section is defined as:

$$\sigma_{\mathrm{a}} = \begin{cases} 50\mathrm{eV} * \left(\frac{\mathrm{E}}{\mathrm{eV}}\right)^{-1/2} \\ 1\mathrm{eV} \end{cases} \tag{C.1}$$

The uniform neutron source is $\mathrm{S}_0 = 1.5 * 10^{18}\ \mathrm{m}^{-3}\mathrm{s}^{-1}$, based on a 3000 MW neutron power, a blanket volume of $320\ \mathrm{m}^3$ and assuming that half of the neutrons are going to the blanket.

- **4-group diffusion theory equations**

Neglecting the leakage term and removing the time dependence the set of equations is:

$$\Sigma_{t0}\Phi_0 = S_0 \tag{C.2}$$

$$\Sigma_{t1}\Phi_1 = \Sigma_{s01}\Phi_0 + \Sigma_{D0}^{6}\Phi_0 + \Sigma_{T0}^{7}\Phi_0 + \Sigma_{D1}^{6}\Phi_1 + \Sigma_{T1}^{7}\Phi_1 \tag{C.3}$$

$$\Sigma_{t2}\Phi_2 = \Sigma_{s02}\Phi_0 + \Sigma_{s12}\Phi_1 \tag{C.4}$$

$$\Sigma_{t3}\Phi_3 = \Sigma_{s13}\Phi_1 + \Sigma_{s23}\Phi_2 \tag{C.5}$$

The groups chosen are:

$$g = 0: E = E_0 \tag{C.6}$$

$$g = 1: E_1 \leq E < E_0 \tag{C.7}$$

$$g = 2: E_2 \leq E < E_1 \tag{C.8}$$

$$g = 3: E < E_2 \tag{C.9}$$

where: $E_0 = 14.1\ \text{MeV}; E_1 = 1\ \text{MeV}; E_2 = 100\ \text{keV}$.

The simplified averaged cross-sections are:

$$\Sigma_{rg} = \frac{\int_{E_g}^{E_{g-1}} \Sigma_r(E)dE}{\int_{E_g}^{E_{g-1}} dE} = \frac{\int_{E_g}^{E_{g-1}} \Sigma_r(E)dE}{E_{g-1} - E_g} \tag{C.10}$$

$$\Sigma_{sg'g} = \frac{\int_{E_{g'}}^{E_{g'-1}} \int_{E_g}^{E_{g-1}} \Sigma_s(E' \to E)dEdE'}{E_{g'-1} - E_{g'}} \tag{C.11}$$

where:

$$\Sigma_{rg} = \sum_A N_A \sigma_{rg}^A \tag{C.12}$$

and $\Sigma_s(E' \to E)$ is the elastic scattering transfer function:

$$\Sigma_s(E' \to E) = \begin{cases} \dfrac{\Sigma_s(E')}{E'(1-\alpha)}; & E \leq E' \leq \dfrac{E}{\alpha}; \\ 0 & \text{otherwise} \end{cases} \qquad \alpha = \left(\frac{A-1}{A+1}\right)^2 \tag{C.13}$$

For a full derivation of the equations see Appendix B.2.

- **Neutron fluxes and breeding ratio comparison**

The program EES (Engineering Equation Solver) has been used to implement the calculations. It has been chosen natural lithium, i.e. 7.5 % ^{6}Li fraction (x=0.075), to make the

neutron flux comparison. It was solved the 4-group model (Φ_{4g}), and the output neutron flux data from the Monte Carlo model was integrated over the energy (Φ_{mc}) to compare fluxes.

Li (x = 0.075)	Φ_{4g} [$cm^{-2}s^{-1}$]	Φ_{mc}[$cm^{-2}s^{-1}$]
E = 14.1 MeV	$2.6 * 10^{13}$	$2.8 * 10^{13}$
1 MeV ≤ E < 14.1M eV	$2.6 * 10^{14}$	$1.1 * 10^{14}$
100 keV ≤ E < 1 MeV	$4.8 * 10^{13}$	$3.1 * 10^{13}$
E < 100 keV	$4.0 * 10^{14}$	$4.1 * 10^{13}$
Total	$7.4 * 10^{14}$	$2.1 * 10^{14}$

Table C.1: Neutron spectrum at ^{6}Li fraction x=0.075. Comparison between 4-group and Serpent results.

The 14.1 MeV neutron flux is a little bit higher in the Monte Carlo model, but in the rest of the groups the 4 energy group model overestimates fluxes, especially in the low-energy group where there is a difference of one order of magnitude.

These results indicate that the breeding ratio is going to be overestimated in the 4-group model.

Li	TBR_{4g}	TBR_{mc}
x = 0.075	1.52	1.18

Table C.2: TBR at ^{6}Li fraction x=0.075. Comparison between 4-group and Serpent results.

Plotting the breeding ratio as a function of ^{6}Li fraction, the difference in the results decreases as increasing the ^{6}Li fraction.

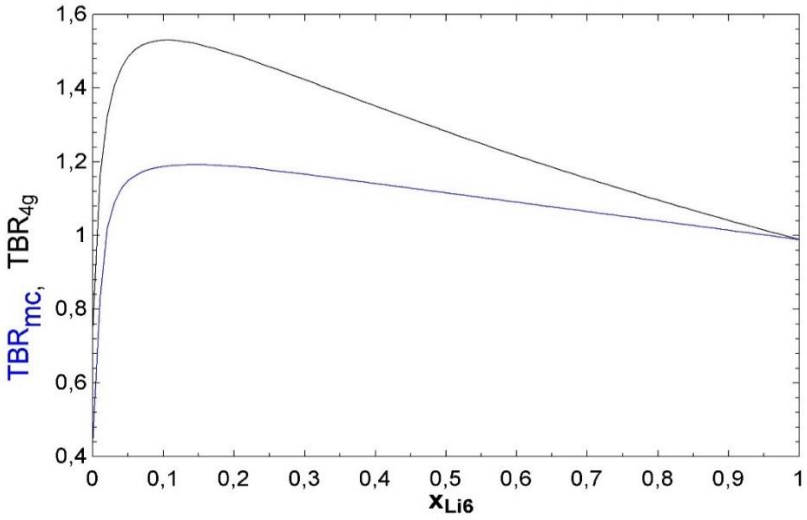

Figure C.1: TBR comparison between Monte-Carlo method and 4-group method, as a function of the ^{6}Li enrichment.

- **Modified 4-group diffusion model**

A very rough assumption solving the 4-group model is not taking into account the neutron flux dependence when calculating the averaged cross-sections. Their proper definition is:

$$\Sigma_{rg} = \frac{\int_{E_g}^{E_{g-1}} \Sigma_r(E)\Phi(E)dE}{\int_{E_g}^{E_{g-1}} \Phi(E)dE} \tag{C.14}$$

$$\Sigma_{sg'g} = \frac{\int_{E_{g'}}^{E_{g'-1}} \int_{E_g}^{E_{g-1}} \Sigma_s(E' \rightarrow E)\Phi(E')dEdE'}{\int_{E_{g'}}^{E_{g'-1}} \Phi(E')dE'} \tag{C.15}$$

To evaluate the importance of this assumption and see how the model can be improved, the neutron flux output data has been taken from the Monte-Carlo model, for natural lithium, and has been used to recalculate the averaged cross-sections of the 4-group model. Running this "modified" 4-group model the following results has been obtained:

Li (x = 0.075)	Φ_{4g} [$cm^{-2}s^{-1}$]	Φ_{4gmod} [$cm^{-2}s^{-1}$]	Φ_{mc}[$cm^{-2}s^{-1}$]
E = 14.1 MeV	$2.6 * 10^{13}$	$2.6 * 10^{13}$	$2.8 * 10^{13}$
1 MeV ≤ E < 14.1 MeV	$2.6 * 10^{14}$	$2.2 * 10^{14}$	$1.1 * 10^{14}$
100 keV ≤ E < 1 MeV	$4.8 * 10^{13}$	$4.4 * 10^{13}$	$3.1 * 10^{13}$
E < 100 keV	$4.0 * 10^{14}$	$3.6 * 10^{13}$	$4.1 * 10^{13}$
Total	$7.4 * 10^{14}$	$3.3 * 10^{14}$	$2.1 * 10^{14}$

Table C.3: Neutron spectrum at ^{6}Li fraction x=0.075. Comparison between 4-group modified-4-group and Serpent results.

The "modified" neutron fluxes are closer to the Monte-Carlo fluxes than the fluxes of the normal 4-group model. Fluxes in groups 1 and 2 decrease a little (10-20 %) and the flux in the group 3 decreases one order of magnitude, being even a little underestimated (14 %) in comparison to the Monte-Carlo model. This can be explained making a comparison between the averaged cross-sections in the 4-group model and the modified model. In general the cross-sections increase in the modified model, but the biggest differences appear in the absorption cross-section of the absorber and in the tritium-reaction cross-section of ^{6}Li:

$\mathbf{Li\ (x = 0.075)}$	σ_a^{4g}	σ_a^{4gmod}	σ_T^{4g}	σ_T^{4gmod}
$\mathbf{g = 0}$	0.01	0.01	0.03	0.03
$\mathbf{g = 1}$	0.02	0.02	0.08	0.11
$\mathbf{g = 2}$	0.08	0.09	0.69	0.74
$\mathbf{g = 3}$	0,32	3,53	1.01	11.01

Table C.4: Absorption and tritium-reaction cross-sections at ^{6}Li fraction x=0.075. Comparison between 4-group and modified-4-group results.

The increase of the cross-sections is huge in the group 3, i.e. for low energies, absorbing more neutrons in this energy range, and causing the decrease of the neutron fluxes.

Calculating the breeding ratio, a value closer to the Monte Carlo's result is obtained:

Li	TBR_{4g}	TBR_{4gmod}	TBR_{mc}
$\mathbf{x = 0.075}$	1.52	1.32	1.18

Table C.5: TBR at ^{6}Li fraction x=0.075. Comparison between 4-group, modified-4-group and Serpent results.

Plotting the breeding ratio as a function of x, the three models can be compared:

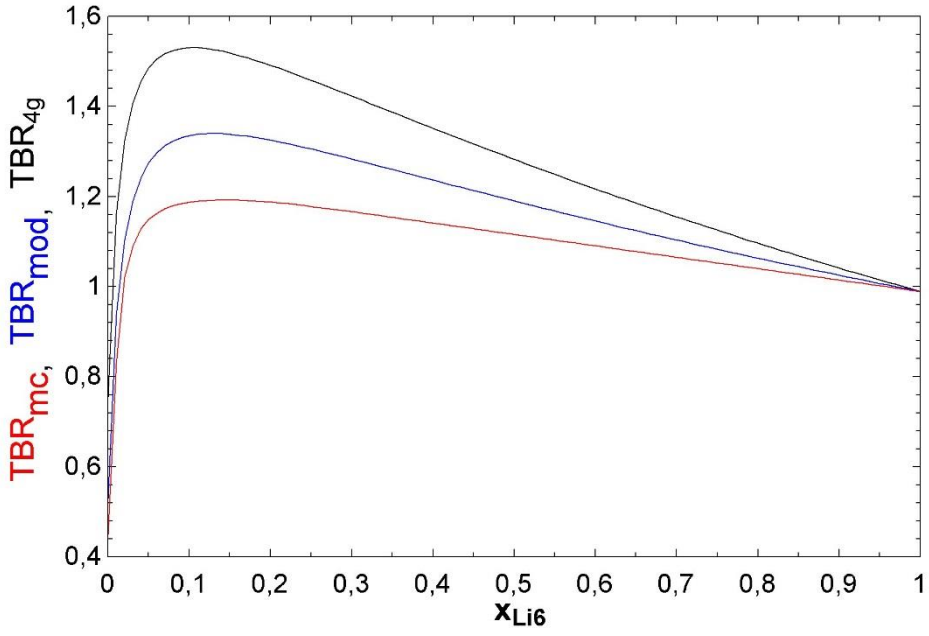

Figure C.2: TBR as a function of the ^{6}Li enrichment. Comparison between 4-group modified-4-group and Monte-Carlo method.

- **Discussion**

The conclusion that can be obtained studying the results is that the main limitation of the 4-group model is the difficulty of taken into account the neutron flux dependence when calculating analytically the averaged cross-sections. This problem can be solved using neutron spectra from Monte Carlo models, as it was done, or using numerical methods.

Other limitations in this case are neglecting the inelastic scattering in the 4 energy groups model (but considering it in the Monte Carlo model), or the assumption of keeping all the born neutrons in the group 1, from reactions $^{6}\mathrm{Li}(\mathrm{n},\mathrm{n}+\mathrm{d})\ ^{4}\mathrm{He}$ and $^{7}\mathrm{Li}(\mathrm{n},\mathrm{n}+\mathrm{t})\ ^{4}\mathrm{He}$.

Appendix D

Design limits for the neutron flux in HCPB and HCLL models

This appendix shows the calculations of the design limits for the total and high-energy neutron fluxes in the HCPB and HCLL blanket models for DEMO, i.e. the maximum neutron flux values allowed in these models (see section 4.3.4.2).

These limits are based on the Serpent results for neutron fluxes in the ITER shielding blanket model (section 5.1.1). The total neutron flux reduction ratio (between flux at first wall and behind the blanket) for this model is $\Phi_{\mathrm{fw}}^{\mathrm{tot}}/\Phi_{\mathrm{bb}}^{\mathrm{tot}} = 114$ (see Table 5.4). (This value is very similar to the one obtained from the graph 3.2 in the 2D model of ITER from reference [7]). As ITER has a high safety factor for the neutron flux when operating at nominal power (500 MW), a lower reduction ratio (around $\gtrsim 0.5 * \Phi_{\mathrm{fw}}/\Phi_{\mathrm{bb}}$) is considered to calculate the design limits for the study. This minimum reduction ratio considered is $\Phi_{\mathrm{fw}}^{\mathrm{tot}}/\Phi_{\mathrm{max}}^{\mathrm{tot}} = 60$. Thus, by using the $\Phi_{\mathrm{fw}}^{\mathrm{tot}}$ value from the shielding blanket model of DEMO ($\Phi_{\mathrm{fw}}^{\mathrm{tot}} = 8.3 * 10^{14}\ \mathrm{cm^{-2}s^{-1}}$) in the former formula, the design limit $\Phi_{\mathrm{max}}^{\mathrm{tot}}$ is calculated:

$$\Phi_{\mathrm{max}}^{\mathrm{tot}} = 1.4 * 10^{13}\ \mathrm{cm^{-2}s^{-1}} \tag{D.1}$$

The design limit for the high-energy neutron flux is calculated by the same procedure. In this case the values are $\Phi_{\mathrm{fw}}^{\mathrm{tot}}/\Phi_{\mathrm{bb}}^{\mathrm{tot}} = 197$ in ITER shielding model, $\Phi_{\mathrm{fw}}^{\mathrm{high}}/\Phi_{\mathrm{max}}^{\mathrm{high}} = 100$ is considered and $\Phi_{\mathrm{fw}}^{\mathrm{tot}} = 4.6 * 10^{14}\ \mathrm{cm^{-2}s^{-1}}$ from the DEMO shielding model. The design limit is:

$$\Phi_{\mathrm{max}}^{\mathrm{high}} = 4.6 * 10^{12}\ \mathrm{cm^{-2}s^{-1}} \tag{D.2}$$

Appendix E

Sample Serpent input files

In this Appendix two Serpent input files are written as example of the tens of simulations run: the shielding blanket model of ITER with Be as first wall and the HCPB-Be blanket model of DEMO with 20 % $^{6}\mathrm{Li}$ enrichment.

E.1 Shielding blanket model of ITER with Be as first wall

```
set title "shield_iter_Be"

set declib "/home/fernana1/endfb7/sss_endfb7.dec"
set nfylib "/home/fernana1/endfb7/sss_endfb7.nfy"
set acelib "/home/fernana1/endfb7/endfb7.serpentxs"

%Geometry normalization: The geometry of the model is the cross-section of the torus
%with the same major radius and first wall surface as the real ITER reactor.
surf 1 cyl 0 0 245
surf 2 cyl 0 0 246
surf 3 cyl 0 0 248
surf 4 cyl 0 0 290
surf 5 cyl 0 0 300
surf 6 cyl 0 0 310

cell 100 0 void -1
cell 101 0 Be 1 -2
cell 102 0 SSH2O 2 -3
cell 103 0 bulk 3 -4
cell 104 0 void 4 -5
cell 105 0 bulk 5 -6
cell 106 0 outside 6
```

```
src Source1 sc 100 se 14.1
set srcrate 3.74E16 %s^-1cm^-1 total neutron yield from the plasma, times the blanket-total_surface %ratio, between the torus perimeter.
set nps 500000 %total number of source neutrons run

mat Be 1.216E-01 rgb 0 255 0
4009.06c 1

mat SSH2O sum rgb 50 100 255 %*10^24
26000.06c 4.211E-2 %NFe=6.016E-2 70%SS 30%H2O
24000.06c 1.163E-2 %NCr=1.662E-2
28000.06c 6.869E-3 %NNi=9.813E-3
1001.06c 2.006E-02 %NH2Opure=3.343E-2cm-3
8016.06c 1.003E-02

mat bulk sum rgb 180 180 180 %*10^24
26000.06c 5.053E-2 %NFe=6.016E-2 84%SS 16%H2O
24000.06c 1.396E-2 %NCr=1.662E-2
28000.06c 8.243E-3 %NNi=9.813E-3
1001.06c 1.07E-02
8016.06c 5.349E-03

plot 3 1000 1000

set nbuf 60

set bc 1 %black

%set egrid 0 1E-9 14.1
%set gcu 0 %group constants in univ 0
set pcc 1  %predictor construction, for burnup
set printm 1 %material composition file

det spectrum1 dc 101 dv 1.543E3 de grid4g %total volume 2.63E5
det spectrum2 dc 102 dv 3.104E3 de grid4g
det spectrum3 dc 103 dv 7.099E4 de grid4g
det spectrum4 dc 104 dv 1.854E4 de grid4g
ene grid4g 1 1E-11 0.1 1 14.05 14.2

det flux1 dc 101 dv 1.543E3
det flux2 dc 102 dv 3.104E3
det flux3 dc 103 dv 7.099E4
det flux4 dc 104 dv 1.854E4
```

```
det flux5 dc 105 dv 1.916E4

det Bealpha dc 101 dr 107 Be9 dv 1.543E3
mat Be9 1.0 4009.06c 1.0
det Be2n dc 101 dr 16 Be9 dv 1.543E3 %the (n,2n) reaction produces Helium through alpha decay

%microscopic cross-section
det sigmaBealpha dc 101 dr 107 Be dt 3 flux1
det sigmaBe2n dc 101 dr 16 Be dt 3 flux1 % times 1E-24, neutron flux, Li6 density and blanket volume
%1.25E9cm^3, gives the total reaction rate
```

E.2 HCPB-Be blanket model of DEMO with 20% 6Li enrichment

```
set title "HCPB_demo_Be"

set declib "/home/fernana1/endfb7/sss_endfb7.dec"
set nfylib "/home/fernana1/endfb7/sss_endfb7.nfy"
set acelib "/home/fernana1/endfb7/endfb7.serpentxs"

%Geometry normalization: The geometry of the model is the cross-section of the torus
%with the same major radius and first wall surface as the real ITER reactor.
surf 1 cyl 0 0 368
surf 2 cyl 0 0 369
surf 3 cyl 0 0 371
surf 4 cyl 0 0 438
surf 5 cyl 0 0 448
surf 6 cyl 0 0 458

cell 100 0 void -1
cell 101 0 Be 1 -2
cell 102 0 SSHe 2 -3
cell 103 0 breeder 3 -4
cell 104 0 void 4 -5
cell 105 0 SS 5 -6
cell 106 0 outside 6

src Source1 sc 100 se 14.1
set srcrate 1.94E17 %s^-1cm^-1 total neutron yield from the plasma, times the blanket-total_surface
%ratio, between the torus perimeter.
set nps 5000000 %total number of source neutrons run

mat Be 1.216E-01 rgb 0 255 0 burn 10
```

```
4009.06c 1

mat SSHe sum rgb 50 100 255 %*10^24
2004.06c 5.861E-4 %NHe=9.769E-4 60%
26000.06c 2.406E-2 %NFe=6.016E-2 40%
24000.06c 6.648E-3 %NCr=1.662E-2
28000.06c 3.925E-3 %NNi=9.813E-3

mat breeder sum rgb 180 180 180 burn 10
2004.06c 1.954E-4 %NHe=9.769E-4 20%
26000.06c 1.504E-2 %NFe=6.016E-2 25%
24000.06c 4.155E-3 %NCr=1.662E-2
28000.06c 2.453E-3 %NNi=9.813E-3
14000.06c 1.146E-3 %NSi=1.146E-2 10%
8016.06c 4.582E-3 %NO=4.582E-2
3006.06c 9.164E-4 %NLi(in Li4SiO4)=4.582E-2; 10%,NLi=4.582E-3, Li6=20%
3007.06c 3.666E-3
4009.06c 5.472E-2 %NBep=1.216E-1 45%

mat SS sum
26000.06c 6.016E-2
24000.06c 1.662E-2
28000.06c 9.813E-3

dep daystep
730.5
730.5
730.5
730.5
730.5

plot 3 1000 1000

set nbuf 60

set bc 1 %black

%set egrid 0 1E-9 14.1
%set gcu 0 %group constants in univ 0
set pcc 1  %predictor construction, for burnup
set printm 1 %material composition file

det spectrum1 dc 101 dv 2.3154E3 de grid4g %total volume 2.63E5
```

```
det spectrum2 dc 102 dv 4.650E3 de grid4g
det spectrum3 dc 103 dv 1.703E5 de grid4g
det spectrum4 dc 104 dv 2.783E4 de grid4g
ene grid4g 1 1E-11 0.1 1 14.05 14.2

det flux1 dc 101 dv 2.3154E3
det flux2 dc 102 dv 4.650E3
det flux3 dc 103 dv 1.7028E5
det flux4 dc 104 dv 2.783E4
det flux5 dc 105 dv 2.846E4

det Li6T dc 103 dr 205 Li6  %7.6E23, times Li6 density gives 1E21s^-1
mat Li6 1.0 3006.06c 1.0

det Li7T dc 103 dr 205 Li7
mat Li7 1.0 3007.06c 1.0

det Bealpha dc 101 dr 107 Be9 dv 2.3154E3 %7.6E23, times Li6 density gives 1E21s^-1
mat Be9 1.0 4009.06c 1.0
det Be2n dc 101 dr 16 Be9 dv 2.3154E3 %the (n,2n) reaction produces Helium through alpha decay

%microscopic cross-section
det sigmaLi6T dc 101 dr 205 Li6 dt 3 flux1
det sigmaLi7T dc 101 dr 205 Li7 dt 3 flux1
det sigmaBealpha dc 101 dr 107 Be dt 3 flux1 % times 1E-24, neutron flux, Li6 density and blanket %volume 1.25E9cm^3, gives the total reaction rate
det sigmaBe2n dc 101 dr 16 Be dt 3 flux1
```

Bibliography

[1] J. Leppänen, *Serpent User Manual*, (retrieved 15/03/2014).

[2] JET, EFDA, http://www.efda.org/jet/.

[3] Fusion cross-sections, IEC Fusion technology, 2007, http://iecfusiontech.blogspot.com.es/2007/07/fusion-cross-sections.html, (retrieved 25/06/2014).

[4] M. Kikuchi, K. Lackner, M. Q. Tran, *Fusion Physics*, IAEA, 2012.

[5] *ITER, the machine*, https://www.iter.org/mach.

[6] D. Maisonnier and the PPCS team, *DEMO and Fusion Power plant Conceptual Studies in Europe,* 2005.

[7] *ITER Nuclear Analysis Report*, Nuclear Analysis Group, ITER Naka&Garching Joint Work Sites, July 2004.

[8] *Planning for Test Blankets Modules radwaste*, ITER newsline 243, October 2012.

[9] L.V. Boccaccini, C. Bachmann, G. Federici, Antonella Li Puma, P. Norajitra, *Design and Development of DEMO Blanket Concepts in Europe*, CEA, 2012.

[10] *Fusion Technology, Annual Report of the Association EURATOM-CEA 2005* http://www-fusion-magnetique.cea.fr/actualites/ra05/eur-cea-technology-2005-full.pdf

[11] F. Cismondia, S. Kecskesb, G. Aiello, *HCPB TBM thermo mechanical design: Assessment with respect codes and standards and DEMO relevancy,* Fusion engineering and design 86 pp. 2228-2232, 2011.

[12] Wolfram Alpha knowledgebase, 2014.

[13] *Lithium silicate (Li4SiO4),* http://www-ferp.ucsd.edu/LIB/PROPS/PANOS/li4sio4.html, (accessed on 28/04/2014).

[14] E. Mas de les Valls , L.A. Sedano, L. Batet, I. Ricapito, A. Aiello, O. Gastaldi d, F. Gabriel, *Lead-lithium eutectic material database for nuclear fusion technology*, Journal of Nuclear Materials 376 pp. 353-357, 2008.

[15] Kaye&Laby, *Tables of Physical and Chemical Constants* http://www.kayelaby.npl.co.uk/toc/.

[16] E. Rabaglino, *Hellium and Tritium in Neutron-irradiated Beryllium,* Forschungszentrum Karlsruhe, FZKA 6939 page 4, December 2004.

[17] J. Roth et al., *Recent analysis of key plasma wall interactions issues for iter*, Journal of Nuclear Materials, vol. 390–391, pp. 1–9, 2009.

[18] S. Brezinsek et al., *Fuel retention studies with the ITER-Like Wall in JET*, IAEA Nuclear Fusion 53, July 2013.

[19] G. Federici, C. Skinner, J. Brooks, J. Coad, C. Grisolia, A. Haasz, A. Hassanein, V. Philipps, C. Pitcher, J. Roth, W. Wampler, and D. Whyte, *Plasma-material interactions in current tokamaks and their impications for next step fusion reactors*, Nuclear Fusion, vol. 41, pp. 1967–2137, 2001.

[20] Fabrizio Franza, *Tritium transport analysis in HCPB DEMO blanket with the FUS-TPC Code*, Karlsruhe Institute of Technology, Kit Scientific Reports 7642, 2013.

[21] L.V. Boccaccini, *Advanced Helium Cooled Pebble Bed Blanket with SiCf/SiC as structural material*, Forschungszentrum Karlsruhe, 1999.

[22] M. Rieth, M.Schirra, A. Falkenstein, P. Graf, S. Heger, H. Kempe, R. Lindau, H. Zimmermann, *EUROFER 97 Tensile, Charpy, Creep and Structural Tests*, Forschungszentrum Karlsruhe, FZKA 6911, 2003.

[23] The JEFF-3.1.2 General Purpose Library, OECD Nuclear Energy Agency Data Bank (February 2014).

[24] The ENDF/B-VII.1 library, BNL National Nuclear Data Center (March 2014).

[25] Cross-Sections Evaluation Working Group, *ENDF-6 Formats Manual,* Brookhaven National Laboratory, July 2010.

[26] The EXFOR library, IAEA Nuclear Data Services (November 2013).

[27] S.A. Klein, *Engineering Equation Solver (EES) Manual* http://www.fchart.com/assets/downloads/ees_manual.pdf.

[28] *Fusion Technology, Annual Report of the Association EURATOM-CEA 2006* http://www-fusion-magnetique.cea.fr/actualites/ra06/eur-cea-2006-full-report.pdf

[29] L.V. Boccaccini, H. Neuberger, X. Jin, R. Meyder, *System Engineering and ITER Integration of the EU HCPB Test Blanket Module System*, P-O Box 3640, D-76021, 2007.

[30] M.R. Gilbert, S.L. Dudarev, S. Zheng, L.W. Packer, and J.-Ch. Sublet, *Transmutation, gas production, and helium embrittlement in materials under neutron irradiation*, CCFE-PR (12)02 page 16, 2010.

[31] D. Stork, *DEMO and the Route to Fusion Energy*, Euratom-UKAEA Fusion Association, September 2009.

[32] S. Hermsmeyer, *Improved Helium Cooled Pebble Bed Blanket*, Forschungszentrum Karlsruhe, FZKA 6399, 1999.

[33] M. Groth, A. Järvinen, Exercises of Fusion Energy Technology https://noppa.aalto.fi/noppa/kurssi/phys-e0463/viikkoharjoitukset.

[34] M.I. Airila, A.T. Salmi, *Tritium breeding ratio and energy amplification in an infinite lithium Blanket*, 2002 (unpublished).

[35] W.M. Stacey, *Nuclear Reactor Physics*, 2nd ed. Wiley, 2007.